Development of a Low-Cost, Low-Weight Flight Control System for an Electrically Powered Model Helicopter

Nicol Carstens

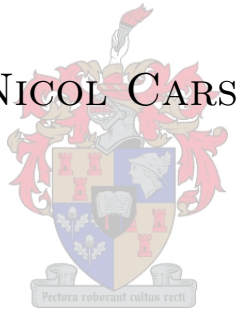

Thesis presented in partial fulfilment of the requirements for the degree of Master of Science in Electronic Engineering with Computer Science at the University of Stellenbosch

Supervisor: Professor Garth W. Milne

April 2005

Declaration

I, the undersigned, hereby declare that the work contained in this thesis is my own original work unless otherwise stated, and has not previously, in its entirety or in part, been submitted at any university for a degree.

.....	.....
Signature	Date

Abstract

This project started a new research area in rotary-wing flight control in the Computer and Control group at the University of Stellenbosch. Initial attempts to build a quad-rotor vehicle exposed difficulties which motivated changing to a standard model helicopter as a test vehicle. A JR Voyager E electrically powered model helicopter was instrumented with low-cost, low-weight sensors and a data communication RF link.

The total cost of the sensor, communication and microcontroller hardware used is approximately US$ 1000 and the added onboard hardware weighs less than 0.4 kg. The sensors used to control the helicopter include a non-differential u-Blox GPS receiver, Analog Devices ADXRS150 rate gyroscopes, Analog Devices ADXL202 accelerometers, a Polaroid ultrasonic range sensor and a Honeywell HMC2003 magnetometer.

Successful yaw, height and longitudinal position control was demonstrated. Significant further work is proposed, based on the literature study performed and the insights and achievements of the first rotary-wing unmanned aerial vehicle project in the group.

Opsomming

Hierdie projek het 'n nuwe navorsings area binne die Rekenaar en Beheer groep van die Universiteit van Stellenbosch ingelyf aangaande die ontwikkel van roterende vlerk onbemande vlieënde voertuie. Aanvanklike mislukte pogings om 'n vier rotor voertuig te ontwikkel het gelei tot die besluit om 'n standaard model helikopter aan te koop as toets voertuig. 'n JR Voyager E elektries aangedrewe model helikopter is geïnstrumenteer met lae koste, lae gewig sensors en data kommunikasie toerusting.

Die totale koste van die sensors, kommunikasie en mikroverwerker hardeware wat gebruik is, is ongeveer US$ 1000 en die massa van die toegevoegde hardeware is minder as 0.4 kg. Die sensors wat gebruik is sluit 'n nie-differensiaal u-Blox GPS ontvanger, Analog Devices ADXRS150 tempo giroskope, Analog Devices ADXL202 versnellingsmeters, 'n Polaroid ultrasoniese afstand sensor en 'n Honeywell HMC2003 magnetometer in.

Gier hoek, hoogte en longitidinale posisie beheer is suksesvol gedemonstreer. 'n Substansiële hoeveel opvolg werk word voorgestel, gebaseer op die literatuur studie wat gedoen is en die insigte en die doelwitte wat bereik is deur die eerste roterende vlerk onbemande vlieënde voertuig projek binne die groep.

Acknowledgements

This project would not have been successful without the guidance from my supervisor, Prof. Garth W. Milne, the financial support provided by Denel Aerospace Systems, the time and effort invested by our helicopter safety pilot, Mike Davis, and the encouragement of my girlfriend, Nadia de Swardt.

Other academic staff from the University of Stellenbosch that provided valuable advice and support were Dr Carl H. Rohwer, Dr Thomas Jones, Mr Johan Treurnicht and Prof. W. H. Steyn. Keith Browne assisted with a diverse number of tasks, ranging from photographer to motor mechanic. For the support and stimulating conversations of fellow students, Iain Peddle, Corné van Daalen, Christiaan Wood and all my other friends in the Electronic Systems Laboratory, I am truly grateful.

A number of people contributed to testbeds, mounts and other mechanical structures: Eddie de Swardt, Ulrich Buttner, Willie Croukamp and Francois Strümpfer. Tim Sindle and Xandri Farr have provided guidance in both the selection and use of the HMC2003 magnetometer. Benjamin Nortier was always willing to lend a helping hand when I had questions regarding GPS problems. Johnny Visagie analyzed the JR Voyager E helicopter as one of his case studies. His work provided a reference to compare my results against.

This document was compiled using the LaTeX template provided by Gert-Jan van Rooyen. I would like to thank him for simplifying the task of compiling a thesis document in LaTeX.

I would like to thank my father who taught me to work with my hands and think for myself, my friend Peter Matthaei who made undergraduate engineering fun and my mother for always loving and supporting me.

Nicol Carstens
December 2004

Contents

Nomenclature

A	rotor disk area
A_b	blade surface area
a	two-dimensional constant lift curve slope
a_0	coning angle of main rotor
a_1	first harmonic coefficient of main rotor longitudinal blade flapping with respect to shaft
a_x,a_y,a_z	accelerometer specific force measured in body axes
b	number of blades
b_1	first harmonic coefficient of main rotor lateral blade flapping with respect to shaft
C_b^n	Direction Cosine Matrix to transform vectors from body reference frame to navigation reference frame
c	mean blade chord length
c_{SB}	mean chord length of aerodynamic blade section of stabilizer bar
g	gravitational acceleration
I_b	moment of inertia of blade about flapping hinge
K	feedback gain
L,M,N	components of moment about the CG, in body frame
l_b	length of aerodynamic blade section of stabilizer bar
l_{SB}	length of stabilizer bar (flybar)
m	mass of helicopter
p, q, r	roll-, pitch- and yaw rate
q_0, q_1, q_2, q_3	attitude quaternions
r_e	rotor efficiency
R	radius of rotor blades
R_0	inner radius of a rotor, where the effective blade section starts
T	thrust of a rotor

u,v,w	velocity components in x, y and z-direction in body frame
U_e,V_e,W_e	trim velocity components in body frame
δ_{thr}	input to the engine throttle
δ_b	input to the longitudinal flapping
δ_a	input to the lateral flapping
δ_r	reference input to the yaw rate feedback system
δ_c	input to the main rotor collective pitch
ϕ	roll angle of Euler angle representation
θ	pitch angle of Euler angle representation
ψ	yaw angle of Euler angle representation
ρ	air density
τ	time constant
τ_e	effective rotor time constant
μ	advance ratio $V/(\Omega R)$
θ_0	collective blade pitch
σ	solidity ratio (ratio of blade area to disc area)
Ω	angular rate of main rotor rotation, quaternion ...

Subscripts

$bias$	bias
HF	high frequency
LF	low frequency
$meas$	measurement
MR	main rotor
N, E, D	North, East, Down
SB	stabilizer bar
TPP	tip path plane
TR	tail rotor

Superscripts

T	transpose

Acronyms and Abbreviations

3D	three-dimensional
ADC	analog to digital converter
AHRS	attitude heading reference system
AHS	American Helicopter Society
AR	aspect ratio
ASCII	American National Standard Code for Information Interchange
CCPM	cyclic collective pitch mixing
COST	commercial off the shelf
CMOS	complementary metal oxide semiconductor
CG	center of gravity
CR	control rotor
DSC	direct servo control, "buddy-plug"
EKF	extended Kalman filter
ESC	electronic speed controller
FCS	flight control system
GPS	Global Positioning System
GSM	Global System for Mobile communications
HILS	hardware-in-the-loop simulation
IARC	International Aerial Robotics Competition
IMU	inertial measurement unit
INS	inertial navigation system
IGE	in ground effect
LOS	line-of-sight
MEMS	micro electro-mechanical systems
MIMO	multi-input multi-output
NED	north, east and down coordinate frame
NGDC	National Geophysical Data Center
NiCd	nickel cadmium

NiMH	nickel metal hydride
NOAA	National Oceanic and Atmospheric Administration
OGE	out of ground effect
PC	personal computer
PPM	pulse position modulation
RC	radio control
RPV	remotely piloted vehicle
RPM	revolutions per minute
RTOS	realtime operating system
RUAV	Rotary-wing Unmanned Aerial Vehicle
RISC	reduced instruction set computer
SAS	stability augmentation system
SISO	single-input single-output
SB	stabilizer bar
TPP	tip path plane
UAV	unmanned aerial vehicle
UART	universal asynchronous receiver/transmitter
US	University of Stellenbosch
USC	University of Southern California
VTOL	vertical take-off and landing

List of Figures

List of Tables

"The thing is, helicopters are different from airplanes. An airplane by its very nature wants to fly and, if not interfered with too strongly by unusual events or by a deliberately incompetent pilot, it will fly. A helicopter does not want to fly. It is maintained in the air by a variety of forces and controls working in opposition to each other and, if there is any disturbance in this delicate balance, the helicopter stops flying; immediately and disastrously. There is no such thing as a gliding helicopter." - Harry Reasoner.

Chapter 1

Introduction and Overview

During the last decade the interest in unmanned aerial vehicles (UAVs) has increased tremendously. Not only are UAVs changing the face of the battlefield as we know it, but the number of potential commercial applications are endless.

Traditionally fixed-wing aircraft have been favoured as UAV platforms due to the structural simplicity and efficiency of these aircraft. Furthermore, fixed-wing aircraft are more stable than helicopters and have relatively simple, symmetric and decoupled dynamics.

Rotary-wing aircraft are becoming increasingly popular as UAV research vehicles. Rotary-wing UAVs offer two attractive capabilities: vertical take-off and landing (VTOL) and the ability to hover.

Although some research groups invest time and money in developing novel rotary-wing unmanned aerial vehicle (RUAV) platforms, most resort to buying radio controlled (RC) model helicopters. These helicopters have proved to be convenient testbeds for RUAV research, offering reasonable endurance and payload at a very reasonable cost. Model helicopters are however also agile, unstable and dangerous vehicles.

1.1 Project Goals

The initial goal of this project was to create a mechanically simple, low-cost, electrically powered rotary-wing vehicle and equip it to fly autonomously. The long term goal was to be able to launch a vehicle, command it to fly to a location, take a picture and return to the launch point.

In order to achieve these goals, the problem was broken up into the following objectives:

1. Design, build and test an electrically powered vehicle.
2. Select sensors and instrument the vehicle.
3. Design and implement a flight control system (FCS).

The goals were found to be too bold and the project definition had to be re-evaluated. The most significant stumbling block at the time was building an electrically powered rotary-wing vehicle. After funding became available, an electrically powered model helicopter was bought. The focus shifted to the development of a low-cost and low-weight flight control system for an electrically powered model helicopter.

Throughout the project Prof. G.W. Milne, the project supervisor, restricted the platform solutions to electrically powered vehicles. The restriction was imposed for the following reasons:

- Electrically powered vehicles can be operated indoors. Not only does this facilitate testing, but also opens opportunities for indoor applications.
- Electric vehicles can be made to hover indefinitely if they are powered by a limited-length tether.
- They start reliably and quickly.

1.2 Project History

In April 1996 a student from the Delft University of Technology, Falco Mooren, compiled a pre-study [39] as part of his practical work experience under the leadership of Prof. Milne. The aim of the HOPTUS (HelicOpter PlaTform of the University of Stellenbosch) project was to design an electrically powered helicopter platform capable of lifting a load for extended periods of time to an altitude of 50 to 100 metres, providing electrical power to the helicopter via a tether.

Mooren came to the conclusion that the coaxial configuration would be mechanically too complex and recommended that the four rotor option be investigated further. Mooren also recommended that a conventional helicopter with a tail rotor be considered as an alternative option.

A feasibility study [66] on the design of an electrically powered rotary-wing vehicle was compiled by Mr Daniel W. Venter, a fourth year student under Prof. M.J. Kamper. Venter also recommended a four rotor configuration.

1.2.1 Coaxial Rotary-Wing Platform

In October 1998 a student from the mechanical engineering department of the University of Stellenbosch designed and built a coaxial rotor platform under the leadership of Mr K. van der Westhuizen [8]. The machine had a fixed pitch rotor system and no other actuators to tilt the tip path plane (TPP) of the main rotor (see figure 1.1).

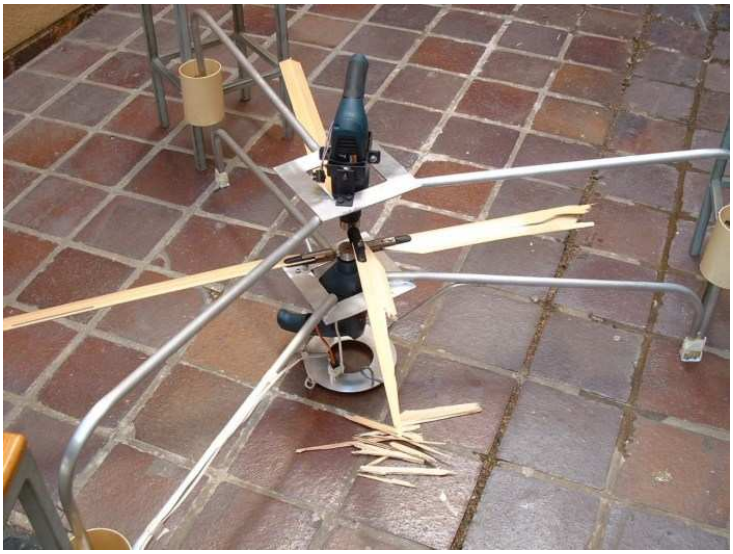

Figure 1.1: *Coaxial rotary-wing platform*

The author abandoned efforts to improve on the existing structure due to the extent of the mechanical inadequacies of the existing coaxial system and the lack of the required expertise to correct the problems. An alternative platform had to be sought. In response to the recommendations provided by the feasibility studies compiled by Mooren [39] and Venter [66], the author constructed a quad rotor structure.

1.2.2 Quad Rotor Vehicle Study

In recent years quad rotor toys have become increasingly popular due to their mechanical simplicity: a fixed cyclic pitch rotor can be used, rather than a feathering/flapping main rotor. A number of quad rotor vehicles have been studied intensively and advanced control theories have been applied to control these vehicles [10, 22, 49].

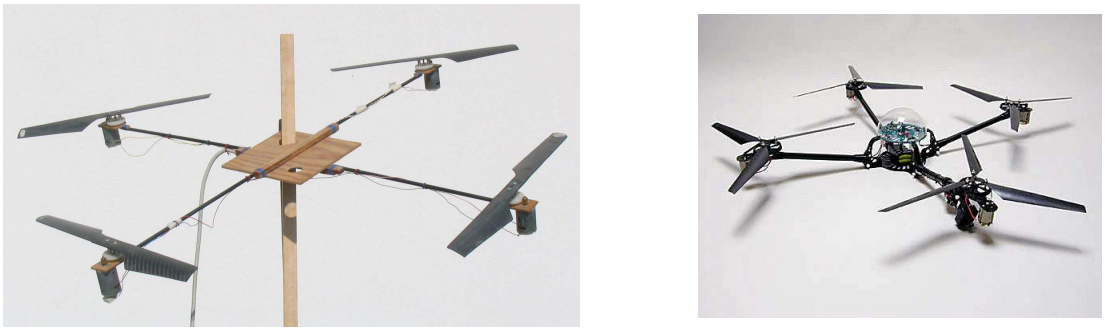

Figure 1.2: *Quad rotor built by the author (left) and Dragan Flyer XP (right)*

However, none of these quad rotor vehicles are flying autonomously. The most significant limitation of this configuration is the low power to weight ratio of existing commercial-off-the-shelf (COTS), small, electrically powered quad rotor vehicles. The only exception to the rule is the Canadian-manufactured [13] Dragan Flyer XP-Pro (see figure 1.2). The Dragan Flyer XP-Pro is capable of lifting a payload of 0.45 kg for 14 to 18 minutes. The Flyer is however not a cheap toy - the XP sells for US$ 5000.

The author invested six months in an attempt to build a rotary-wing vehicle. After a number of failed attempts to create a simple, low complexity rotary-wing vehicle with a reasonable power to weight ratio, the efforts were abandoned. The reasons for the failures can be summarised as follows:

Experience: It is common practice to build fixed-wing RC aircraft, but hardly any pilots manufacture their own helicopters. Neither the author, nor any of the staff that assisted him, had the required expertise to build a successful rotary-wing vehicle within the time and financial constraints.

Money: The power plants for the coaxial rotor vehicle were standard hand drills. Hairdryer motors were used to power the quad rotor vehicle. Although the motors might have produced sufficient thrust to lift the structures, the efficiency of the subsystems and motors were too low to carry the weight of the required sensors and control electronics.

Time: If more time was available it might have been possible to source the required parts and expertise to build a suitable vehicle.

In order to save time, the decision was made to buy an electrically powered RC model helicopter. An additional benefit offered by a COTS vehicle is that parts are COTS available when accidents occur.

1.3 Achievements and Future Projects

A small, electrically powered RC model helicopter, a JR Voyager E, was purchased (see figure 1.3). The focus shifted from building a vehicle to selecting and integrating the required sensors to be able to construct a flight control system (FCS) that could demonstrate basic, autonomous hover. Payload-, financial-, experience- and time limitations had to be weighed against anticipated performance in order to obtain the best possible solution within the existing boundaries. The following has been achieved since the RC model helicopter was acquired:

- The various autonomously flying model helicopter systems and the recommendations provided by successful teams have been studied extensively.
- The hardware required to stabilise a model helicopter has been designed and evaluated.
- The dynamic models presented by other authors have been studied and a hover and slow speed controller has been designed and simulated.
- The heading, altitude and longitudinal motion of the acquired JR Voyager E helicopter has been regulated successfully.

Figure 1.3: *Standard JR Voyager E with hoola-hoop*

To the knowledge of the author, at the time of writing, no autonomously free-flying sub-one-metre rotor diameter, electrically powered RC helicopter system exists. The majority of university projects are all making use of larger, glow- or gasoline[1] powered RC helicopters, using expensive, high quality differential global positioning systems (DGPS) and/or high grade inertial sensors to perform state estimation.

Unlike most other RUAV systems, the focus of this project has been to develop a simple, low-cost vehicle and FCS capable of performing basic, autonomous near-hover flight. Throughout the document the results obtained by other institutions are used as a reference, while similarities and differences between this and other projects are highlighted.

This project was a single student effort. Neither the author, nor his supervisor, had any prior RC helicopter experience. It was the first project in the Electronic Systems Laboratory (ESL) of the University of Stellenbosch making use of a RC vehicle and has been the seed from which a UAV group involving two lecturers and four students has formed. The experience gained through this project, together with the infrastructure that has been created, paves the way for future low cost model helicopter FCS development at the ESL.

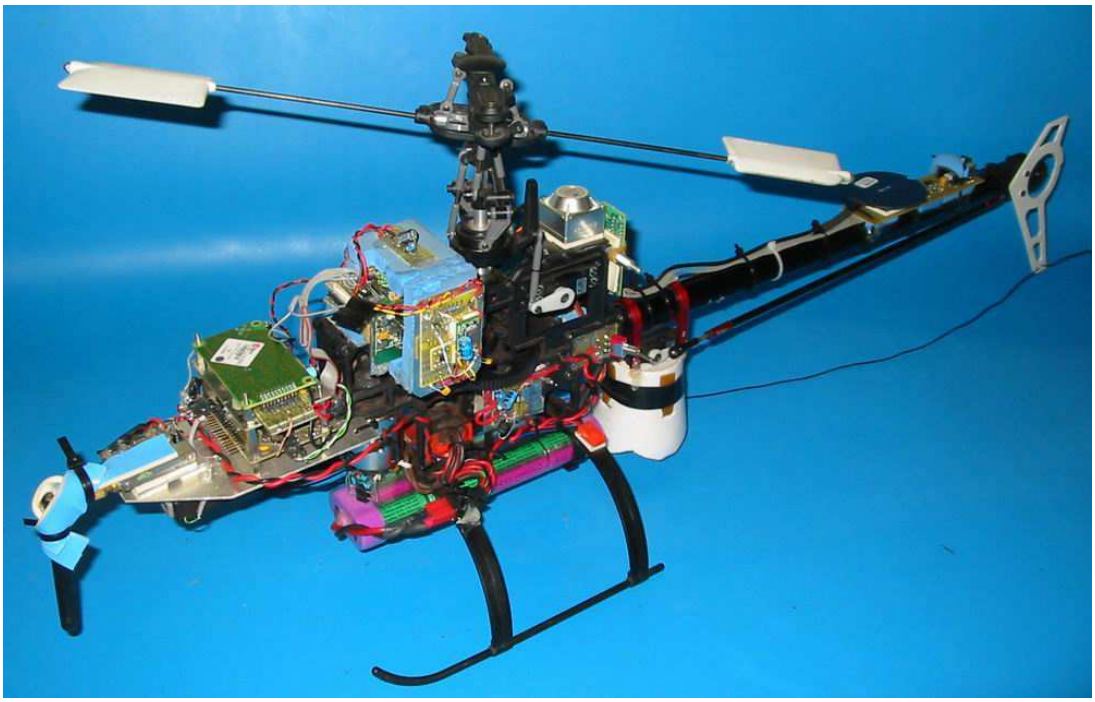

Figure 1.4: *JR Voyager E with all onboard subsystems mounted*

[1]RC helicopter pilots refer to "glow" powered motors to distinguish between glow- and spark plug engines. "Glow-Fuel" consists of Methanol (CH_3OH) as base fluid and is usually mixed with Castor/Synthetic Oil and Nitro Methane (CH_3NO_2).

1.4 Thesis Outline

The work performed by the author will be presented as follows:

Chapter 2: The dynamics of model helicopters are investigated. The properties of the Voyager E are compared to those of other glow and gasoline powered helicopters.

Chapter 3: The state estimators that were designed and implemented are presented. Some of the popular techniques used by other institutions are outlined.

Chapter 4: A systems overview is provided and the hardware used is described. The selection and evaluation of the helicopter, sensors and communication links are discussed.

Chapter 5: An overview of the software that was written for the three 8-bit microcontrollers and the desktop PC that was used to control the helicopter, is provided.

Chapter 6: A theoretical control system design and the simulations are presented.

Chapter 7: The control system implementation is discussed. The flight test responses are compared to simulations.

Chapter 8: The document is concluded with an assessment of the work and recommendations for future projects.

Chapter 2

Dynamics of RC Helicopters

A vast amount of effort has been invested by other institutions in identifying models for glow and gasoline powered helicopters. The most useful work in this field has been the work that presents a linearised model that describes the influence of the Bell-Hiller stabiliser bar[1] on the dynamics of the RC helicopter [36, 37]. Mettler *et al.* [33] have looked into the scaling effects and dynamic characteristics of miniature rotorcraft. Limited success has been achieved through attempts to adapt existing models for full-size helicopters to obtain accurate models for much smaller, more agile RC model helicopters.

No publications have been dedicated to describing the dynamics of a small, electrically powered, free flying RC helicopter that is not equipped with a rotor speed governor. Although a lot can be learned from the larger RC helicopters, most pilots describe the smaller helicopters as more sensitive to disturbances and mechanically less robust, and therefore more difficult to fly.

The goal of this chapter is not to derive a complete model for an RC helicopter from first principals. The models that have been presented by other authors will be used as the point of departure. The results that have been obtained by others will be summarized and applied to the JR Voyager E helicopter. The differences and similarities between the smaller, electrically powered helicopter and the larger gasoline and glow powered counterparts will be investigated.

The goal is to derive a model that is sufficient to design and simulate a FCS, without getting entangled in the intricate details of helicopter modelling. A decoupled model,

[1]The Bell-Hiller stabiliser bar (SB) is a combination of the classic Bell stabiliser bar and the Hiller servo rotor (SR) or control rotor (CR). The system consists of a "flybar", "paddles" and a number of linkages to the swashplate and main rotor cyclic pitch arms.

linearised near hover, will be used to design the estimators in chapter 3 and to close the control loops in chapters 6 and 7.

2.1 Control Mechanisms

Most full size and model helicopters (with only one set of main rotor blades and one set of tail rotor blades) are controlled using five control inputs:

- input to main rotor longitudinal cyclic blade pitch angle (δ_b),
- input to main rotor lateral cyclic blade pitch angle (δ_a),
- input to main rotor collective blade pitch angle (δ_c),
- input to tail rotor collective blade pitch angle (δ_r), and
- engine throttle (δ_{thr}).

If we consider a basic, decoupled model of a helicopter performing hover (and near-hover) flight, the main rotor blades can be viewed as a disc producing lift. The longitudinal- and lateral cyclic control movements (δ_b, δ_a) enable the pilot to tilt the tip path plane (TPP) of this disc relative to the body of the helicopter. These flapping angles (a_1, b_1) will induce moments about the center of gravity (CG) of the helicopter. The attitude of the body and blades controls the orientation of the thrust vector, causing lateral and longitudinal accelerations. The longitudinal cyclic can be viewed as the dominant pitch angle and longitudinal acceleration control input. Similarly, the lateral cyclic controls the roll angle and lateral acceleration, velocity and position.

The magnitude of the thrust produced by the main and tail rotor blades is determined by the collective pitch and rotation rate of the main and tail rotor blades. The input to the main rotor collective pitch (δ_c) is the dominant control to increase or decrease the vertical climb rate of the helicopter. If no vertical acceleration is present, the thrust produced is exactly equal to the weight of the helicopter.

Some systems require that the pilot also controls the rotational speed of the main rotor blades (Ω) by adjusting the power to the engine (δ_{thr}). Most RC helicopters have an engine speed governor to ensure that the revolutions per minute (RPM) of the main rotor blades are kept constant. If the helicopter is not equipped with an engine governor, the engine power is controlled open loop by programming the throttle control (δ_{thr}) to be a function of the main rotor collective pitch angle command.

The input to tail rotor collective blade pitch angle (δ_r) is used to command a yaw rate, changing the heading of the helicopter. A fixed gear ratio between the tail rotor shaft and main rotor shaft determines the angular rotation speed of the tail rotor blades relative to the main rotor angular rotation speed. It also implies that a load on either the tail rotor or main rotor will influence the other. This is an example of the cross-coupling that exists between the yaw rate and the climb rate.

A significant amount of cross-coupling exists between the various states and control mechanisms. For example: if the collective pitch on the main rotor blades is increased (to increase the vertical rate of climb) a yaw moment will be induced by the main rotor drag and a yaw control input will have to be applied by adjusting the collective pitch of the tail blades. A change in collective pitch on the tail rotor blades will also induce lateral acceleration of the helicopter body. A roll angle correction needs to be applied to compensate for the change in lateral force.

RC model helicopters are equipped with stability augmentation systems of which a Bell-Hiller stabiliser bar and a yaw rate feedback system are two commonly found examples. The Bell-Hiller stabiliser bar is a mechanical component that forms part of the helicopter rotor mechanics. The yaw rate stability augmentation system is an electronic subsystem that will be discussed in chapter 4.

2.2 Hover Thrust

Thrust calculations that were performed to predict the maximum payload a helicopter can carry are studied in this section. To verify the equations used, the thrust calculations were also performed for other model helicopters and compared with published results.

A helicopter can lift a higher payload in ground effect (IGE) than out of ground effect (OGE). Since the goal of this project was to be able to perform slow movements out of ground effect, the added lift provided IGE and at higher advance ratios will be ignored. Since the flight tests were performed at altitudes less than 150 metres above sea level, the calculations are performed for a helicopter flying at sea level.

According to Stepniewski and Keys [59], the thrust produced by the main rotor can be calculated using:

$$T = 4\pi R^2 \rho {V_t}^2 \left[A^2 r_e^2 + \frac{1}{3} B r_e^3 + \frac{4A(2A^2 - 3Br_e)(A^2 + Br_e)^{\frac{3}{2}}}{15B^2} \right] \tag{2.1}$$

with

$$A = \frac{\sigma a}{16}, \text{ and } B = \frac{\sigma a \theta_0}{8}$$

and assuming $r_e = 0.95$ is a good approximation for the rotor efficiency. Equation 2.1 was used to calculate the thrust for various RC model helicopters and can be seen in table 2.1.

Table 2.1: *Mass vs calculated thrust for various helicopters*

Helicopter	Mass [kg]	T [kg]	Ω [rad/s]	θ_0 [deg]
Voyager E	2.0	2.10	157.1 (1500 RPM)	9°
X-Cell	4.9	4.85	172.8 (1650 RPM)	5°
R-50	44	38.25	91.1 (870 RPM)	6.2°

The helicopter used in this project and other helicopters that are not equipped with a governor to maintain constant main rotor RPM, have a "throttle- and collective curve" programmed into the standard model helicopter transmitter. By moving the left-hand[2] collective stick forward, the pilot is commanding increased power to the engine and also increased main rotor collective pitch. In figure 2.1 the collective pitch angle and the engine throttle are plotted against the "throttle-collective" stick movement from zero to 100 %.

In the case of the electrically powered helicopter that was used, the thrust produced due to a fixed "throttle-collective stick" command decreases as the battery voltage decreases. Ideally a governor would be used to maintain the main rotor RPM. Due to the combined throttle and main rotor collective pitch angle controls, both the throttle and collective pitch angles are increased to keep the helicopter at the same altitude while the voltage of the batteries decreases. The increase in command deflection measured during a flight is roughly 10% of the total actuator movement.

2.3 Linear State Space Models

This section presents the linearised dynamic models that will be used in section 2.4.

[2]This helicopter radio gear has been set up to use "mode two": main rotor collective-engine throttle and tail rotor collective on the left hand, and pitch- and roll cyclic on the right hand.

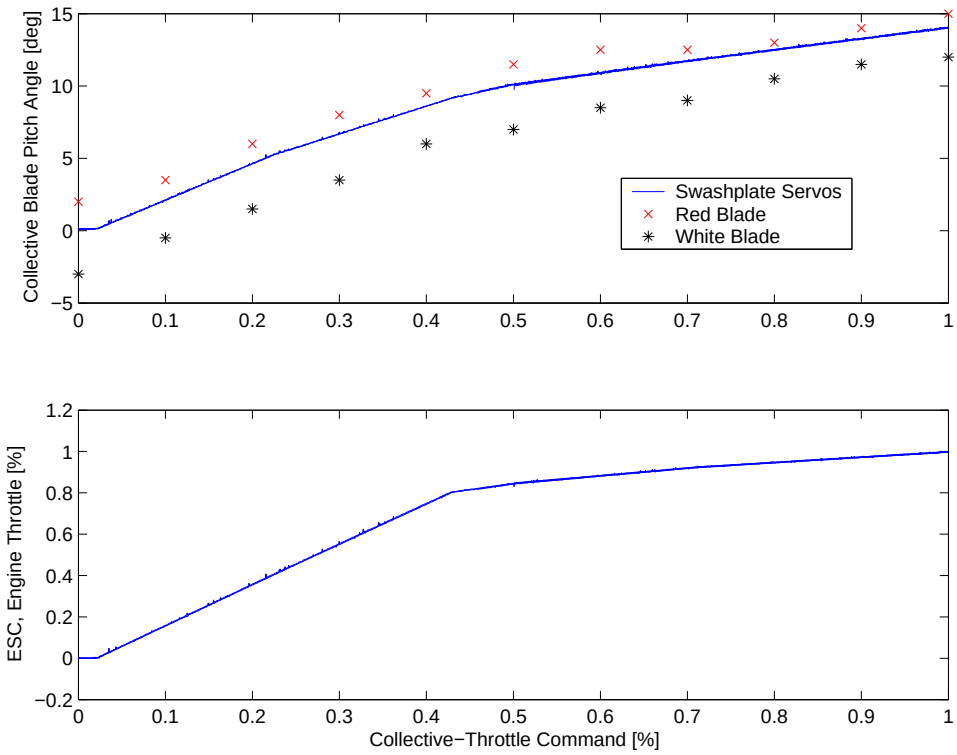

Figure 2.1: *Main rotor collective pitch angle and throttle vs "throttle-collective" input*

2.3.1 Eleven State Model

The eleven state model was the first model to be published by Mettler *et al.* [36]. The control and stability derivatives were identified for a Yamaha R-50 performing near-hover flight. The model did not include the flapping angles of the stabiliser bar in the state vector.

$$\begin{bmatrix} \dot{u} \\ \dot{v} \\ \dot{p} \\ \dot{q} \\ \dot{\phi} \\ \dot{\theta} \\ \dot{a_1} \\ \dot{b_1} \\ \dot{w} \\ \dot{r} \\ \dot{r_{fb}} \end{bmatrix} = \begin{bmatrix} X_u & 0 & 0 & 0 & 0 & -g & X_{a_1} & 0 & 0 & 0 & 0 \\ 0 & Y_v & 0 & 0 & g & 0 & 0 & Y_{b_1} & 0 & 0 & 0 \\ L_u & L_v & 0 & 0 & 0 & 0 & L_{a_1} & L_{b_1} & 0 & 0 & 0 \\ M_u & M_v & 0 & 0 & 0 & 0 & M_{a_1} & M_{b_1} & 0 & 0 & 0 \\ 0 & 0 & 1 & 0 & 0 & 0 & 0 & 0 & 0 & 0 & 0 \\ 0 & 0 & 0 & 1 & 0 & 0 & 0 & 0 & 0 & 0 & 0 \\ 0 & 0 & 0 & -1 & 0 & 0 & \frac{-1}{\tau_e} & 0 & 0 & 0 & 0 \\ 0 & 0 & -1 & 0 & 0 & 0 & B_{a_1} & \frac{-1}{\tau_e} & 0 & 0 & 0 \\ 0 & 0 & 0 & 0 & 0 & 0 & Z_{a_1} & Z_{b_1} & Z_w & Z_r & 0 \\ 0 & N_v & N_p & 0 & 0 & 0 & 0 & 0 & N_w & N_r & N_{rfb} \\ 0 & 0 & 0 & 0 & 0 & 0 & 0 & 0 & 0 & K_r & K_{rfb} \end{bmatrix} \begin{bmatrix} u \\ v \\ p \\ q \\ \phi \\ \theta \\ a_1 \\ b_1 \\ w \\ r \\ r_{fb} \end{bmatrix} + \begin{bmatrix} 0 & 0 & 0 & 0 \\ 0 & 0 & 0 & 0 \\ 0 & 0 & 0 & 0 \\ 0 & 0 & 0 & 0 \\ 0 & 0 & 0 & 0 \\ 0 & 0 & 0 & 0 \\ A_{\delta_a} & A_{\delta_b} & 0 & 0 \\ B_{\delta_a} & B_{\delta_b} & 0 & 0 \\ 0 & 0 & 0 & Z_{\delta_c} \\ 0 & 0 & N_{\delta_r} & N_{\delta_c} \\ 0 & 0 & 0 & 0 \end{bmatrix} \begin{bmatrix} \delta_a \\ \delta_b \\ \delta_r \\ \delta_c \end{bmatrix}$$

Shim [56] designed and implemented a number of controllers based on the eleven state model. Shim made use of a Yamaha R-50 and Kyosho Concept 60[3] helicopter. The control

[3]RC pilots typically refer to a "60 size" helicopter, which implies a helicopter that was designed to use a 0.6 cubic inch methanol motor.

and stability derivatives were identified for both the Concept 60 and the R-50. The work published by Shim *et al.* has proved to be a valuable reference during the development of this project. Table 2.2 presents the eigenvalues of the model identified by Shim for a Concept 60 helicopter. The model identified by Shim will be used in chapter 6.

Table 2.2: *Identified Eigen Values for a Concept 60 RC Helicopter*

-1.3195	Heave
$-6.2640 \pm 7.6859i$	Yaw
$-1.5261 \pm 15.8488i$	Roll
$-2.8241 \pm 14.1320i$	Pitch
$-0.0101 \pm 0.6021i$	Phugoid 1
$-0.0018 \pm 0.2443i$	Phugoid 2

2.3.2 Thirteen State Model

Mettler *et al.* [35] went on to use a thirteen state model to describe a Yamaha R-50 helicopter performing both near-hover ($\mu \approx 0$) and cruise flight ($\mu = 0.07$ to $\mu = 0.14$).

Two more state variables are introduced: the longitudinal (c) and lateral (d) flapping angles of the stabiliser bar. Mettler *et al.* acknowledge [37] that the flapping angles of the stabiliser bar are not required to be included as states in the model to fit flight data well. The motivation for adding the two states is that the new model gives better insight into the physical motion described by the model.

Mettler also included the stability derivatives L_w and M_w and control derivatives Y_{δ_r} and M_{δ_c}. The derivatives L_w and M_w are zero during hover and are therefore often absent in models used to describe near-hover flight.

$$\begin{bmatrix} \dot{u} \\ \dot{v} \\ \dot{p} \\ \dot{q} \\ \dot{\phi} \\ \dot{\theta} \\ \dot{a_1} \\ \dot{b_1} \\ \dot{w} \\ \dot{r} \\ \dot{r_{fb}} \\ \dot{c} \\ \dot{d} \end{bmatrix} = \begin{bmatrix} X_u & 0 & 0 & 0 & 0 & -g & X_{a_1} & 0 & 0 & 0 & 0 & 0 & 0 \\ 0 & Y_v & 0 & 0 & g & 0 & 0 & Y_{b_1} & 0 & 0 & 0 & 0 & 0 \\ L_u & L_v & 0 & 0 & 0 & 0 & 0 & L_{b_1} & L_w & 0 & 0 & 0 & 0 \\ M_u & M_v & 0 & 0 & 0 & 0 & M_{a_1} & 0 & M_w & 0 & 0 & 0 & 0 \\ 0 & 0 & 1 & 0 & 0 & 0 & 0 & 0 & 0 & 0 & 0 & 0 & 0 \\ 0 & 0 & 0 & 1 & 0 & 0 & 0 & 0 & 0 & 0 & 0 & 0 & 0 \\ 0 & 0 & 0 & -1 & 0 & 0 & \frac{-1}{\tau_{MR}} & A_{b_1} & 0 & 0 & 0 & A_c & 0 \\ 0 & 0 & -1 & 0 & 0 & 0 & B_{a_1} & \frac{-1}{\tau_{MR}} & 0 & 0 & 0 & 0 & B_d \\ 0 & 0 & 0 & 0 & 0 & 0 & Z_{a_1} & Z_{b_1} & Z_w & Z_r & 0 & 0 & 0 \\ 0 & N_v & N_p & 0 & 0 & 0 & 0 & 0 & N_w & N_r & N_{rfb} & 0 & 0 \\ 0 & 0 & 0 & 0 & 0 & 0 & 0 & 0 & 0 & K_r & K_{rfb} & 0 & 0 \\ 0 & 0 & 0 & -1 & 0 & 0 & 0 & 0 & 0 & 0 & 0 & \frac{-1}{\tau_{SB}} & 0 \\ 0 & 0 & -1 & 0 & 0 & 0 & 0 & 0 & 0 & 0 & 0 & 0 & \frac{-1}{\tau_{SB}} \end{bmatrix} \begin{bmatrix} u \\ v \\ p \\ q \\ \phi \\ \theta \\ a_1 \\ b_1 \\ w \\ r \\ r_{fb} \\ c \\ d \end{bmatrix} + \begin{bmatrix} 0 & 0 & 0 & 0 \\ 0 & 0 & Y_{\delta_r} & 0 \\ 0 & 0 & 0 & 0 \\ 0 & 0 & 0 & M_{\delta_c} \\ 0 & 0 & 0 & 0 \\ 0 & 0 & 0 & 0 \\ A_{\delta_a} & A_{\delta_b} & 0 & 0 \\ B_{\delta_a} & B_{\delta_b} & 0 & 0 \\ 0 & 0 & 0 & Z_{\delta_c} \\ 0 & 0 & N_{\delta_r} & N_{\delta_c} \\ 0 & 0 & 0 & 0 \\ 0 & C_{\delta_b} & 0 & 0 \\ D_{\delta_a} & 0 & 0 & 0 \end{bmatrix} \begin{bmatrix} \delta_a \\ \delta_b \\ \delta_r \\ \delta_c \end{bmatrix}$$

2.3.3 Longitudinal-Vertical/Lateral-Directional Model

It is common to decouple the dynamics of fixed-wing aircraft into simpler longitudinal-vertical and lateral-directional models. The linear models presented by Gavrilets *et al.* [19, 20] are similar to the eleven and thirteen state models as provided in subsections 2.3.1 and 2.3.2. The only major difference is that the models have been broken up to describe longitudinal-vertical and lateral-directional motion, with some cross-coupling terms having been neglected. The focus of these publications has been to describe a model helicopter performing aggressive manoeuvres.

> *"Based on flight experiments, longitudinal-vertical and lateral-directional dynamics of the X-Cell in low advance ratio flight (up to $\mu = 0.15$) are sufficiently decoupled to design separate feedback controllers"* - Gavrilets *et al.* [20].

The state and control vectors for the longitudinal-vertical model are:

$$\mathbf{x}_{long-vert} = \begin{bmatrix} u & a_1 & q & w & \theta \end{bmatrix}^T \tag{2.2}$$

$$\delta_{long-vert} = \begin{bmatrix} \delta_b & \delta_c \end{bmatrix}^T \tag{2.3}$$

and

$$\mathbf{x}_{lat-direc} = \begin{bmatrix} v & b_1 & p & r & \phi \end{bmatrix}^T \tag{2.4}$$

$$\delta_{lat-direc} = \begin{bmatrix} \delta_a & \delta_r \end{bmatrix}^T \tag{2.5}$$

for the lateral-directional model. The two models obtained in this way neglect coupling between pitch and roll motions (including the motion of the main rotor and Bell-Hiller stabiliser bar), as well as heave and lateral/yaw motion.

2.4 Linear, Decoupled Models

In this section the linear eleventh order model will be decomposed into lower order models describing vertical, directional, longitudinal and lateral motion. Although the eleventh order model will still be used during some simulations, the decoupled subsystems will later be used to design some of the control laws and provide an understanding of the fundamental motion of a model helicopter performing near-hover flight.

2.4.1 Heave Dynamics

In their eleven state model Mettler *et al.* [37] make use of the follow set of equations to describe the heave dynamics of a model helicopter:

$$\dot{w} = Z_{a_1}a_1 + Z_{b_1}b_1 + Z_w w + Z_r r + Z_{\delta_c}\delta_c \tag{2.6}$$

$$\dot{z} = w \tag{2.7}$$

They have identified the parameters through rigorous system identification using high quality sensors. From the eleven state model it can be seen that if a collective-throttle command is applied, it will only affect the climb rate (w) and the yaw rate (r) directly. The influence of the collective command on the yaw is one of the primary reasons why model helicopters are equipped with active yaw rate damping subsystems.

Mettler *et al.* [37] proceed by stating that a first-order system model adequately describes the heave dynamics of a RC helicopter performing near-hover manoeuvres:

$$\dot{w} = Z_w w + Z_{\delta_c}\delta_c \tag{2.8}$$

$$\dot{z} = w \tag{2.9}$$

The heave damping derivative (Z_w) is derived by Padfield [47] to be:

$$Z_w = \frac{2aA_b\rho(\Omega R)\lambda_i}{(16\lambda_i + a_0\sigma)M_a} \tag{2.10}$$

where A_b is the blade area and σ the ratio of blade area to disc area (solidity ratio). This expression was not derived specifically for RC helicopters, but the results obtained using it were compared with the identified heave damping derivative of other model helicopters. The results obtained are presented in table 2.3. Since no measurement of the main rotor rotation speed or collective pitch angles of the Voyager E were available, nominal, near-hover values were assumed.

Table 2.3: *Identified vs Predicted heave damping derivatives (Z_w) for RC helicopters*

Helicopter	Identified	Calculated
Voyager E	-1.10	-0.98
Concept 60	-1.35 [54]	-1.16
R-50	-0.61 [37]	-0.64

The identified value of Z_w in table 2.3 for the JR Voyager E was obtained through "curve fitting". A step command was applied to the collective-throttle control channel (see figure 2.2). An 8 % (of full deflection) command was applied to the control channel. The Matlab GUI Curve Fitting Tool (`cftool`) was used to identify the value of Z_w. Through a steady state analysis Z_{δ_c} was calculated to be between 12 and 15.

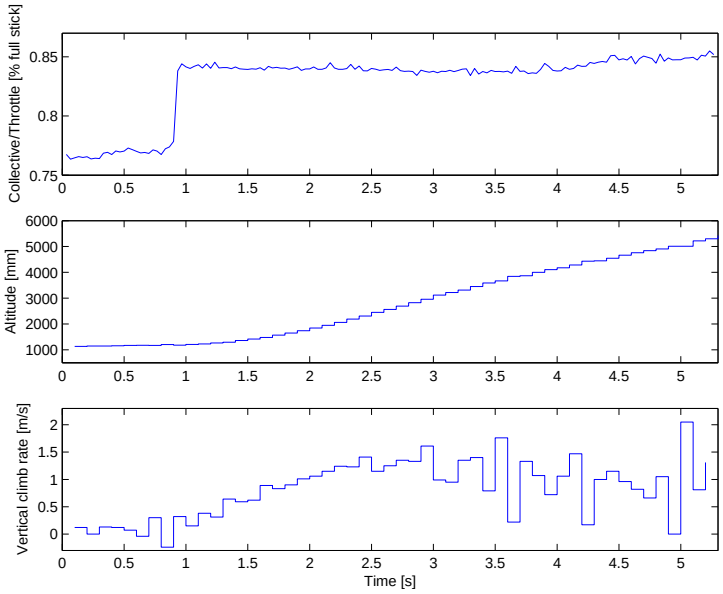

Figure 2.2: *Step command on collective-throttle control channel*

In equation 2.8 the assumption is made that the main rotor rotation rate is kept constant under increasing and decreasing loads on the main and tail rotor blades. As mentioned in section 2.2, this will not be the case if there is no controller regulating the rotation rate, especially not in the case of an electrically powered helicopter of which the battery voltage drops during the flight.

Identification of the heave parameters is complicated by noisy measurements at low update rates. No negative step commands were applied due to the risks involved in such tests. The helicopter lacks power to stop an aggressive descent and therefore it was decided not to perform negative step command experiments.

2.4.2 Yaw Dynamics

It is a challenging task to describe the yaw rate response of a model helicopter. The air flow over the tail rotor varies drastically over the flight envelope of the helicopter. The response of the tail rotor is coupled to the main rotor via the driving system. Furthermore, even if only near-hover manoeuvres are considered, yaw rate damping is provided by an

ill-identified yaw rate stability augmentation system. The command signal from the pilot is fed through this electronic subsystem to the trail rotor collective pitch servo. The yaw rate feedback system can be operated in "heading hold" or "rate damping" mode. For the purposes of this project it was set up to damp the yaw rate.

The yaw dynamics are described as follows in the eleventh order state space model in section 2.3.1:

$$\dot{r} = N_v v + N_p p + N_w w + N_r r + N_{r_{fb}} r_{fb} + N_{\delta_c} \delta_c + N_{\delta_r} \delta_r \tag{2.11}$$

$$\dot{r_{fb}} = K_r r + K_{r_{fb}} r_{fb} \tag{2.12}$$

The dominant response to tail rotor collective pitch perturbations is described using the following model [36]:

$$\dot{r} = N_r r + N_{r_{fb}} r_{fb} + N_{\delta_r} \delta_r \tag{2.13}$$

$$\dot{r_{fb}} = K_r r + K_{r_{fb}} r_{fb} \tag{2.14}$$

with $K_{r_{fb}}$, N_r and $N_{r_{fb}}$ identified as negative values.

Due to the active yaw rate damping subsystem, the yaw dynamic response of the helicopter is slow and stable. Furthermore, the heading of the helicopter can be measured accurately and does not need to be controlled to within less than $\pm 10^\circ$ since the stability of the helicopter is not dependant on the heading [41]. Controlling the heading during hover has proved to be simple compared to the other degrees of freedom.

2.4.3 Pitch and Roll Dynamics

According to Mettler *et al.* [37] the dynamics of a small-scale rotorcraft are governed by the first-order effects: *"In particular, the rotor forces and moments clearly dominate the vehicle dynamics, as demonstrated by the distinctly second-order characteristic of the roll and pitch dynamics"*.

Gavrilets *et al.* [18] agree that first order models of the tip-path-plane flapping dynamics are sufficient for control system design. Describing the fundamental pitch and roll dynamics of the RC helicopter requires two steps:

1. describing the flapping of the rotor blades (a_1, b_1) which is dominated by the response of the stabiliser bar, and

2. describing the pitch and roll rate of the helicopter (q, p) in response to the flapping of the blades.

Mettler *et al.* [36] proposed the following model to describe the the angular rate dynamics and the blade flapping of a R-50 helicopter:

$$\dot{b_1} = -\frac{b_1}{\tau_e} - p + B_{a_1}a_1 + B_{\delta_a}\delta_a + B_{\delta_b}\delta_b \tag{2.15}$$

$$\dot{a_1} = -\frac{a_1}{\tau_e} - q + A_{b_1}b_1 + A_{\delta_a}\delta_a + A_{\delta_b}\delta_b \tag{2.16}$$

$$\dot{p} = L_u u + L_v v + L_{b_1}b_1 + L_{a_1}a_1 \tag{2.17}$$

$$\dot{q} = M_u u + M_v v + M_{b_1}b_1 + M_{a_1}a_1 \tag{2.18}$$

In [37], and subsequent articles, Mettler neglects M_{b_1} and L_{a_1}.

The main rotor blade time constant (τ_{MR}) is much smaller than the time constant of the stabiliser bar (τ_{SB}). In the thirteen state model that includes the flapping angle of the stabiliser bar, a distinction is made between τ_{MR} and τ_{SB}, but in the eleven state model, only the effective time constant (τ_e), that is approximately equal to the stabiliser bar time constant, is used.

Gavrilets *et al.* [18] and Mettler *et al.* [33] argue that since there is almost an order of magnitude difference between the cross-coupling derivatives $(A_{b_1}, B_{a_1}, A_{\delta_a}, B_{\delta_b})$ and the direct derivatives $(A_{a_1}, B_{b_1}, A_{\delta_b}, B_{\delta_a})$ of their X-Cell, the cross-coupling derivatives can be neglected. The stability derivatives L_w and M_w are zero near hover. It is assumed that the longitudinal and lateral velocities can be modelled and controlled independently, as was assumed by Gavrilets *et al.* [19, 20]. The model reduces to

$$\dot{b_1} = -\frac{b_1}{\tau_e} - p + B_{\delta_a}\delta_a \tag{2.19}$$

$$\dot{a_1} = -\frac{a_1}{\tau_e} - q + A_{\delta_b}\delta_b \tag{2.20}$$

$$\dot{p} = L_v v + L_{b_1}b_1 \tag{2.21}$$

$$\dot{q} = M_u u + M_{a_1}a_1 \tag{2.22}$$

for near-hover flight, which yields the second order, lightly damped transfer function from cyclic input to body angular rotation [18, 34]:

$$\frac{q}{\delta_b} \approx \frac{A_{\delta_b}\omega_{nq}^2}{s^2 + s/\tau_e + \omega_{nq}^2} \tag{2.23}$$

$$\frac{p}{\delta_a} \approx \frac{B_{\delta_a}\omega_{np}^2}{s^2 + s/\tau_e + \omega_{np}^2} \tag{2.24}$$

with

$$\omega_{nq}^2 = M_{a_1} = \frac{Th_{MR} + K_\beta}{I_{yy}} \tag{2.25}$$

$$\omega_{np}^2 = L_{b_1} = \frac{Th_{MR} + K_\beta}{I_{xx}} \tag{2.26}$$

The thrust produced by the main rotor (T) is approximately equal to the weight of the helicopter (mg) during hover and near-hover flight. If the location of the CG is known, then the distance between the rotors and CG (h_{MR}) can be measured. The moments of inertia can be estimated or measured. The hub torsional stiffness (K_β) is the only parameter remaining and can be calculated from the above.

The natural frequencies can be identified by analysing the recorded step response of the second order systems. Figure 2.3 presents an example of a step command that was applied to the longitudinal cyclic input of the Voyager E. The damping ratio $\zeta = 0.086$ and a natural frequency $\omega_n = 18.4\,\text{rad/s}$ was identified using the Matlab "Curve Fitting Tool".

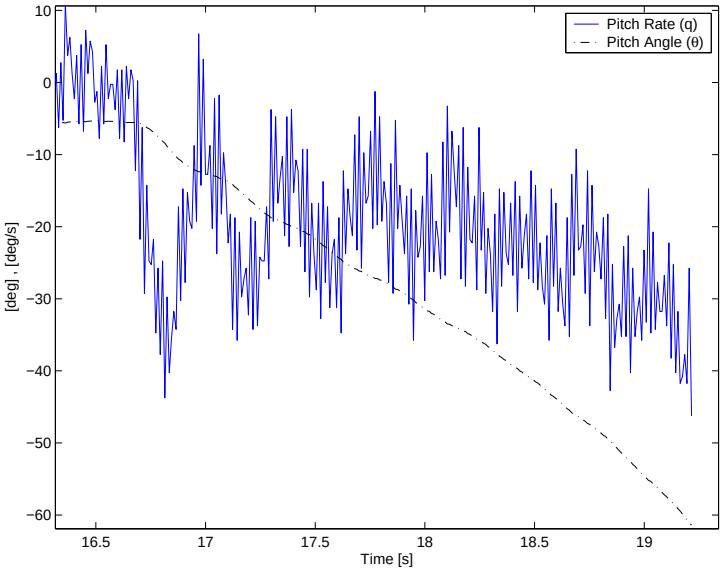

Figure 2.3: *Step command on longitudinal cyclic input*

The Yamaha R-50 has a teetering hinge and an independent blade flapping hinge for each blade [33], while the X-Cell, Concept 60 and Voyager E have unhinged teetering heads - as is typically found on standard RC model helicopters.

Table 2.4 gives the natural frequencies and damping ratios for different helicopters calculated from their respective linear, identified models. The models were identified by various authors using instrumented helicopters and therefore the parameters describe the

dynamics of the various instrumented helicopters. The values were calculated [35, 37] from equations 2.25, 2.26 and

$$1/\tau_e \approx 2\zeta_q\omega_{nq} \tag{2.27}$$

$$1/\tau_e \approx 2\zeta_p\omega_{np} \tag{2.28}$$

The identified values for the Voyager E are also included in table 2.4. It can be seen from the table that the damping ratio is lower for the roll rate response than the pitch rate response. The pitch rate frequency is also lower than the roll rate natural frequency. These two properties can be attributed to the higher pitching moment of inertia (I_{yy}) compared to the rolling moment of inertia (I_{xx}). The identified pitch rate damping for the Voyager E is the lowest, while the pitch rate natural frequency is the highest of all of the helicopters.

Table 2.4: *Identified pitch and roll rate natural frequencies and damping ratios for different helicopters*

Helicopter	ω_{nq} [rad/s]	ζ_q	ω_{np} [rad/s]	ζ_p	τ_e [s]
R-50 [36]	8.3	0.20	11.9	0.14	0.30
X-Cell [18]	14.6	0.25	20.1	0.18	0.13
Concept 60 [54]	14.8	0.15	15.4	0.14	0.23
Voyager E	18.4	0.09	n.a.	n.a.	0.09

Unfortunately the experiment that yielded figure 2.3 led to a crash and severe damage to the Voyager E helicopter. Care must be taken not to apply too large pitch rate step commands for too long.

Bell-Hiller Stabiliser Bar

The Bell-Hiller stabiliser bar, integrated into the control mechanisms of almost all RC helicopters, performs two functions:

- increases the effective time constant of the main rotor, and
- reduces the control forces that have to be applied by the servos [33].

From [37] the response time of the main and servo rotors can be calculated using

$$\tau = \frac{16}{\gamma\Omega} \tag{2.29}$$

where the non-dimensional Lock number γ is defined by

$$\gamma = \frac{\rho c a \left(R^4 - r^4\right)}{I_b}. \tag{2.30}$$

The Lock number is a scaling coefficient describing the ratio of aerodynamic to inertial forces acting on a rotor blade [47].

Munzinger [40] calculated the linear lift curve slope (a) as a function of the blade aspect ratio (AR) using

$$a = \frac{2\pi}{1 + \frac{2}{AR}} \tag{2.31}$$

with

$$AR = \frac{l_{SB}^2}{l_b c_{SB}}. \tag{2.32}$$

Table 2.5 provides a summary of the dynamic properties of the servo rotors for a R-50, X-Cell and Voyager E helicopter (assuming use of standard size and weight flybar and paddles for the respective helicopters).

Table 2.5: *Stabiliser bar parameters and theoretical time constants*

	R-50	X-Cell	Voyager E	Units
flybar length (l_{SB})	1.130	0.450	0.440	[m]
flybar weight	n.a.	0.0419	0.0231	[kg]
paddle chord (c_{SB})	0.100	0.050	0.039	[m]
paddle length (l_b)	0.150	0.075	0.070	[m]
paddle weight	n.a.	0.0198	0.0099	[kg]
moment of inertia (I_b)	n.a.	0.959e-3	0.479e-3	[kg.m^2]
SB Lock number (γ)	n.a.	0.6919	0.997	-
SB time constant (τ_{SB})	0.3021	0.1352	0.094	[s]

The time constants are dependant, among others, on the rotor blade speed, the exact size, weight and distribution of components and instrumentation, and the density of the air in which the helicopter is flying. Consequently, the numbers published by different research groups will differ, even though the same type of helicopter was used.

The theoretically predicted time constants are presented in table 2.5. Gavrilets *et al.* [18] make use of equation 2.30 without corrections from [47] to describe the X-Cell SE platform being used at MIT. The Lock number is calculated to be ≈ 0.8, and the corresponding settling time is 0.144 s. Given the available information, the author calculated a

$\tau_{SB} = 0.1352\,\text{s}$ for a standard X-Cell. Shim [56] published the time constant of their R-50 (Ursa Mangna 2) to be $\tau_{SB} = 0.29\,\text{s}$, while Mettler *et al.* published a value of $\tau_{SB} = 0.36\,\text{s}$ for their R-50. The τ_{SB} of the Voyager E was calculated to be 0.094 s. Although slightly faster than the predicted and measured time constants for the X-Cell and Concept 60, the time constant of the stabiliser bar of the Voyager E is in line with the values for the bigger glow powered helicopter.

The above equations explain why pilots use heavy stabiliser bar paddles when they participate in competitions that require slow, accurate movements. The higher the inertia of the stabiliser bar, the larger the time constant of the stabiliser bar (and consequently the pitch and roll dynamics).

2.4.4 Horizontal Velocity Dynamics

The influence of wind (both constant and gusts) will be ignored in this analysis since the safety pilot struggles to fly the helicopter in wind speeds exceeding 10 km/h. The Voyager E helicopter is small and responds fast and violently to wind gusts. Larger glow and gasoline powered helicopters are less responsive to wind disturbances.

Mettler *et al.* [37] present the following linearised model for the horizontal velocity dynamics:

$$\dot{u} = X_u u - g\theta + X_{a_1} a_1 \tag{2.33}$$

$$\dot{v} = Y_v v + g\phi + Y_{b_1} b_1 + Y_{\delta_r} \delta_r \tag{2.34}$$

with a_1 and b_1 the longitudinal and lateral rotor flapping angles, $X_u = -0.05$, $Y_v = -0.15$, $-X_{a_1} = Y_{b_1} = g$ and $Y_{\delta_r} = 11.23$ identified for a R-50 model helicopter.

Assuming the helicopter is kept near hover, the changes in tail rotor collective and engine RPM are small and the lateral acceleration due to the tail rotor can be ignored [36]. Equations 2.33 and 2.34 can be simplified to

$$\dot{u} = X_u u - g(\theta + a_1) = X_u u - g(\theta_{TPP}) \tag{2.35}$$

$$\dot{v} = Y_v v + g(\phi + b_1) = Y_v v + g(\phi_{TPP}) \tag{2.36}$$

Shim *et al.* [55] made use of equations 2.35 and 2.36 to model their 0.60 cubic inch Concept 60 helicopter.

The velocities and body rates can be measured, but one problem remains: it is very difficult to measure the flapping angle between the body of the helicopter and the rotor

blades. It is not trivial estimating this angle either (even though this angle is strongly dependant on pilot commands).

Christoph Eck presents a simplified model in his thesis [15]. The helicopter frame and blades are approximated as a rigid body:

$$\dot{u} = X_\theta \theta \approx -g\theta \tag{2.37}$$

$$\dot{v} = Y_\phi \phi \approx g\phi \tag{2.38}$$

for small values of θ and ϕ.

Equations 2.37 and 2.38 were used to design the pitch and roll attitude and velocity estimators. These estimators have been tested on post flight data and in realtime. It has proved to be sufficiently accurate to control the helicopter near hover.

2.5 Conclusion

The nonlinear equations describing the motion of RC helicopters is a field of research that has received limited attention [19]. The complications introduced by the addition of a stabilizer bar, the stiffness of the rotor head, and the large ratio of control forces and moments to mass, distinguish model helicopters from their bigger counterparts.

This chapter has provided an overview of the models that have been used to describe the response of model helicopters performing near-hover manoeuvres. Extensive work has been invested in the identification of helicopters such as the Yamaha R-50, Miniature Aircraft X-Cell and Kyosho Concept 60.

The parameters of the JR Voyager E that were identified through curve fitting and theoretical prediction were presented and compared to the identified and predicted values of the other helicopters.

Since the ultimate goal of the project is to develop a basic, low closed loop bandwidth FCS, a highly accurate model is not required. It is important to understand the fundamental dynamics and the potential risks.

Chapter 3

State Measurement and Estimation

To be able to control a vehicle, information about the states of the vehicle is required. In some cases the states can be measured directly to a sufficient level of accuracy using one or more sensors, but this is not always possible. It might be physically impossible to measure the state, or the noise on a single sensor might be too high, or the update rate too low. If a model of the plant exists, it might be possible to estimate the state using one or more sensors. In some applications the measurements from multiple sensors can be used to estimate a state more accurately than a single sensor can measure the state.

Three sets of states are required to control a RC helicopter successfully: attitude, velocity and position. Altitude and heading are fairly simple to measure during near-hover flight. A number of sensors exist to measure velocity and position.

Measuring pitch and roll angles is more difficult since high bandwidth, high resolution estimates are required to keep the helicopter stationary. Measuring the attitude of the vehicle is the primary focus of this chapter. The estimators and filtering techniques used will be described. Some of the techniques used by other institutions will also be investigated. The acquired hardware will be described in chapter 4.

State estimation and measurement is arguably the most important and complex section of the problem - especially for projects that aim to provide a solution at the lowest possible cost.

3.1 Altitude

Feron *et al.* [21, 58] describe using a barometric pressure sensor to measure altitude. This sensor is not commonly used to measure the altitude of a RC helicopter due to

the difficulty to obtain sufficient resolution, and distortion of the measurement in ground effect. The helicopter used by Feron *et al.* has been instrumented to perform aggressive aerobatic manoeuvres.

The University of Queensland and CSIRO have successfully employed a stereo camera system to measure altitude very effectively [12].

A GPS receiver is capable of measuring three dimensional position and can therefore be used to measure the altitude of a helicopter. Low cost commercial GPS receivers are notorious for poor altitude measurements. A differential GPS offers high accuracy measurements at high update rates. A number of teams competing in the IARC used a complementary filter to fuse the data from their NovAtel DGPS with the readings from an ultrasonic sensor or laser range finder. Amidi [1] makes use of a laser rangefinder to measure altitude at 20 Hz.

Although ultrasonic range sensors are very susceptible to vibrations, the sensors have been used successfully as altitude sensors [28]. The author also made use of an ultrasonic sensor to measure altitude. The sensor is simple to use, reliable (if mounted correctly) and light. An indication of climb rate can be obtained using the difference between consecutive measurements. The hardware used will be discussed in more detail in section 4.4.2.

3.2 Heading

One of the properties of a helicopter that distinguishes it from a conventional fixed-wing aircraft is its ability to change its heading when stationary. In the absence of a cross-wind, the heading of a fixed wing aircraft flying straight and level can be measured by merely measuring the direction of the velocity using a GPS receiver. Not only can a helicopter change direction while remaining stationary, it can also fly sideways without any forward speed. It is thus essential to be able to measure the heading of a helicopter.

It is possible to measure the complete attitude (pitch, roll and yaw angles) of a vehicle using only carrier phase GPS. Conway [11] used this technique to demonstrate the first fully autonomous RC helicopter flight in 1996. It is a novel technique and not a cheap COTS solution.

The heading of a vehicle can be calculated through measurement of the magnetic field of the earth. If the pitch and roll angles of the vehicle are known, the heading of the vehicle can be calculated accurately from the measurements of a three-axis magnetometer. A number of factors that complicate the determination of heading include magnetic

inclination, magnetic declination, hard and soft iron effects.

A three axis magnetometer was used to measure the magnetic field of the earth at a 10 Hz update rate.

3.3 Pitch and Roll Angles

Although it is theoretically possible to measure the attitude of a body using only rate gyroscopes (given that the initial orientation of the body is known), rate gyroscopes capable of measuring attitude to a high degree of accuracy over an extended period of time are very expensive. Errors in the orientation solution accumulate due to bias drift, random walk, numerical integration errors and other noise factors, making it impossible in practice to determine the attitude of a RC helicopter using only low cost rate gyroscopes.

The quality of affordable, small, low cost rate gyroscopes has been increasing significantly during the last few years. Rate gyroscope sensors are capable of providing good high frequency attitude rate measurements, but measurements from additional sensors are required to ensure low frequency stability and accuracy. A number of absolute pitch and roll attitude determination systems exist:

- sensing the orientation of the horizon using a camera [16] or IR detector system [61] (assuming the horizon is visible and horizontal),
- identifying a known pattern [53] (markings or an array of lights) and
- multi-antenna GPS attitude determination [11].

The last two of these attitude determination systems can also be used to determine velocity and position and offer good solutions for landing and take-off.

3.3.1 Integrated GPS and INS

In an age where processing power is constantly decreasing in price and weight, full state estimators (estimating attitude, acceleration, velocity, position, gravity vector and sensor biases simultaneously) are becoming increasingly popular and practical to implement. No knowledge about the dynamics of the vehicle is required and no simplifying assumptions need to be made about sensor properties. The price being paid to obtain these attractive qualities is that these filters are:

- computationally demanding,
- complex and
- a number of fair quality, accurately mounted sensors are required to obtain high quality estimates.

The majority of RUAV research projects are making use of high (twelve to seventeen) state Extended Kalman filters to combine accurate DGPS measurements and high quality rate gyroscopes measurements. These filters require powerful processors. Examples of these estimators can be found in [15, 48, 51, 65]. Aaron Kahn has also made an example available through a Sourceforge project [26].

3.3.2 Accelerometer Measurements

It is common practice to use measurements from accelerometers to calculate the pitch and roll angles of a stationary object. However, as soon as the unit is accelerating, more information is required to estimate the attitude of the vehicle correctly.

> "*Accelerometers, however, are unable to separate the total acceleration with respect to inertial space, from that caused by the presence of a gravitational field. These sensors do in fact provide measurements of the difference between the true acceleration in space and the acceleration due to gravity. This quantity is the non-gravitational force per unit mass exerted on the instrument, referred to in this text for brevity as specific force*" - Titterton [62].

Accelerometers typically contain a small proof mass, supported by a spring or flexure. Deflection of the mass is measured to determine the force applied to the proof mass. Accelerometers thus measure the specific force - the force applied to a unit mass. Other accelerometers implementations can be shown to measure the same parameter.

If we ignore the rotation rate of the earth, and assume low velocities, the relationship between acceleration, specific force and gravitational acceleration can mathematically be described as follows [48, 62]:

$$\begin{bmatrix} \ddot{x}_N \\ \ddot{x}_E \\ \ddot{x}_D \end{bmatrix} = C_b^n \begin{bmatrix} a_x \\ a_y \\ a_z \end{bmatrix} + \begin{bmatrix} 0 \\ 0 \\ g \end{bmatrix} \tag{3.1}$$

with C_b^n the Direction Cosine Matrix to transform the specific force measurements (a_x, a_y, a_z) from body reference frame to navigation reference frame, and $\ddot{x}_N$, $\ddot{x}_E$ and $\ddot{x}_D$ the true accelerations of the vehicle.

Thus if the position (double integral of $\ddot{\mathbf{x}}$) of an object is bounded within a limited area, the average of its acceleration is near zero and therefore the average direction of the specific force must equal the gravity vector, which is vertical.

Kingston *et al.* [30] describe an algorithm to estimate the attitude of a fixed-wing aircraft using only a set of accelerometers, three low cost rate gyroscopes and a low cost GPS. It is assumed that the heading of the aircraft can be calculated using only the GPS velocity measurement. Crosswinds are assumed small relative to the longitudinal velocity. Alternatively a three axis magnetometer can be added to the sensor array to estimate the heading of the vehicle. The magnetometer hardware increases the complexity and requires additional calibrated hardware. The algorithm of Kingston *et al.* is an example of an attitude determination algorithm, making use of the measurements from accelerometers to determine the attitude of a vehicle without assuming that accelerometers measure only forces opposing gravity acceleration.

From this section it can be concluded that accelerometers are valuable sensors to assist in solving the attitude determination problem. However, additional sensors are required to determine the attitude of an accelerating body.

3.3.3 Simple Complementary Filters

A number of articles have been published [3, 5, 26, 41, 58] describing complementary filtering techniques that have been used to combine the low frequency accelerometer measurements with high frequency rate gyroscope measurements to obtain pitch and roll angle state estimates - specifically for helicopter control. The most extreme example is the MIT helicopter performing aerobatic manoeuvres using a simple complementary filter.

MIT Complementary Filter

The inertial measurement unit used by MIT is a very high quality unit compared to the sensors used in this and other projects like those of CSIRO [52], Technical University of Berlin (MARVIN) [42] and Rotomotion [26]. The rate gyroscopes used by MIT feature bias drift rates of an order of magnitude lower than the bias drift rates of the best small, low cost MEMS rate gyroscopes currently available.

The filter is presented to illustrate how accelerometer measurements can be used to aid in calculation of pitch and roll angles, especially if high quality rate gyroscopes are used in conjunction with the accelerometers. Accelerometers can even be used to aid in estimating the attitude of a helicopter performing very aggressive manoeuvres if the quality of the rate gyroscopes is high enough. The filter design is based on an example by McRuer *et al.* "Aircraft Dynamics and Automatic Control" [32] and presented by Sprague *et al.* from MIT [58].

First, the estimation of the pitch angle $(\hat{\theta})$[1] will be investigated. Let us assume that sensors exist that can measure the pitch angle and the pitch rate of a vehicle. The rate sensor's measurements only contain good high frequency information. The angle sensor provides measurements of the absolute angle, but has a limited bandwidth.

In the complementary filter the angle measurements are low-pass filtered to obtain θ_{LF}. The angular rate measurements are integrated and high-pass filtered to obtain θ_{HF}. The estimated pitch angle is obtained through summation of θ_{LF} and θ_{HF} (see the block diagram in figure 3.1).

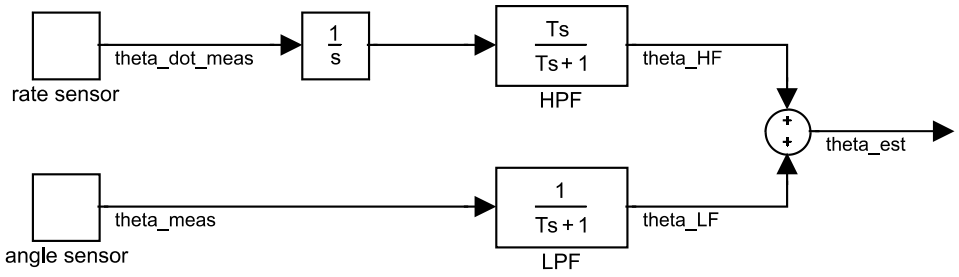

Figure 3.1: *Complementary filter for estimation of the body pitch angle*

Let us call the rate measurement $\dot{\theta}_{meas}$ while the pitch angle measurement is referred to as θ_{meas}. From the block diagram:

$$\theta_{HF} = \dot{\theta}_{meas}\left(\frac{1}{s}\right)\left(\frac{s\tau_a}{s\tau_a + 1}\right) \tag{3.2}$$

with τ_a the filter time constant. $\dot{\theta}_{HF}$ can thus be expressed as:

$$\dot{\theta}_{HF} = \frac{-1}{\tau_a}\theta_{HF} + \dot{\theta}_{meas} \tag{3.3}$$

[1]Estimates are indicated using a hat.

In a similar fashion, from the block diagram we find θ_{LF}:

$$\theta_{LF} = \theta_{meas}\left(\frac{1}{s\tau_a + 1}\right) \tag{3.4}$$

$$\Rightarrow \dot{\theta}_{LF} = \frac{-1}{\tau_a}\theta_{LF} + \frac{1}{\tau_a}\theta_{meas} \tag{3.5}$$

Exactly the same procedure can be used to calculate $\dot{\phi}_{LF}$ and $\dot{\phi}_{HF}$ from the roll rate sensor ($\dot{\phi}_{meas}$) and the measured roll angle (ϕ_{meas}), giving:

$$\dot{\phi}_{HF} = \frac{-1}{\tau_a}\phi_{HF} + \dot{\phi}_{meas} \tag{3.6}$$

$$\dot{\phi}_{LF} = \frac{-1}{\tau_a}\phi_{LF} + \frac{1}{\tau_a}\phi_{meas} \tag{3.7}$$

One problem still needs to be solved: finding sensors that are capable of measuring the pitch and roll angles and rates. Knowing that the filter is used to combine rate gyroscope measurements and accelerometer measurements to estimate pitch and roll angles, we turn our attention to some useful facts. For a non-accelerating vehicle

$$\phi_{meas} = arctan(\frac{a_y}{a_z}) \tag{3.8}$$

$$\theta_{meas} = arctan(-\frac{a_x}{a_z}\cos\phi) \tag{3.9}$$

From [51, 62]:

$$\dot{\phi} = p + \tan\theta(q\sin\phi + r\cos\phi) \tag{3.10}$$

$$\dot{\theta} = q\cos\phi - r\sin\phi \tag{3.11}$$

which yields

$$\dot{\phi}_{meas} = p_{meas} + \tan\hat{\theta}(q_{meas}\sin\hat{\phi} + r_{meas}\cos\hat{\phi}) \tag{3.12}$$

$$\dot{\theta}_{meas} = q_{meas}\cos\hat{\phi} - r_{meas}\sin\hat{\phi} \tag{3.13}$$

It would be better to use the estimated angles in equations 3.12 and 3.13 to calculate the angular rates. The estimates would yield more accurate results than the raw measurements. Substitution of 3.12 in 3.6, 3.13 in 3.3, 3.8 in 3.7 and 3.9 in 3.5, results in the equations published in [58]:

$$\dot{\phi}_{HF} = -\frac{1}{\tau_a}\phi_{HF} + p_{meas} + \tan\hat{\theta}(q_{meas}\sin\hat{\phi} + r_{meas}\cos\hat{\phi}) \tag{3.14}$$

$$\dot{\theta}_{HF} = -\frac{1}{\tau_a}\theta_{HF} + q_{meas}\cos\hat{\phi} - r_{meas}\sin\hat{\phi} \tag{3.15}$$

$$\dot{\phi}_{LF} = -\frac{1}{\tau_a}\phi_{LF} + \frac{1}{\tau_a}\arctan\left(\frac{a_y}{a_z}\right) \tag{3.16}$$

$$\dot{\theta}_{LF} = -\frac{1}{\tau_a}\theta_{LF} + \frac{1}{\tau_a}\arctan\left(-\frac{a_x}{a_z}\cos\hat{\phi}\right) \tag{3.17}$$

with

$$\hat{\dot{\phi}} = \dot{\phi}_{HF} + \dot{\phi}_{LF} \tag{3.18}$$

$$\hat{\dot{\theta}} = \dot{\theta}_{HF} + \dot{\theta}_{LF} \tag{3.19}$$

Now let us inspect the influence of noisy measurements, accelerations and non-ideal sensors on the performance of the filter. For simplicity, consider the zero roll angle case ($\phi = 0$), which simplifies the pitch angle estimate to:

$$\dot{\theta}_{HF} = -\frac{1}{\tau_a}\theta_{HF} + q_{meas} \tag{3.20}$$

$$\dot{\theta}_{LF} = -\frac{1}{\tau_a}\theta_{LF} + \frac{1}{\tau_a}\arctan\left(-\frac{a_x}{a_z}\right) \tag{3.21}$$

In the analysis below the bias drift on rate gyroscopes is included. Since the term $\arctan\left(-\frac{a_x}{a_z}\right)$ only equals θ when the body is not accelerating [30], any accelerations are regarded as high frequency perturbations and represented by the symbol θ_p. The rate gyroscope has a bias output (b_{gyro}) for zero physical rate. The accelerometers and rate gyroscope sensor measurements are thus represented as follows:

$$q_{meas} = \dot{\theta}_{true} + b_{gyro} \tag{3.22}$$

$$\arctan\left(-\frac{a_x}{a_z}\right) = \theta_{true} + \theta_p \tag{3.23}$$

which are substituted in equations 3.20 and 3.21 to give

$$\dot{\theta}_{HF} = -\frac{1}{\tau_a}\theta_{HF} + (\dot{\theta}_{true} + b_{gyro}) \tag{3.24}$$

$$\dot{\theta}_{LF} = -\frac{1}{\tau_a}\theta_{LF} + \frac{1}{\tau_a}(\theta_{true} + \theta_p) \tag{3.25}$$

Adding equations 3.24 and 3.25 as described in equation 3.19 gives the estimated pitch angle in transfer function form as

$$\hat{\theta}(s) = \theta_{true}(s) + \frac{\theta_p(s)}{\tau_a s + 1} + \frac{b_{gyro}(s)\tau_a}{\tau_a s + 1} \tag{3.26}$$

Equation 3.26 shows that the rate gyroscope bias produces a offset in $\hat{\theta}$ of $b_{gyro}\tau_a$. Figure 3.1 shows that making $\tau_a = \infty$ is equivalent to removing the accelerometers, and thus causes the steady state offset in $\hat{\theta}$ to become infinite. *The fundamental role of the accelerometers is thus to bound the steady state error of the pitch angle estimate derived from integrating the rate gyroscope measurements.*

Equation 3.26 also shows that the acceleration-induced perturbations are filtered by a single pole with time constant, τ_a. The MIT team is making use of $\tau_a = 150\,\mathrm{s}$, implying that for fast aerobatic manoeuvres the acceleration information is not used. The low frequency gain of the rate gyroscope bias drift is proportional to τ_a, and is high for the MIT case.

Equation 3.26 provides a good explanation as to why the complementary filter works well for the MIT group but not for projects using low cost rate gyroscopes. If the rate gyroscope sensor has a bias offset of $0.1°/s$, the pitch angle estimate offset is equal to 15°. After the signal conditioning of the pitch rate gyroscope sensor, the pitch rate resolution equaled approximately $0.5°/s$. The drift rate of the bias of the low cost Tokin rate gyroscopes is typically $0.15°/s$ in one minute.

The above analysis shows that accelerometers can play a valuable role in attitude estimators.

The greatest advantage of the above approach is that knowledge about the dynamics of the vehicle and sensor characteristic is only used to set the bandwidth of these complementary filters. The system constructed using such a filter can be used to measure the attitude of any vehicle - assuming limited amplitude and duration acceleration of the vehicle. The accuracy of the solution is dependant on the magnitude of the drift and random walk caused by integration of the noisy, sampled rate gyroscopes, as well as the nature of the motion of the vehicle on which the system is mounted. The higher the quality of the rate gyroscopes and the resolution of the analog to digital converters, the more accurate the filter will be, being less dependant on the accelerometer measurements.

The gravity vector can also be used to correct the bias drift on mechanical attitude gyroscopes. Amidi [1] mentions using mechanical gyroscopes that "incorporate a pendulous inner gimbal, using the gravity vector to eliminate long-term drift". Bryson [4] describes a similar mechanical system.

3.3.4 Kahn-Hudson Extended Kalman Filter

The IMU acquired from Rotomotion (that will be described in section 4.4.4) was supplied with open source software that was developed by Aaron Kahn and Trammell Hudson. No thorough theoretical treatment of the filter exists and will therefore be derived in detail. A similar filter has recently been published by Kingston *et al.* [30]. The Kahn-Hudson EKF as was implemented by Kahn and Hudson assumes that three rate gyroscopes, two two-axis accelerometers and a three axis magnetometer are used to construct an AHRS.

Zarchan [68] gives the standard formulation of the Extended Kalman Filter (EKF):

$$\dot{\mathbf{x}} = f(\mathbf{x}) + \mathbf{w} \tag{3.27}$$

$$\mathbf{z} = h(\mathbf{x}) + \mathbf{v} \tag{3.28}$$

with $\mathbf{x}$ the state vector, $\mathbf{z}$ the output vector. The corrected state estimates ($\hat{\mathbf{x}}_k$) and the predicted estimates ($\bar{\mathbf{x}}_k$) are calculated from the measurement and time update equations [68]:

$$\bar{\mathbf{x}}_k = \hat{\mathbf{x}}_{k-1} + f(\hat{\mathbf{x}}_{k-1})T_s \tag{3.29}$$

$$\hat{\mathbf{x}}_k = \bar{\mathbf{x}}_k + \mathbf{K_k}[\mathbf{z}_k - h(\bar{\mathbf{x}}_k)] \tag{3.30}$$

with T_s the sampling time.

"Because the system and measurement equations are nonlinear [equations 3.27 and 3.28], *a first-order approximation is used in the continuous Riccati equations for the system dynamics matrix* $\boldsymbol{F}$ *and the measurement matrix* $\boldsymbol{H}$*. The matrices are related to the nonlinear system and measurement equations according to* [equation 3.31 and 3.32]*."* - from Zarchan [68].

$$\mathbf{F} = \left.\frac{\partial f(\mathbf{x})}{\partial \mathbf{x}}\right|_{x=\hat{x}} \tag{3.31}$$

$$\mathbf{H} = \left.\frac{\partial h(\mathbf{x})}{\partial \mathbf{x}}\right|_{x=\hat{x}} \tag{3.32}$$

The discrete Riccatti equations required to compute the Kalman gains, using $\mathbf{Q}_k \approx \mathbf{I} + \mathbf{F}T_s$, are provided in Zarchan [68] as:

$$\mathbf{M}_k = \mathbf{\Phi}\mathbf{P}_{k-1}\mathbf{\Phi}_k^T + \mathbf{Q}_k \tag{3.33}$$

$$\mathbf{K}_k = \mathbf{M}_k\mathbf{H}^T(\mathbf{H}\mathbf{M}_k\mathbf{H}^T + \mathbf{R}_k)^{-1} \tag{3.34}$$

$$\mathbf{P}_k = (\mathbf{I} - \mathbf{K}_k\mathbf{H})\mathbf{M}_k \tag{3.35}$$

For our application we chose to include the attitude quaternions and the rate gyroscope biases in the state vector ($\mathbf{x}$):

$$\mathbf{x} = \begin{bmatrix} q_0 & q_1 & q_2 & q_3 & p_{bias} & q_{bias} & r_{bias} \end{bmatrix}^T \tag{3.36}$$

The quaternion representation is preferred to the Euler angle representation for state propagation since no singularities exist at any attitude. A further advantage is that the time derivative of the quaternion is a simple function of the measurable body-axis angular rates as given in [51, 62]:

$$\dot{\mathbf{q}} = \begin{bmatrix} \dot{q_0} \\ \dot{q_1} \\ \dot{q_2} \\ \dot{q_3} \end{bmatrix} = \frac{1}{2}\Omega(p,q,r)\mathbf{q} = \frac{1}{2}\begin{bmatrix} 0 & -p & -q & -r \\ p & 0 & r & -q \\ q & -r & 0 & p \\ r & q & -p & 0 \end{bmatrix}\begin{bmatrix} q_0 \\ q_1 \\ q_2 \\ q_3 \end{bmatrix} \tag{3.37}$$

The true angular rates are given by the difference between the measurements from the rate gyroscopes and their biases:

$$\begin{bmatrix} p \\ q \\ r \end{bmatrix} = \begin{bmatrix} p_{meas} - p_{bias} \\ q_{meas} - q_{bias} \\ r_{meas} - r_{bias} \end{bmatrix} \tag{3.38}$$

Knowing that the biases vary slowly and are therefore regarded as constants with respect to the system dynamics ($\dot{p}_{meas} = \dot{q}_{meas} = \dot{r}_{meas} = 0$), equation 3.37 will provide $f(\mathbf{x})$ in equation 3.27 as:

$$\dot{\mathbf{x}} = f(\mathbf{x}, p_{meas}, p_{meas}, r_{meas}) = \frac{1}{2}\begin{bmatrix} \Omega(p,q,r) & 0_{4\times 3} \\ 0_{3\times 4} & 0_{3\times 3} \end{bmatrix}\mathbf{x} \tag{3.39}$$

It is found that $f(\mathbf{x})$ is a function of the state vector and the rate gyroscope measurements.

We chose the output vector $\mathbf{z}$ to be the Euler angles since they are easily interpreted:

$$\mathbf{z} = \begin{bmatrix} \phi \\ \theta \\ \psi \end{bmatrix} \tag{3.40}$$

During non-accelerating flight, the pitch and roll angles of the helicopter body can be calculated from the measurements from the three accelerometers [30]:

$$\theta_{meas} = -\arcsin\left(\frac{a_x}{g}\right) \tag{3.41}$$

$$\phi_{meas} = \arctan\left(\frac{a_y}{a_z}\right) \tag{3.42}$$

The magnetic heading of the helicopter can be obtained from a magnetic sensor, but a complex calculation using the estimated (or measured during initialisation) pitch and roll angles is required. Using the magnetometer measurements (M_x, M_y and M_z), the magnetic heading is calculated as follows [9]:

$$\psi_{meas} = \arctan\left(\frac{M_y\cos\theta + M_z\sin\theta}{M_x\cos\phi + M_y\sin\theta\sin\phi - M_z\cos\theta\sin\phi}\right) \tag{3.43}$$

Now we turn our attention to determining $h(\mathbf{x})$. The attitude is represented in the state vector in terms of attitude quaternions, while the filter output is defined and calculated from measurements as Euler angles. The elements of the quaternion and Euler description of the Direction Cosine Matrix (C_b^n) are compared ($C_b^n(\phi,\theta,\psi) = C_b^n(q_0,q_1,q_2,q_3)$) to find the equations to transform from quaternions to Euler angles [62]:

$$\phi = \arctan\left(\frac{C_{b,32}^n}{C_{b,33}^n}\right) = \arctan\left(\frac{2(q_2q_3+q_0q_1)}{1-2(q_1^2+q_2^2)}\right) \tag{3.44}$$

$$\theta = \arcsin\left(-C_{b,31}^n\right) = \arcsin\left(-2(q_1q_3-q_0q_2)\right) \tag{3.45}$$

$$\psi = \arctan\left(\frac{C_{b,21}^n}{C_{b,11}^n}\right) = \arctan\left(\frac{2(q_1q_2+q_0q_3)}{1-2(q_2^2+q_3^2)}\right) \tag{3.46}$$

The Euler angles can be described in terms of quaternions using equations 3.44, 3.45 and 3.46 [30, 51]. Equations 3.44, 3.45 and 3.46 are used to calculate the estimated Euler angle outputs from the quaternions. Therefore $h(\mathbf{x})$ is found by substituting equations 3.44, 3.45 and 3.46 into equation 3.40.

For initialisation of the estimated quaternions, the Euler angles are measured and transformed to quaternions using equations 3.47, 3.48, 3.49 and 3.50 [15, 51, 62].

$$q_0 = \cos(\tfrac{\phi}{2})\cos(\tfrac{\theta}{2})\cos(\tfrac{\psi}{2}) + \sin(\tfrac{\phi}{2})\sin(\tfrac{\theta}{2})\sin(\tfrac{\psi}{2}) \tag{3.47}$$

$$q_1 = \sin(\tfrac{\phi}{2})\cos(\tfrac{\theta}{2})\cos(\tfrac{\psi}{2}) - \cos(\tfrac{\phi}{2})\sin(\tfrac{\theta}{2})\sin(\tfrac{\psi}{2}) \tag{3.48}$$

$$q_2 = \cos(\tfrac{\phi}{2})\sin(\tfrac{\theta}{2})\cos(\tfrac{\psi}{2}) + \sin(\tfrac{\phi}{2})\cos(\tfrac{\theta}{2})\sin(\tfrac{\psi}{2}) \tag{3.49}$$

$$q_3 = \cos(\tfrac{\phi}{2})\cos(\tfrac{\theta}{2})\sin(\tfrac{\psi}{2}) - \sin(\tfrac{\phi}{2})\sin(\tfrac{\theta}{2})\cos(\tfrac{\psi}{2}) \tag{3.50}$$

$$\mathbf{F} = \left.\frac{\partial f(\mathbf{x})}{\partial \mathbf{x}}\right|_{x=\hat{x}} = \frac{1}{2}\left[\begin{array}{ccccccc} 0 & -\hat{p} & -\hat{q} & -\hat{r} & \hat{q_1} & \hat{q_2} & \hat{q_3} \\ \hat{p} & 0 & \hat{r} & -\hat{q} & -\hat{q_0} & \hat{q_3} & -\hat{q_2} \\ \hat{q} & -\hat{r} & 0 & \hat{p} & -\hat{q_3} & \hat{q_0} & \hat{q_1} \\ \hat{r} & \hat{q} & -\hat{p} & 0 & -\hat{q_2} & -\hat{q_1} & \hat{q_0} \\ \hline \multicolumn{7}{c}{0_{3\times 7}} \end{array}\right] \tag{3.51}$$

with

$$\left[\begin{array}{c} \hat{p} \\ \hat{q} \\ \hat{r} \end{array}\right] = \left[\begin{array}{c} p_{meas} - \hat{p}_{bias} \\ q_{meas} - \hat{q}_{bias} \\ r_{meas} - \hat{r}_{bias} \end{array}\right] \tag{3.52}$$

Using equations 3.44, 3.45 and 3.46 the Jacobian $\mathbf{H}$ may be calculated [30, 51, 56]:

$$\mathbf{H} = \left.\frac{\partial h(\mathbf{x})}{\partial \mathbf{x}}\right|_{x=\hat{x}} = \left.\left[\begin{array}{ccccccc} \frac{\partial\phi}{\partial q_0} & \frac{\partial\phi}{\partial q_1} & \frac{\partial\phi}{\partial q_2} & \frac{\partial\phi}{\partial q_3} & 0 & 0 & 0 \\ \frac{\partial\theta}{\partial q_0} & \frac{\partial\theta}{\partial q_1} & \frac{\partial\theta}{\partial q_2} & \frac{\partial\theta}{\partial q_3} & 0 & 0 & 0 \\ \frac{\partial\psi}{\partial q_0} & \frac{\partial\psi}{\partial q_1} & \frac{\partial\psi}{\partial q_2} & \frac{\partial\psi}{\partial q_3} & 0 & 0 & 0 \end{array}\right]\right|_{x=\hat{x}} \tag{3.53}$$

$$= \left[\begin{array}{ccccccc} \frac{2\hat{q}_1 d_{33}}{d_{33}^2+d_{32}^2} & \frac{2\hat{q}_0 d_{33}+2\hat{q}_1 d_{32}}{d_{33}^2+d_{32}^2} & \frac{2\hat{q}_3 d_{33}+\hat{q}_2 d_{32}}{d_{33}^2+d_{32}^2} & \frac{2\hat{q}_2 d_{33}}{d_{33}^2+d_{32}^2} & 0 & 0 & 0 \\ \frac{2\hat{q}_2}{\sqrt{1-d_{31}^2}} & \frac{-2\hat{q}_3}{\sqrt{1-d_{31}^2}} & \frac{2\hat{q}_0}{\sqrt{1-d_{31}^2}} & \frac{-2\hat{q}_1}{\sqrt{1-d_{31}^2}} & 0 & 0 & 0 \\ \frac{2\hat{q}_3 d_{11}}{d_{11}^2+d_{21}^2} & \frac{2\hat{q}_2 d_{11}}{d_{11}^2+d_{21}^2} & \frac{2\hat{q}_1 d_{11}+2\hat{q}_2 d_{21}}{d_{11}^2+d_{21}^2} & \frac{2\hat{q}_0 d_{11}+2\hat{q}_3 d_{21}}{d_{11}^2+d_{21}^2} & 0 & 0 & 0 \end{array}\right] \tag{3.54}$$

with

$$d_{11} = 1 - 2(\hat{q}_2^2 + \hat{q}_3^3) \tag{3.55}$$

$$d_{21} = 2(\hat{q}_1\hat{q}_2 + \hat{q}_0\hat{q}_3) \tag{3.56}$$

$$d_{31} = 2(\hat{q}_1\hat{q}_3 - \hat{q}_0\hat{q}_2) \tag{3.57}$$

$$d_{32} = 2(\hat{q}_2\hat{q}_3 + \hat{q}_0\hat{q}_1) \tag{3.58}$$

$$d_{33} = 1 - 2(\hat{q}_1^2 + \hat{q}_2^3) \tag{3.59}$$

One problem remains before the standard discrete Extended Kalman filter equations can be used to estimate the attitude: selecting the process noise ($\mathbf{Q}_k$) and measurement noise ($\mathbf{R}_k$) covariance matrices. These matrices determine the time constants of the Kalman filter. Initial values were provided by the IMU manufacturer, but the values of $\mathbf{Q}_k$ and $\mathbf{R}_k$ were later selected through trial and error. Although guidelines exist to aid with the selection of $\mathbf{Q}_k$ and $\mathbf{R}_k$ based on the noise power spectral density of the

measurement noise, it is known that some trial and error selection of $\mathbf{Q}_k$ and $\mathbf{R}_k$ is required to find good values for these matrices.

Equations 3.41 and 3.42 will only provide correct measurements of the helicopter pitch and roll angles if the helicopter is not accelerating. It would be possible to make corrections for the accelerations if the acceleration of the vehicle could be measured [30, 43]. Research groups that make use of high quality DGPS or vision aiding, perform these corrections.

Other groups assume that the acceleration is low and of short duration. Therefore, if too much weight is placed on the attitude measurements, the filter corrects false offsets in attitude (due to manoeuvring) too quickly. If too much weight is placed on the rate gyroscopes, the random walk of the filter is too large.

The Kahn-Hudson Extended Kalman Filter was initially used to estimate the pitch and roll angles. These estimates were used to conduct initial attitude control tests.

The level of accuracy required to hover the helicopter within a confined space is high. Using the estimates from the EKF, inconsistencies were found between attitude estimates, velocity measurements and the basic dynamic model of the vehicle. The inconsistent behaviour of the EKF was attributed to resolution and drift of the rate gyroscope sensors. The problem was solved by replacing the rate gyroscope sensors with higher quality sensors, and using a simple estimator based on the basic dynamics model of the helicopter. The dynamic model based filter will be described in the next section.

The Kahn-Hudson EKF is still being used to estimate the heading, since, with the active yaw rate damping subsystem activated, a high accuracy heading estimate is not required to be able to control the helicopter during near-hover flight. Furthermore the filter allows calculation of the heading without having to fly the helicopter. The filter also estimates the absolute attitude of the helicopter body, not the attitude of the TPP like the filter that will be presented in section 3.3.5.

3.3.5 Vehicle Kinematics Based

The simplified equations that describe the relationship between the angular rates and the velocity of a RC helicopter were presented in section 2.4.4. These equations were used by the author to design an attitude estimator that was successfully used to control the longitudinal position of the helicopter.

Unlike most of the estimators used by others, the method does not estimate the absolute attitude of the body, but the attitude of the TPP relative to the attitude that will

cause no acceleration of the body. The filter structure is shown in figure 3.2. The assumption is made that the heading of the vehicle does not change. Expanding modifications will be required to allow heading changes.

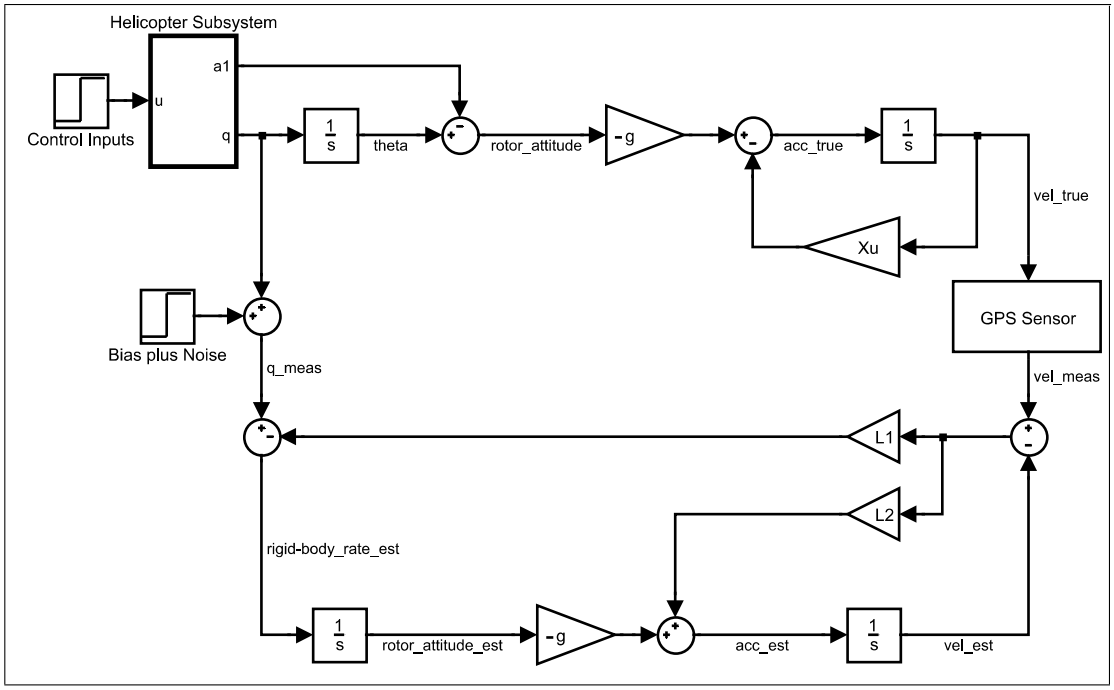

Figure 3.2: *Block diagram of the vehicle kinematic-based pitch angle and longitudinal velocity estimator*

From figure 3.2 the steady state errors in velocity and attitude caused by bias offsets on the rate gyroscope signals can be calculated as follows:

$$\hat{u}(0) = \frac{q_{bias}}{L_1} \tag{3.60}$$

$$\hat{\theta}_{TPP}(0) = \frac{q_{bias} L_2}{g L_1} \tag{3.61}$$

with q_{bias} in radians. Therefore, with a rate gyroscope bias of 0.5°/s (which is a realistic number after an one minute flight), and gains $L_2 = 1$ and $L_1 = 0.1$, the velocity will have an offset of 0.087 m/s and the pitch angle will have an offset of 0.51°. The values have been verified through simulation.

One drawback of the estimator is that it is only possible to estimate the attitude of the vehicle if the vehicle is flying. The helicopter can not be strapped onto the roof of a car to test the estimator. However, the filter was designed and tested using raw sensor measurements captured during a real flight. The accuracy of the filter was judged based on the difference between the estimated velocity and the GPS receiver velocity measurements (the innovations).

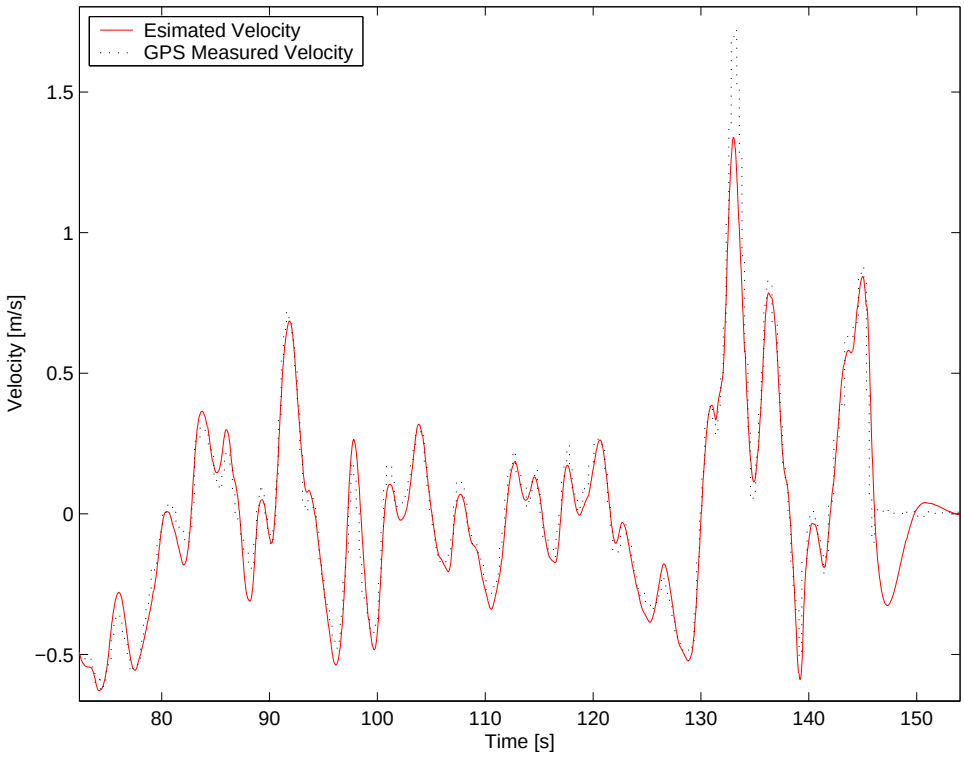

Figure 3.3: *GPS measured velocity (after latency correction) vs estimated velocity*

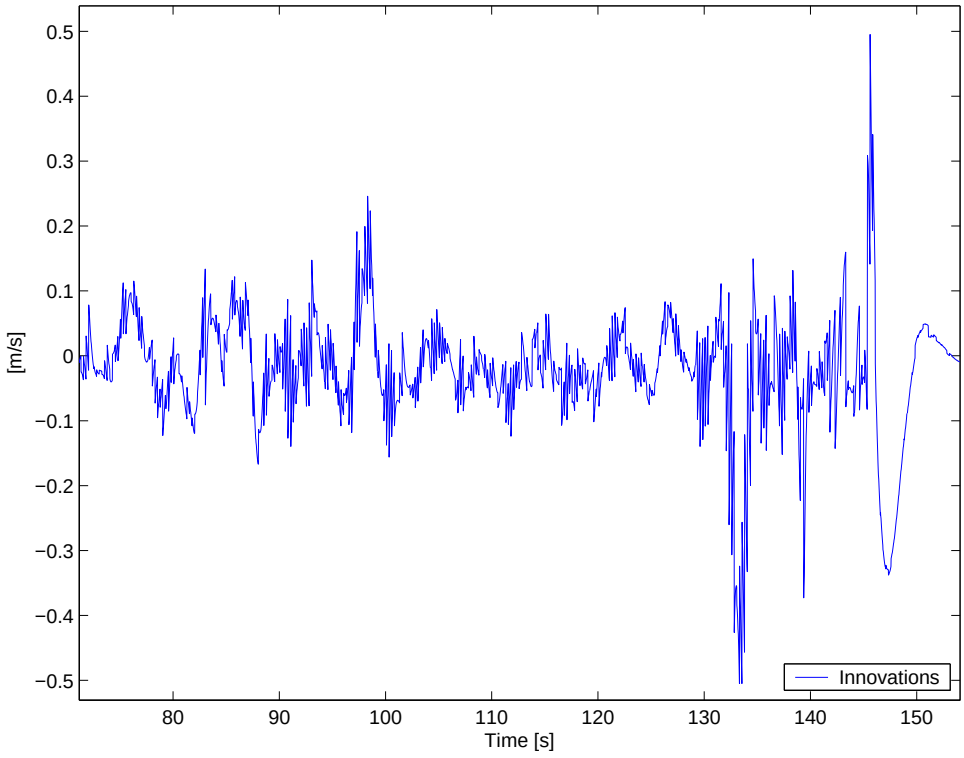

Figure 3.4: *Difference between GPS velocity measurements and estimated velocity*

It is important not to over estimate the quality of the longitudinal velocity measured using the GPS and compass. The velocity measurements, the heading measurements and the model contains errors. The model used to design the estimator is only valid for near-hover attitudes. The accuracy of the estimator will deteriorate if the near-hover condition is not satisfied. If too much value is placed on small velocity innovation errors, the attitude estimates become noisy due to the errors in the velocity measurements.

In theory the latency of the GPS needs to be accounted for if the filter is to perform correctly, especially if high gains are used to feed back the velocity innovations (implying high filter bandwidth). However, if the gains on the velocity innovations are too high, the attitude estimates will respond drastically to any errors in the velocity measurements (which can be caused by GPS measurement errors or heading estimate errors). It is not desirable to have GPS measurement errors causing violent attitude errors, since the inertial sensors are capable of measuring high frequency motion with high accuracy. Reasonably good estimates could be achieved without compensation for the GPS latency while using low feedback gains on the innovations.

The flight that yielded measurements that were used to generate figures 3.3, 3.4 and 3.5 will be discussed in more detail in chapter 7. The flight was a test of the longitudinal position controller. The section of the flight seen in figures 3.3, 3.4 and 3.5 is the last half of the flight, starting while under computer control, with control taken over by the pilot at time 131 s and the pilot landing the helicopter at time 146 s, within 10 cm from the take-off position.

A further drawback of the state estimator can be seen in figures 3.3 and 3.4: during transition from being stationary on the ground to free flight, the state estimates will be corrupted due to forces acting on the body that are not included in the model. For example, sections of the undercarriage applying forces on the body. The high innovations can be seen in figures 3.4 and 3.3 during the landing (landing taking place at time 146 s). The model does not make provision for the transition from being stationary to free flight, or from free flight to landing.

The majority of estimation problems encountered were due to sensor inadequacies. The estimators can not be fully evaluated without considering the sensors used. The Kahn-Hudson filter was used and evaluated using the Rotomotion IMU and a 1 Hz update rate Sigtec Navigation GPS receiver. The vehicle kinematics based filter made use of measurements from a 4 Hz update rate u-Blox GPS receiver and a higher quality Analog Devices ADXRS150 rate gyroscope.

In figure 3.5 the pitch angle output from the Kahn-Hudson EKF is compared to

the estimator designed using the vehicle dynamics. It is important to remember that the Kahn-Hudson filter estimates the absolute attitude of the helicopter body, while the vehicle dynamics describes the attitude of the main rotor TPP relative to the attitude that will yield zero acceleration. From figure 3.5 it is clear that the two estimators are not a perfect match, but that there are strong similarities between the estimates that were obtained using completely different hardware and algorithms to obtain estimates of strongly related states.

Knowing that the helicopter is hovering till time 131 s, it can be seen from figure 3.5 that the pitch angle of the helicopter changes less than $\pm 4^\circ$ while in hover. Pitch angles of $\pm 8^\circ$ yield significant accelerations (see both figures 3.5 and 3.3).

The estimator yields a solution sufficiently accurate to control the helicopter near-hover and requires only two rate gyroscopes, GPS velocity measurements and the heading of the helicopter to estimate the pitch and roll attitude as well as the horizontal velocity at 60 Hz. Furthermore, the estimator requires minimal processing power.

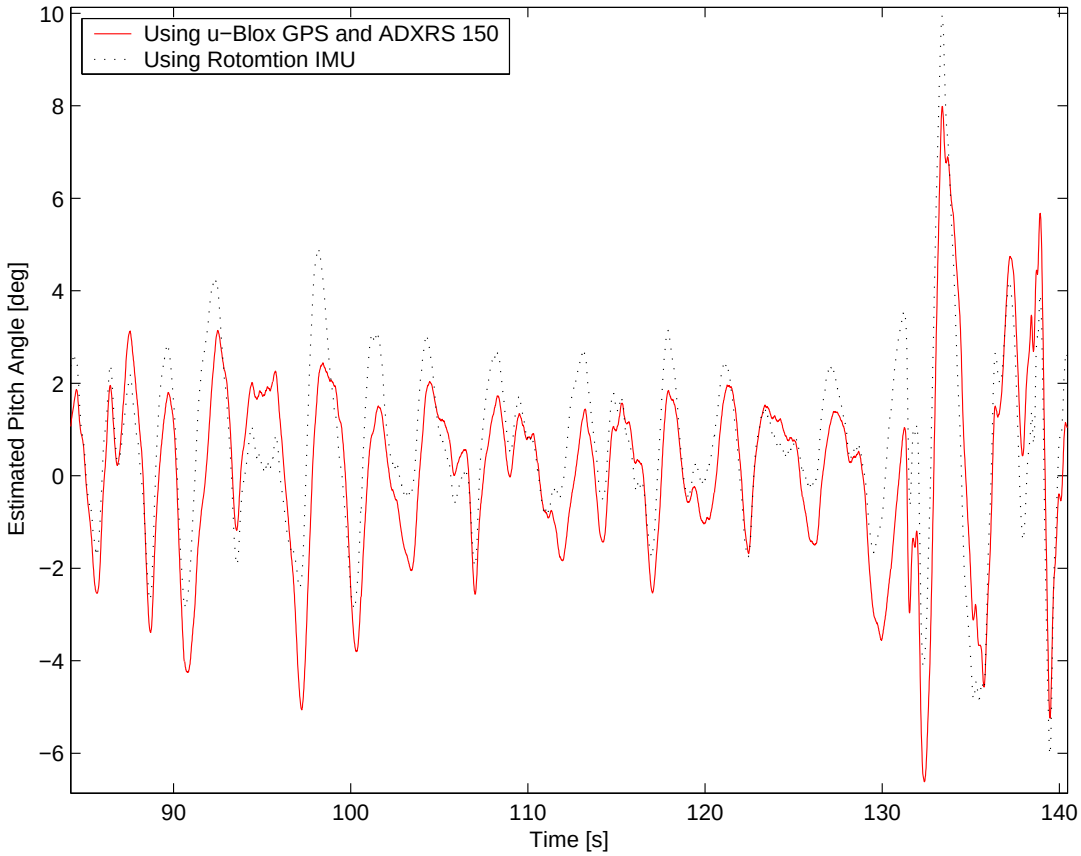

Figure 3.5: *Pitch angle estimates using Kahn-Hudson EKF and vehicle kinematic-based estimator*

3.4 Horizontal Position and Velocity

The kinematics of the helicopter were used to develop the state estimators in section 3.3.5. Rate gyroscopes and a GPS receiver were used to provide measurements of the inputs and velocities. The velocity of the helicopter is also estimated in the process. Although the direct GPS velocity measurements obtained were of fair quality, the estimators provide velocity estimates at much higher update rates than the GPS receiver. The estimated longitudinal velocity was used to control the helicopter.

It is known that low cost GPS receivers are capable of measuring velocity to a higher degree of accuracy (typically $< 0.2\,\mathrm{m/s}$) than position (typically CEP $= 5\,\mathrm{m}$ with a drift rate of up to $0.9\,\mathrm{m/s}$) over a short period of time - depending on a large number of factors like agility of vehicle movement and satellite visibility. It was found that integration of the velocity yields more accurate relative position measurements than calculated from the GPS receiver position fixes. The integrated velocity estimates were therefore used to control the position of the helicopter. The hardware used and the results obtained will be discussed in sections 4.4.6 and 7.3.2.

3.5 Summary

Limited effort has been invested by other international groups in the development of low cost, low weight ($< 0.5\,\mathrm{kg}$) FCS and state estimators for rotary-wing vehicles. This chapter presented an overview of technologies that have been investigated to measure and estimate the attitude, velocity and position of RUAV's.

Although the mechanics of RC helicopters are capable of performing highly agile manoeuvres, it has been assumed that the first goal is to stabilise and control a helicopter during slow near-hover manoeuvres.

The challenge of measuring the pitch and roll angles has received special attention due to the importance of having accurate estimates of these states to be able to stabilise and control a RUAV near-hover. High quality rate gyroscopes can significantly simplify the problem of estimating the pitch and roll angles accurately.

The EKF that was implemented by Kahn and Hudson was mathematically derived. Due to problems experienced using the Kahn-Hudson filter and Rotomotion inertial measurement unit (IMU), a computationally simple filter, based on the kinematics of the vehicle, was developed. The vehicle kinematics-based filter not only succeeds in estimat-

ing the attitude of the helicopter tip path plane, but also estimates the velocity of the helicopter between GPS receiver updates.

The designed vehicle kinematics-based estimator meets the needs of the problem to control the helicopter near-hover, providing the heading remains fixed. Extending the design to allow heading changes is not complex.

Chapter 4

System Overview and Hardware

This chapter provides an overview of the system and a detailed description of the hardware utilised. The selection of equipment is motivated and the performance of the equipment is evaluated. A number of unique hardware challenges were encountered due to the low cost of the sensors and the payload restrictions of the helicopter.

This chapter consists of the following sections:

- Section 4.1 describes what has been achieved and investigated by other research groups.
- Section 4.2 describes the layout of the system developed in this project. The relationships between the hardware subsystems are briefly outlined.
- Section 4.3 presents the helicopter and some of the subsystems of a standard RC helicopter.
- Section 4.4 treats the selection of sensors and the results obtained using these sensors.
- Section 4.5 discusses the communication links used to transfer data and control commands between the helicopter, the pilot and the ground station.

4.1 Overview of RC Helicopter FCS

This section will provide an overview of the evolution of FCSs for RC model helicopters, with special reference to the IARC participants. The IARC has inspired a vast amount of published research on RUAV systems.

A number of RUAV systems have been developed by private companies for military and commercial use. Little is known about many of these systems. For a list of published projects and commercial products, refer to appendix A.

4.1.1 International Aerial Robotics Competition

The International Aerial Robotics Competition (IARC) was initiated in 1990 at Georgia Institute of Technology by Professor Robert Michelson, past president of the Association for Unmanned Vehicle Systems International (AUVSI). The mission objectives typically include search and rescue missions to be performed by autonomously flying vehicles.

Three years after the initiation of the competition, the team from Georgia Institute of Technology was the first team to successfully demonstrate autonomous take-off and landing.

In 1995 Team Hummingbird from Stanford University became the first team to successfully complete the first mission objective of the competition: develop a robot that can fly autonomously, find and pick up randomly placed objects and transport them to another location [67]. The only sensors used were a pair of Trimble GPS receivers operating using Differential Carrier Phase calculations [11].

The 1996 competition was won by the team from the MIT Draper Laboratory. The new mission required that the autonomous vehicles navigate through a toxic waste dump, locating, identifying and reporting the locations of barrels marked with labels. The sensors consisted of a Systron-Donner MotionPak IMU, a NovAtel RT-20 DGPS, a digital compass and an ultrasonic altimeter.

The Robotics Institute at Carnegie-Mellon won the 1997 competition using a Yamaha R-50 helicopter ($\approx$ US\$ 100 000) as platform. The group also became the first contender to demonstrate vision-only based navigation [1]. The onboard vision processor provided information such as attitude, velocity and position.

The Technical University of Berlin (MARVIN) took honours in both the 1999 and the 2000 Millennium Disaster Search and Rescue Missions. A custom built IMU, using low cost Murata ENV5 rate gyroscopes, and a NovAtel RT-2 DGPS system was used by the team.

The hardware used by the teams participating in the IARC have the following in common:

- all of the helicopters used to date were glow- or gasoline powered helicopters with 0.60 cubic inch or larger engines,
- the mass of the mountings, sensors, communication equipment and processors is in excess of 3 kg, and
- the cost of COTS DGPS and IMU systems is in excess of US$ 5 000.

4.1.2 Electrically Powered RC Helicopter Projects

The following research has been performed using electrically powered helicopters as platforms:

- The University of South California is working towards demonstrating formation flight using electrically powered model helicopters as followers. To date, only the proposed hardware of one of these helicopters has been published [44].
- The Robotics Institute at Carnegie-Mellon [1] and the Swiss Federal Institute of Technology Zürich (ETHZ) [60] made use of restrained, tethered, electrically powered RC helicopters during their early years of FCS development. The position of the helicopters was measured using external instruments like potentiometers and cameras.
- California Institute of Technology used a brushless, tethered RC helicopter (Kyosho) on a training stand (Whiteman Inc), with a Polhemus Inside Track system to measure the position of the helicopter [69].

To the knowledge of the writer, no autonomously free-flying sub-one-metre rotor diameter electrically powered helicopter system exists, in spite of the growing interest in RUAVs. A number of fixed-wing electrically powered aeroplanes are flying autonomously [14, 16].

4.1.3 Other Valuable Projects

Mettler, Tischler and Kanade [36, 37] have contributed significantly to the field of RC model helicopter system identification. Once a student at Carnegie Mellon University, Mettler has worked with Amidi and his team who won the 1997 IARC. Mettler is currently working with Frazzoli [17], Sprague [58], Feron and Gavrilets [19, 21] at MIT. The team

from MIT became the first research group to perform autonomous aerobatic manoeuvres with a RC model helicopter.

A group of private individuals, located in the USA, has been working towards making autonomously flying helicopters more affordable and accessible for the general public. Trammell Hudson (founder) and Aaron Kahn (graduate student from Georgia Institute of Technology [28]) have been the main contributors to the "Source Forge Autopilot Project" [27]. As a result of this work a company known as Rotomotion[1] has been established [26].

4.2 System Overview

Although a host of RC helicopter FCS projects have been presented during the last decade, the location of the main processor, the size and type of helicopter and the cost of the sensors used in this project distinguishes this project from the rest. The controller code is running on a standard desktop PC (see figure 4.1), transmitting the commands to the helicopter via the direct servo control (DSC) plug[2] located at the back of a standard RC transmitter. A microcontroller (Atmel 8-bit AVR) was used to convert commands from the PC UART port to pulse position modulation (PPM) commands that can be fed into the DSC port of the RC transmitter. Onboard the helicopter there is very little interference with standard control hardware (see figures 4.1 and 4.2). However, for the purpose of debugging, the pulse position modulation (PPM) signals were measured inside the JR receiver, using a 16-bit timer of an AVR micro controller. The PPM signals were recorded to be able to correlate commands from the pilot to the response of the helicopter.

4.3 JR Voyager E Helicopter

Gasoline powered helicopters have proved themselves as powerful workhorses. Glow engines are however the most popular RC helicopters amongst model helicopter pilots. Glow engines offer higher power to weight ratios compared to gasoline and electrically powered helicopters of the same price. The main drawbacks of both glow and gasoline engines are

[1]Throughout this document the author will refer to Rotomotion as synonymous with the Source Forge Autopilot project. Hardware is bought from Rotomotion, but this hardware should be compatible with the software developed by the Source Forge Autopilot group.

[2]This interface is also known as the "buddy plug". It is used to train student pilots. An experienced pilot acts as the master, taking initial control of the vehicle. The master pilot can pass control over to a student (slave) by pulling a switch, and regain control by letting go of the switch.

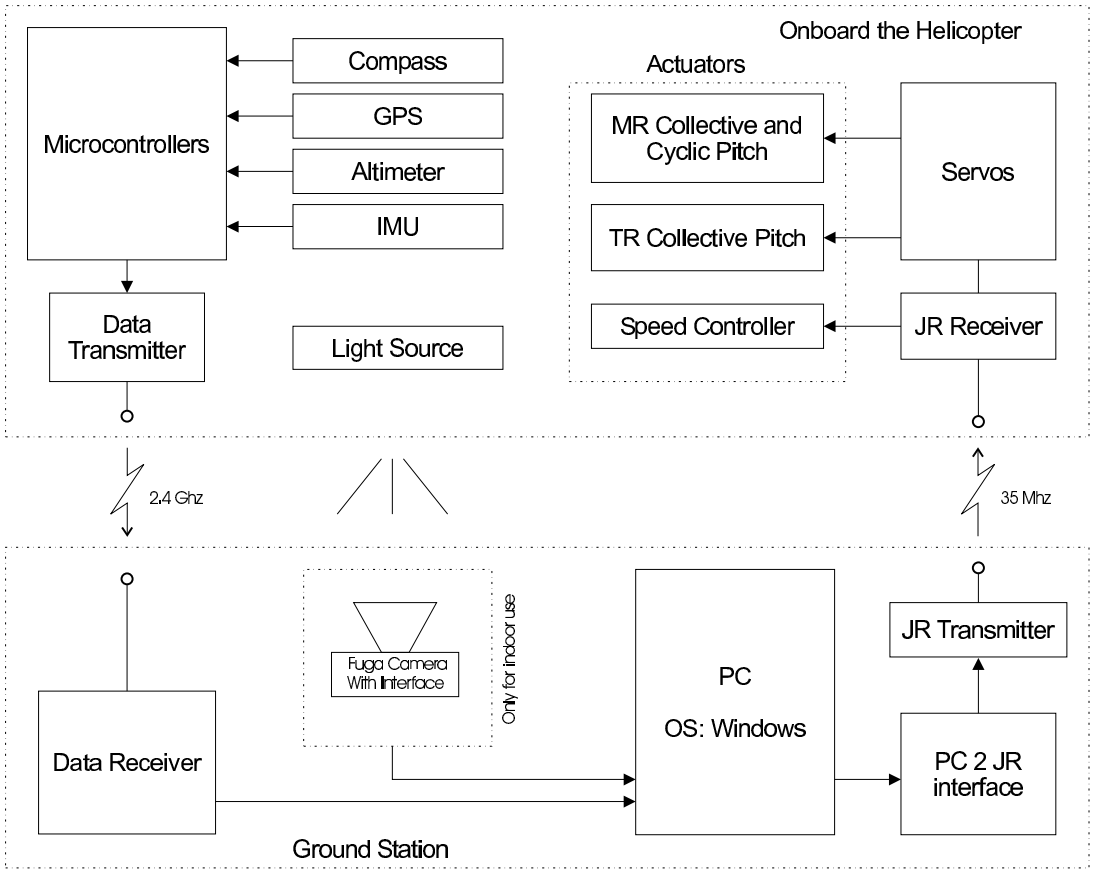

Figure 4.1: *System Layout*

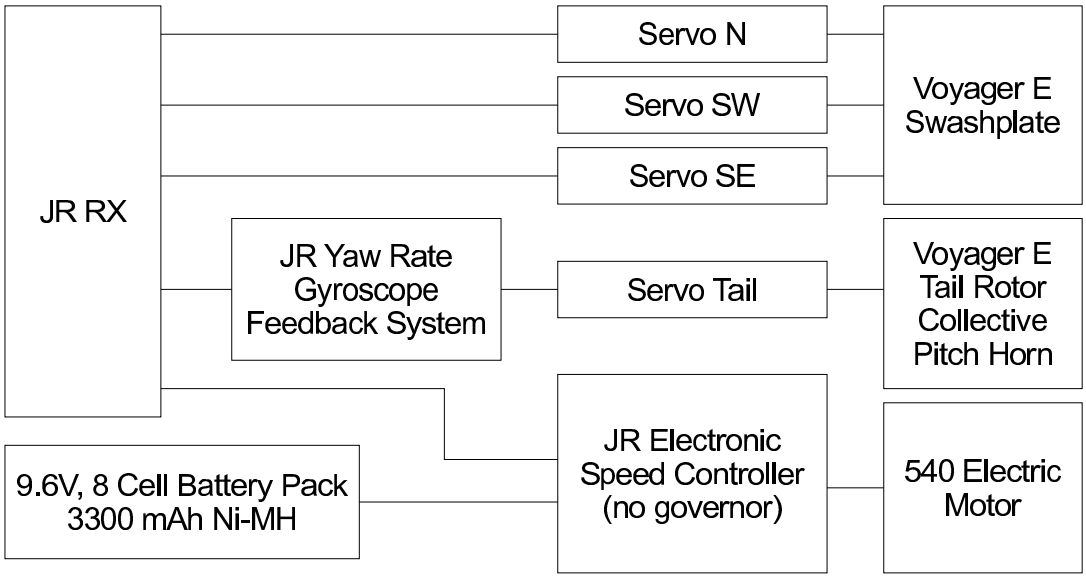

Figure 4.2: *Onboard JR receiver, servos and other standard JR equipment*

the high noise levels and emissions caused by these engines. The advantages of glow and gasoline powered helicopters are:

- large payload carrying capability that varies from 4 kg to 25 kg,
- flight times in excess of 15 minutes (depending on the amount of payload that is sacrificed to carry fuel and batteries),
- fast turnaround time between flights (being able to land, refuel and continue flying), and
- the reliability and robustness of the heavier mechanics.

The mechanics of a standard glow- or gasoline powered helicopter are more robust than the mechanics of a smaller electrically powered helicopter. Due to the limited thrust of electrically powered helicopters, the weight of the mechanics has to be kept to a bare minimum. Consequently manufacturers have to reduce the weight of components and sacrifice robustness in order to keep the cost reasonable. For example: the Voyager E has no bearing in the tail collective pitch arm. The repeated failure of the tail collective pitch mechanism endangered the vehicle and terminated flight testing a number of times (see appendix B).

Two main classes of electrically powered helicopters exist: very small indoor toys and larger helicopters capable of tolerating low wind speeds. The JR Voyager E was chosen since it is the best supported, medium size, electrically powered RC helicopter locally available. The assembly of the helicopter proved to be as easy as promised by the manufacturers. Appendix B provides details regarding modifications made, suggested alterations and maintenance problems encountered.

The first flight tests were conducted in very close proximity of the pilot at a maximum altitude of 1 metre. The ability of the helicopter to fly with a payload was tested using a training aid known as “hoola-hoop” (see figure 1.3). A total of 500 g was lifted for 2 minutes before the helicopter started moving around “uncomfortably”. The flight time of nearly two minutes compared well to the flight time of two and a half minutes obtained without the 500 g payload. The tests were conducted 100 metres above sea level, using a standard JR/Sanyo SCR 2400 mAh 8.4 V 7-cell NiCd battery pack.

4.3.1 Battery Packs

The standard battery pack sold by JR for use with the Voyager E helicopter is a 7-cell Sanyo 2400 mAh NiCd SCR battery pack. Very few hobbyists use the standard 7-cell

battery pack and the standard brushed motor to power their Voyager E helicopters. Most pilots upgrade their Voyager E's to use brushless motors with appropriate battery packs. Flight times of ten to fifteen minutes are typically achieved using brushless motors with 10-cell battery packs. The rest of the pilots use 8-cell battery packs with the standard motor. Lithium Polymer battery packs are becoming more popular and affordable.

Table 4.1: *Comparison of battery packs used in this project*

	8.4 V JR/Sanyo	9.6 V Sanyo	9.6 V GP	Units
Type	NiCd	NiCd	NiMH	-
Capacity	2400	2400	3300	mAh
Maximum discharge rate	> 40	> 40	> 30	A
Average flight duration	2 : 30	4 : 00	4 : 40	min
Cost	103	74	98	US$
Weight	0.413	0.486	0.521	kg

The 8-cell NiCd battery pack only survived half a year of frequent use. Currently four 8-cell NiMH GP3300 battery packs are being used to conduct flight tests. The length of the flights have not increased significantly following the switch to a higher capacity battery pack, but the helicopter behaves more consistently for the duration of the flight.

The angular rotation rate of the main rotor blades is dependant on the voltage of the battery pack. The collective pitch of the main rotor blades is used to vary the amount of thrust produced. With an 8-cell battery pack the RPM of the main rotor blades starts at 1560 RPM (26 Hz) and drops to 1320 RPM (22 Hz) towards the end of the flight. With a 7-cell battery pack the RPM starts at 1140 RPM (19 Hz). See section 4.4.4 for more details on the influence of the battery voltage on vibrations.

The same battery pack that is used to supply power to the motor, is also used to power the control- and sensor electronics.

4.3.2 Active Yaw Rate Damping Subsystem

It is very difficult to fly a model RC helicopter without the aid of an active yaw rate damping subsystem[3]. The yaw rate damping system receives a yaw command from the pilot via the standard RC transmitter/receiver system (see figure 4.2) and measures the yaw rate using a rate gyroscope. The required control output is calculated and applied

[3]Typically just referred to as a "gyro" by most pilots.

to the servo that controls the collective pitch of the trail rotor.

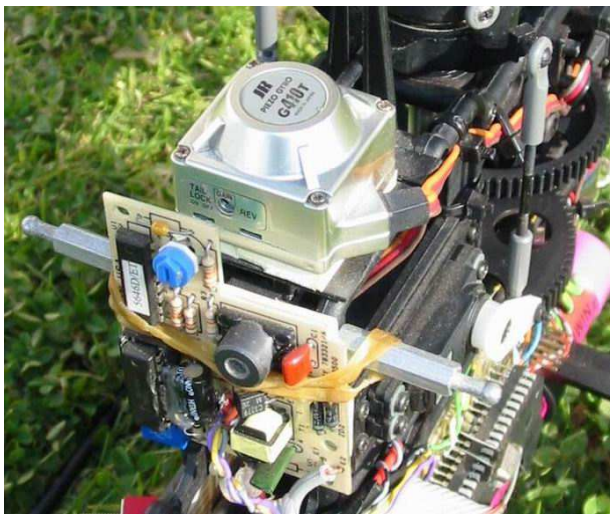

Figure 4.3: *JR active yaw rate damping system (top) and the Polaroid Ultrasonic processor PCB (bottom left)*

The standard yaw rate damper subsystem was retained (see figure 4.3) since a human safety pilot had to perform most of the flying - even when the developed control system was bypassed or in case of failure of the developed control system. Since the aim of this project was to control the helicopter, there was no need to remove the added damping provided by this small, lightweight subsystem.

4.3.3 120 Degree CCPM

Most standard fixed-wing aeroplanes use a single servo (or transmitter "channel") to command each actuator: elevator, ailerons, rudder or throttle. The Voyager E has a 120° cyclic collective pitch mixing (CCPM) servo system. The three servos that control the movement of the swashplate, which determines the cyclic and collective feathering of the main rotor blades, are space with a 120° angle between adjacent servos.

A set of linear equations can be derived to calculate the servo positions for each of the three servos (servo_N, servo_{SW}, servo_{SE}) in response to the control inputs (δ_b, δ_a, δ_c). For a 120° CCPM system, the following set of equations describes the relationship between commands and servo positions [27]:

$$\begin{bmatrix} \text{servo}_N \\ \text{servo}_{SE} \\ \text{servo}_{SW} \end{bmatrix} = \begin{bmatrix} 1 & \cos(0°) & \sin(0°) \\ 1 & \cos(-120°) & \sin(-120°) \\ 1 & \cos(120°) & \sin(120°) \end{bmatrix} \begin{bmatrix} \delta_c \\ \delta_b \\ \delta_a \end{bmatrix} \tag{4.1}$$

The equations can also be rewritten to obtain the control inputs (δ_b, δ_a, δ_c) from measured servo positions. The inversion was performed to determine pilot and computer commands from telemetered servo control pulses. It is typical amongst RC manufacturers to use a 9-bit or 10-bit timer to represent the width of these pulses (for example JR's ZPCM (9-bit) and SPCM (10-bit)). It was therefore decided to use the 16-bit timer of the microcontroller, rather than an 8-bit timer, to sample the PPM pulse train. This train of pulses is updated at approximately 45.87 Hz and each of the pulses is between 1 ms and 2 ms wide. The servo command pulses (PPM signals) were transmitted to the ground station and logged with the rest of the sensor and other data (see figure 4.4).

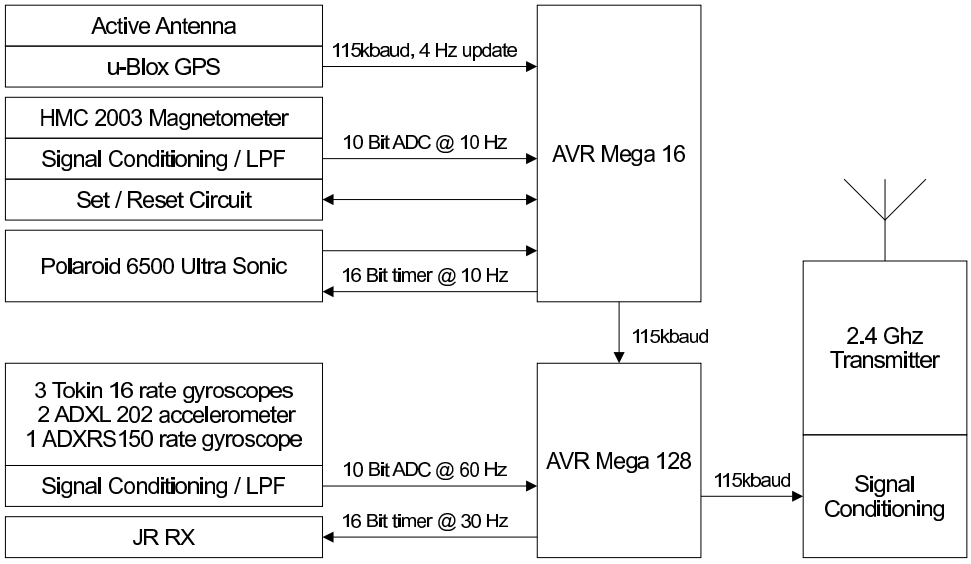

Figure 4.4: *Developed onboard electronics (excluding standard JR systems)*

Care needs to be taken when setting up the travel and bias (not just command trims) of the servo positions. The calibration process needs to be repeated every time the mechanical or RC transmitter setup of the helicopter changes, for example when the safety pilot changes the travel of a servo or a servo is broken (see appendix B).

4.3.4 Direct Servo Control Plug

It was decided to run the filters and control equations on a remote PC due to power and weight constraints. Furthermore, one of the goals of this project was to make the system as cheap and simple as possible. By using the DSC plug to command the helicopter, it would be possible to strap the necessary sensors onto any helicopter and control the helicopter from a standard RC transmitter, literally replacing the pilot with a PC.

The PC is treated like a student (slave) pilot, while the safety pilot remains the master. The safety pilot can take the helicopter to a safe altitude and pass control to the "student"

controls being received via the DSC plug. The DSC trainer system can be used to either transfer full control of all servos to a student pilot, or just a subset of channels (while the transmitter continues to perform the CCPM servo mixing).

The longitudinal cyclic, lateral cyclic and main rotor collective pitch can be commanded separately via the DSC trainer facility. The servo mixing is performed by the JR transmitter, not the student (PC). Changing the bias of the longitudinal cyclic, lateral cyclic or main rotor collective, does not require any bias changes by the student. The master transmitter takes care of the trim positions of the individual servos. The greatest advantage is the ability to safely hand over one degree of freedom at a time: longitudinal cyclic, lateral cyclic or main rotor collective pitch. Being able to transfer one, or all, degrees of freedom to the student, reduces complexity and risks during flight testing.

There are a number of advantages to transmitting the control signals to the helicopter via the DSC plug:

- Limited modifications to standard RC systems (which reduces risks),
- Reduced complexity,
- Less computational power is required onboard the platform, and
- Lower payload carrying ability required.

Using the DSC function has the following dangers and drawbacks:

- Dependency on two communication links,
- Time delay introduced by the communication links,
- Difficulty to maintain realtime synchronisation, and
- Not being able to separate the collective and throttle commands (not on the JR transmitter system).

Currently, no other helicopter project is making use of the direct servo control (DSC) plug to send commands to its helicopter, but a very successful fixed-wing UAV project is making use of the DSC plug to control its vehicle [14].

4.3.5 Weight Budget

The Voyager E was not designed to carry a payload. Instead of removing weight (like most RC pilots do) weight was added to the system. Table 4.2 provides a summary of the weight that was added to the helicopter frame.

Table 4.2: *Breakdown of weight added to helicopter*

Part	Weight [g]
2.4GHz TX	27.1
2.4GHz antenna	11.1
u-Blox OEM GPS	23.6
GPS antenna	34.5
Magnetometer sensors	24.7
Magnetometer AVR board	19.3
IMU sensors	≈ 86
IMU, Power AVR board	21.7
Polaroid transducer	11.7
Polaroid board	16.9
Mounting plate	36.1
Bolts, cables, etc	≈ 73
Δ Larger battery pack	≈ 108
Total	≈ 494

The total mass of the current helicopter, including all sensors and additional electronics, an 8-cell battery pack, mini servos and receiver is 2.02 kg. JR recommends a flying weight of less than 1.58 kg. The additional load has contributed to the early failure of two engines during the last year of test flying and the short lifespan of brushes. From flight experiments it is clear that the payload is at a limit.

4.3.6 Servos

The JR Voyager E is sold with plastic mountings to enable pilots to use mini servos rather than standard servos. The advantage of using mini servos is a reduction in weight, at the cost of speed and torque. Since the goal of the project was not to fly aggressive manoeuvres that would have required high speed and high torque servos, mini servos were used.

The small signal bandwidth of a servo is not a common specification provided by man-

ufacturers. The small signal bandwidth is not really important to RC model pilots since humans are not capable of controlling helicopters at the high bandwidths that computers are capable of. MIT has identified the small signal bandwidth of the Futaba S9402 and JR DS8417 high speed servos (see table 4.3).

Table 4.3: *Servo properties*

	Eagle	Futaba	JR	Units
Model	E381	S9402	DS8417	-
Size	mini	standard	standard	-
Torque	4.1	8.0	6.5	kg.cm
Voltage	4.8	6	4.8	V
Slew Rate	273	667	750	°/s
Bandwidth	n.a.	7 [58]	7 [21]	Hz
Weight	22.5	55	60	g
Price	40	80	115	US$

It is not possible to determine the small signal bandwidth of a servo by comparing the slew rates of the servos. The maximum frequency that can be applied without distorting the sinusoidal command due to slew rate is:

$$f = \frac{SLEW}{2\pi V_p} \tag{4.2}$$

where V_p is the peak of the sinusoidal signal (in degrees) to be followed, and the $SLEW$ is the servo slewrate in degrees per second. The Eagle E381 servos used in this project have very high slew rates for mini servos, yet have less than half the slew rate of the other two servos listed in table 4.3.

It is important that servos are not commanded to positions that are located beyond the maximum positions that the actuators allow[4]. It has been found that it does not take much effort to strip the gearbox of the mini servos. A Windows graphics user interface (GUI) was developed by the author to set the travel limits on the individual servos.

[4]RC modelers refer to reaching this limit as “binding” (jamming).

4.4 Sensors

The most important factors that had to be considered during selection of the sensors were: price, availability, size, weight and quality. Together with the requirements that have been presented in chapter 2 and chapter 3, this section will focus on what sensors were used, why the sensors were chosen and the problems experienced in using them.

4.4.1 Magnetometer

Magnetic Field Measurements

A number of students [25, 57] at the University of Stellenbosch have made use of the Honeywell HMC2003 three axis magnetometer. Since it has proved to be a sensor offering high accuracy, it was the sensor of choice to determine heading.

For high accuracy magnetic field measurements, a set/reset pulse is required to re-align the Magneto Resistive Crystals of the sensor [23]. A circuit was built and tested to perform the set/reset function. It was found that the crystal alignment errors did not dominate the calculated heading error and the circuit was therefore not used during flight testing.

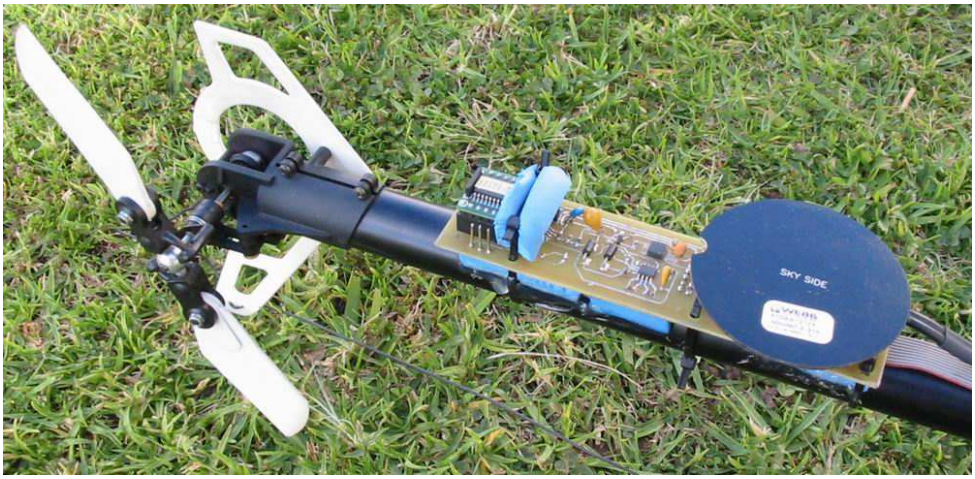

Figure 4.5: *Developed HMC2003 three axis magnetometer sensor system and GPS receiver antenna mounted on tail boom*

The PCB of the magnetometer sensor was designed to be mounted on the tail boom of the helicopter (see figure 4.5) to provide good separation from the electric motor, ferrous metals and other electronics. The PCB was also designed to provide space for mounting the GPS receiver antenna.

Heading Angle Calculation

The magnetic heading of the helicopter is calculated from equation 3.43. According to the calculations of the National Geophysical Data Center (NGDC) of the National Oceanic and Atmospheric Administration (NOAA), the magnetic declination in Stellenbosch was 22° and 25 min West and the inclination 65° and 36 min up on 9 January 2004. Thus, roughly 22.5° needs to be subtracted from the magnetic bearing to give the true heading.

The four primary factors contributing to errors in heading calculations are:

- Inaccurate corrections for pitch and roll angles of the sensor,
- Calibration errors,
- Hard iron, and
- Soft iron effects.

The sensor measurements proved to be sufficiently accurate to obtain heading estimates within ±10° during flight - even though only rough pitch and roll angle estimates were available. The output resolution and accuracy is sufficiently accurate for stabilising a helicopter in hover and performing near-hover flights.

The resolution and accuracy of the magnetic field measurements (and therefore the calculated heading) can be improved significantly by using a 12-bit or 16-bit ADC and higher accuracy pitch and roll angle corrections [9].

In near-hover flight a simple complementary filter can be used to fuse the measurements from the magnetometer and the yaw rate gyroscope to give a higher yaw sensor bandwidth.

4.4.2 Ultrasonic Range Sensor

The Polaroid 6500 ultrasonic sensor is commonly used as a height meter, in conjunction with DGPS receiver systems, by teams participating in the IARC. Due to the popularity, low price, low weight and quality of the sensor, this sensor was chosen as a low altitude ($< 10\,\mathrm{m}$) sensor. Table 4.4 summarises the properties of the Polaroid sensor.

Aaron Kahn [28] describes the sensitivity of the sensor to vibration and provides a detailed description of the mounting that he used to mount two Polaroid sensors on the 0.60 size X-Cell helicopter of Georgia Institute of Technology.

Table 4.4: *Polaroid 6500 ultrasonic sensor*

	Value	Units
Minimum range	0.4	m
Maximum range	9	m
Resolution	< 1	cm
Update rate	10	Hz
Cost	≈ 57	US$

In spite of precautions taken by the author, erratic response was intermittently observed: during some flights it was impossible to measure altitudes exceeding 1 metre above ground level (AGL). The mounting was changed a number of times and yet the problem persisted. The helicopter was dismantled in an attempt to identify the cause of the erratic measurements. The problem was identified to be the location of the Polaroid decoder board: the board had to be moved relative to the battery of the helicopter. Moving the board solved the problem and the sensor has been providing measurements over the altitude range since the alteration.

Although the sensor will reliably provide measurements, the measurements are sometimes noisy and needs to be filtered. Figure 4.6 provides an example of what are now considered to be reasonably good altitude measurements while figure 4.7 is regarded as an unusually noisy set of height measurements.

In section 2.4.1 figure 2.2 is an example of a main rotor collective step command. It can be seen that the differences between consecutive altitude measurements are smooth during the first section of the step command, but only up to approximately 3.5 m AGL, from where on the difference contains increased noise levels. The noise on the height measurements is a function of the vibrations of the helicopter and the terrain beneath it.

It is important to be able to measure the climb rate to be able to control the altitude of the helicopter accurately. During some flights the climb rate had to be filtered, while during other flights no filtering was required. The vibration levels of the airframe as well as the reflection surface are two important factors that influence the performance of the sensor.

For future work it is recommended that an estimator using measurements from the ultrasonic range sensor and the accelerometers, be investigated. Although the ultrasonic sensor succeeded in measuring the height accurately during most indoor flights, the outdoor climb rate estimates could be improved on by utilising additional sensors to estimate the climb rate [1, 6].

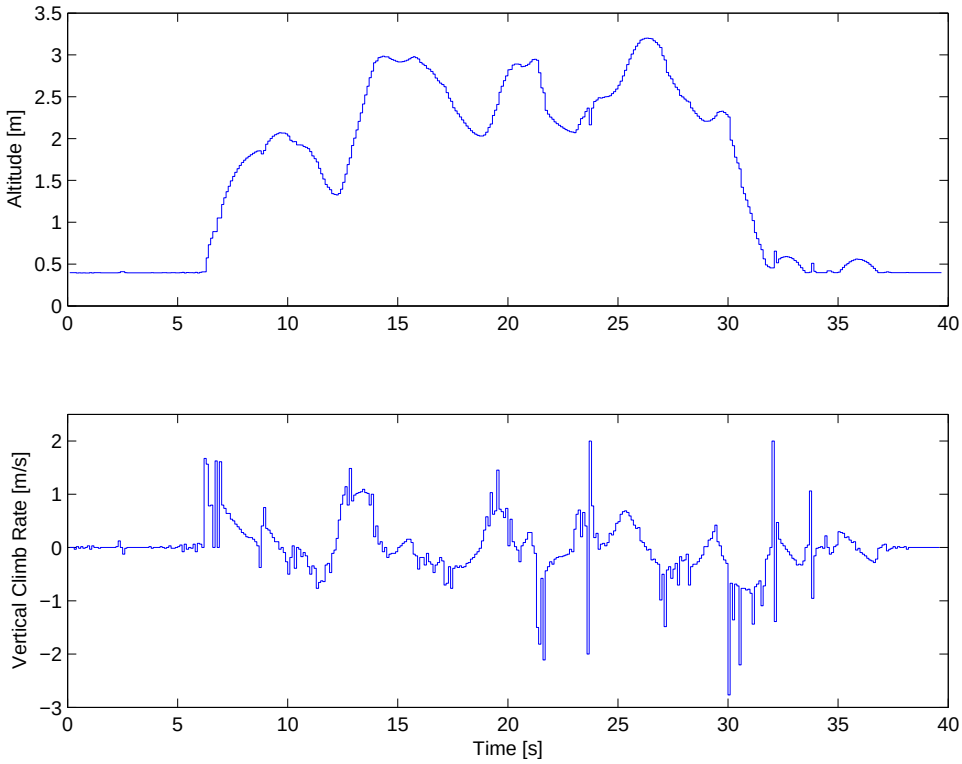

Figure 4.6: *Ultrasonic altitude measurement with average mechanical vibration*

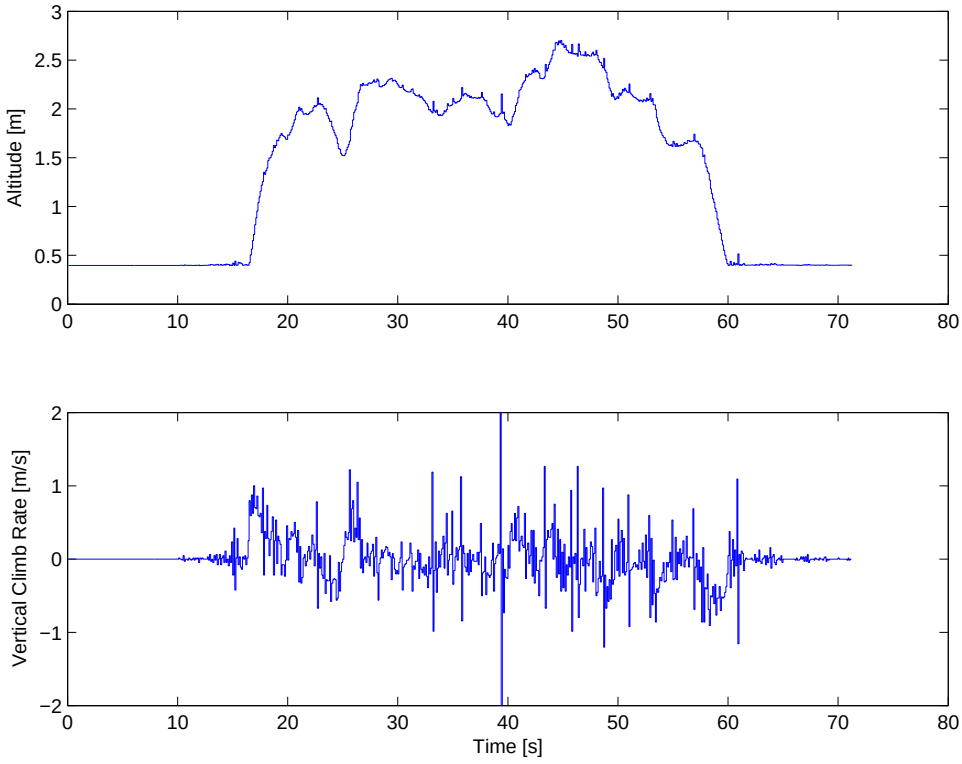

Figure 4.7: *Ultrasonic altitude measurement with high mechanical vibration*

4.4.3 Accelerometer and Rate Gyroscope Selection

Accelerometer Selection

The number of small accelerometers that are locally available at a reasonable price is limited. The Analog Devices ADXL accelerometers offer good value for money, are easy to obtain and are small. Most low cost (< US$ 1 000) IMU and autopilots make use of the Analog Devices accelerometers, for example O-Navi [46], MGL Avionics [31], Cloud Cap Technology [64], Rotomotion [26], Microstrain [2] and MicroPilot [38].

Table 4.5: *Analog Devices ADXL202 accelerometer properties*

	Value	Units
Range	±2	g
Supply voltage	5	V
Bias voltage	2.5	V
Scale factor	312	mV/g
Cost	≈ 16	US$
Unfiltered Bandwidth	6	kHz

Rate Gyroscope Selection

Due to the payload constraints, most rate gyroscopes, IMU and AHRS units used in similar projects were not only too expensive, but too heavy to be used as inertial sensors. Table 4.6 lists the most popular sensors that have been used by competitors in the IARC and other RC helicopter projects.

Table 4.6: *Examples of IMUs and rate gyroscopes used by other research groups*

Rate Gyroscope	Group	Comments
Murata ENV5	MARVIN	not available
Murata ENC3	CSIRO	low quality
Microstrain IMU	WARG	small, but medium price
BOEING DQI-NP INS/GPS	Berkeley	too heavy and expensive
ISIS-IMU	MIT, Gatech	too heavy and expensive
CrossBow VGX IMU	USC	too heavy and expensive

The decision had to be made whether to buy an IMU or individual sensors. The main advantage of buying an assembled unit is the development time saved for the relatively

small price difference between individual sensors and an assembled unit. The sensors were narrowed down to two IMU's: the Rotomotion IMU (using Tokin CG-16D rate gyroscopes) and the MicroStrain IMU (using Murata ENC3 rate gyroscopes at the time). The Microstrain IMU was four times more expensive than the Rotomotion IMU. At the time no other available rate gyroscope sensors offered significantly better quality than the Tokin CG-16D rate gyroscopes. The reduced development time made it worthwhile buying an assembled unit, rather than building an IMU using similar quality sensors. Unlike most other AHRS and IMU units, the source code for the Rotomotion IMU was available.

A few months after the Rotomotion IMU was bought, Analog Devices began shipping the first samples of the ADXRS150 rate gyroscopes. Since the third quarter of 2003 these sensors have become tremendously popular. Manufacturers like Cloud Cap [64], Microstrain [2] and MicroPilot [38] have changed existing products to utilise the ADXRS rate gyroscope sensors, replacing existing sensors on award-winning products. After extensive testing of the Rotomotion IMU, the author acquired two ADXRS150 rate gyroscopes from MGL Avionics [31] in March 2004. The bias stability, scaling and linearity of the Analog Devices rate gyroscopes proved to be superior to any of the other rate gyroscopes in this price class.

The bias drift of both the Tokin and Analog Devices rate gyroscopes are poorly described by the manufacturers. The only bias specification provided in the datasheet of the Tokin CG-16D sensor states that the zero rate of the sensor is $\pm 300\,\text{mV}$ at 25°C. Whether the specification indicates the drift of a single sensor over time or the maximum offset of any randomly selected sensor, is not clear. It has been found that the zero rate voltage offset can exceed the full scale voltage range of the sensor ($\pm 99\,\text{mV}$). Drift rates in the order of $0.26°/\text{s}$ over one minute have been recorded in an environment without significant temperature changes.

The datasheet of the Analog Devices sensor only provides a specification of the temperature related bias drift of the sensor. Drift rates in the order of $0.07°/\text{s}$ over one minute have been reported for the Analog Devices ADXRS150 [31].

4.4.4 Rotomotion IMU

A Rotomotion IMU was acquired and the majority of flight tests were performed using it. The IMU utilises three Tokin CG-16D rate gyroscopes and two two-axis Analog Devices ADXL202 accelerometers, forming a triad of accelerometers.

Table 4.7: *Tokin CG-16D and Analog Devices ADXRS150 rate gyroscopes*

	Tokin CG-16D	ADXRS150	Units
Range	±90	±150	°/s
Supply voltage	5	5	V
Bias voltage	2.4	2.5	V
Scale factor	1.1	12.5	mV/°/s
Bandwidth	100	40	Hz
Cost	≈ 25	≈ 72	US$

A number of problems had to be solved and precautions taken to obtain maximum accuracy from the Rotomotion IMU:

- Vibration isolation mounting
- Low pass filter cut-off frequency
- Order of low pass filters
- Sampling rate
- Amplification of rate gyroscope signals
- Temperature insulation
- Supply voltage regulation

As an initial test, the IMU was rigidly strapped to the frame of the helicopter without any mechanical vibration isolation. The main rotor blade frequency could be measured using the rate gyroscopes, but not by the accelerometers. The reading from the accelerometers showed a bias movement, but no high (≈ 25 Hz) frequency content. The IMU was then mounted onto a 300 g aluminium block which was mounted onto a piece of closed cell foam, and the foam then mounted onto the frame. With the new mounting, the vibrations could also be measured using the accelerometers.

Closed cell foam was used as a first layer of insulation (see figure 4.8). The improvements were immediately visible. The largest components of vibration corresponded with the expected frequency of the main rotor ($23 - 26$ Hz) and the first and second harmonics of the main rotor blade rotation speed [15, 21]. In order to prevent aliasing, the sampling frequency was chosen as 112 Hz for initial vibration isolation tests.

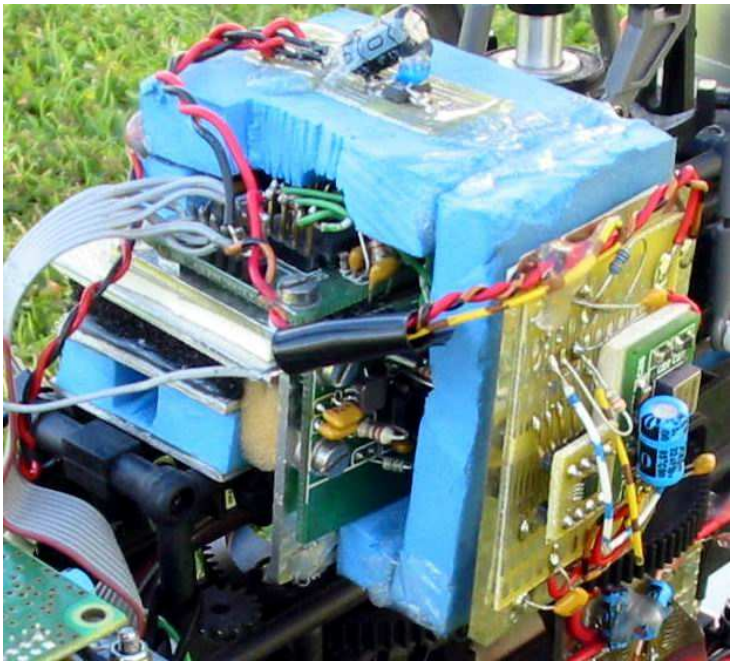

Figure 4.8: *Rotomotion IMU mounted in and on closed cell foam*

From these tests it became clear that the 50 Hz and 72 Hz cut-off frequencies of the accelerometer and rate gyroscope low pass filters were too high for this application. The −3 dB cut-off was moved to 7 Hz for the rate gyroscopes and 10 Hz for the accelerometers. The frequency contents of the pitch and roll rate gyroscope signals are presented in figure 4.9, using the original 7 cell battery pack and original Rotomotion IMU and filters. Figure 4.10 displays the results obtained once the cut-off frequencies of the filters were lowered, and an 8 cell battery pack was used. The increased main rotor speed ($17 - 25$ Hz) and less movement due to the servo rotor ($3 - 4$ Hz) can be noted between the two figures. Although the amplitude of the main rotor frequency is slightly higher in figure 4.10, the most important change is the reduced amplitude of all frequencies above the Nyquist frequency of 30 Hz for the intended sampling rate of 60 Hz. As an additional counter measure, the first and second order low pass filters between the microcontroller ADC board and the sensors were increased to third and fourth order low pass filters.

It is possible that the mechanical filtering that was used by Rotomotion provided sufficient mechanical low pass filtering of the vibrations and thus less harsh signal conditioning was required. The much higher weight (≈ 3 kg) of the Rotomotion box, carrying the sensors and processors, could have provided sufficient vibration isolation.

The IMU was bought as a unit that outputs serial data from its AVR microcontroller. The 10-bit AVR ADC is used to sample the Tokin rate gyroscopes. The Tokin sensors have a nominal sensitivity of 1.1 mV/°/s. To make maximum use of the 4.88 mV increments

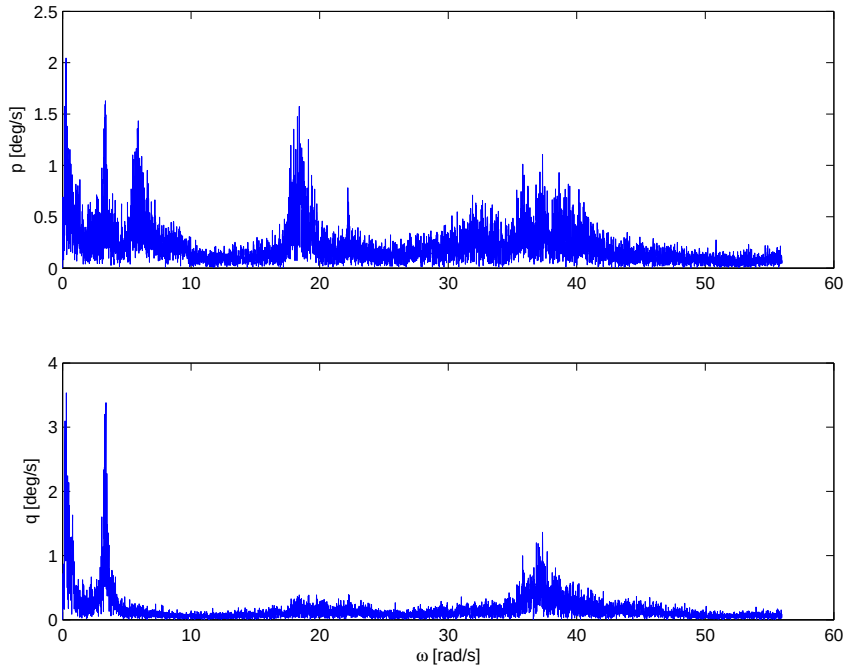

Figure 4.9: *Rotomotion IMU measurements using standard filtering and 7 cell battery*

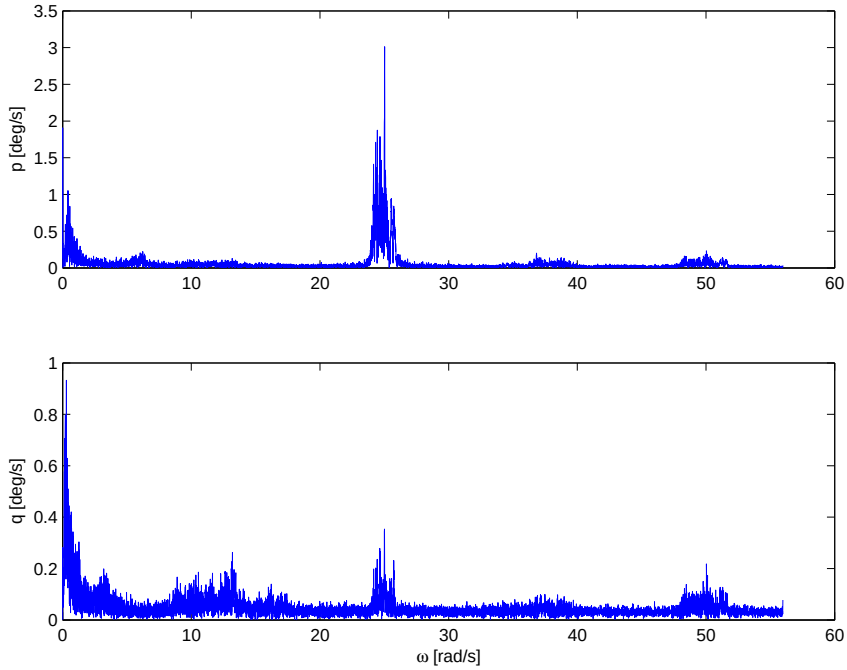

Figure 4.10: *Rotomotion IMU measurements after first changes to filters and 8 cell battery*

of the 10-bit AVR microcontroller ADC, the gain of the signal conditioning amplifiers used between the Tokin rate gyroscopes and the 10-bit AVR ADC was increased from 4.7 to 10. The increased gain had the desired effect of increasing the resolution from 0.94°/sec/bit to 0.44°/sec/bit, but also amplified the bias drift of the sensors. The bias movement of the Tokin rate gyroscope sensors is significant if the rate gyroscope is exposed to ambient temperature changes. Closed cell foam was used to protect the rate gyroscopes from direct sunlight exposure and main rotor blade downwash (see figure 4.8). Covering the rate gyroscopes in closed cell foam successfully reduced the sensor bias response to ambient temperature changes.

Rotomotion used a resistor network to provide a 2.5 V reference for the accelerometers. The output of the accelerometer amplifiers intermittently contained high frequency noise components. Adding a separate voltage regulator to the sensor board solved the problem.

A number of the problems encountered were due to inadequate protection of the inertial sensors against temperature fluctuations and vibrations. If it were possible to mount a large, heavy sensor and processor box, mounted on rubber dampers, some of the above mentioned problems might never have occurred. Due to the payload and space constraints of the helicopter, it was not possible to mount the sensors and other electronics as a single unit.

Rate gyroscope measurements taken indoors without the motor running can be seen in figure 4.11. The rate gyroscopes were switched on for more than 10 minutes before the measurements were taken. In figure 4.11 the bias of the roll rate gyroscope drifted roughly 0.26°/s in one minute. The quantisation of 0.44°/s can also be seen.

In spite of the changes made to the Rotomotion hardware, the resolution and bias drift of the Tokin rate gyroscopes after signal conditioning remained poor. The results obtained using the Rotomotion sensor and Kahn-Hudson EKF combination will be described in more detail in section 7.3.1. Alternative sensors and methods to determine pitch and roll angles were investigated.

4.4.5 Analog Devices Rate Gyroscopes

When the Analog Devices ADXRS150 rate gyroscopes became available, these sensors were acquired as alternative rate sensors. The Analog Devices rate gyroscopes were ultimately used in the state estimator that stabilised the longitudinal motion of the helicopter.

Due to the bias drift and the scaling factor of the Tokin rate gyroscopes it was not possible to increase the resolution of the rate gyroscopes without numerous modifications

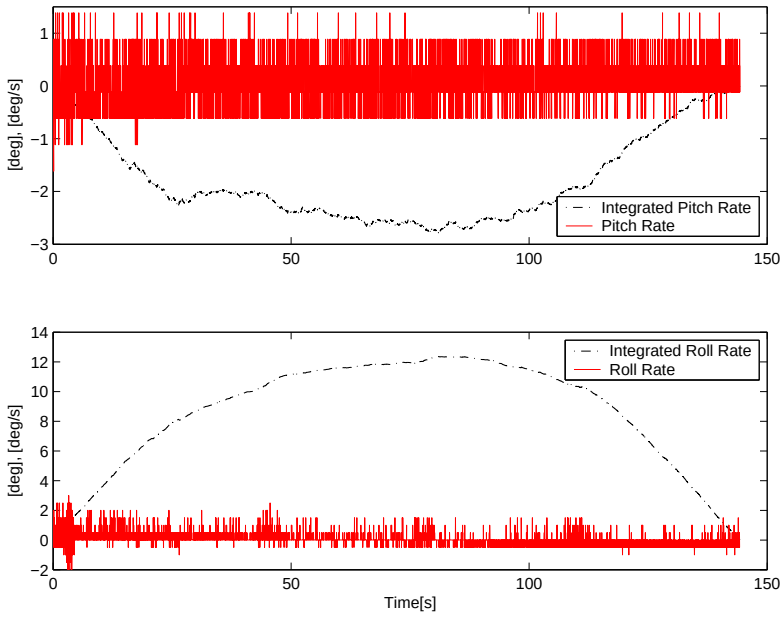

Figure 4.11: *Tokin CG16-D rate gyroscope measurements on stationary vehicle with no vibration*

to the existing PCB. The most time effective method to incorporate the ADXRS sensor was to add an operational amplifier to scale the output of the Analog Devices rate gyroscope to give $\pm 70°/s$ range over the 10-bit ADC range.

The two main advantages of the Analog Devices sensors for this project proved to be:

1. bias stability and
2. analog output voltage range scaling.

It is recommended that a higher resolution ADC (external to the microcontroller) and higher sampling rates be used in future[5]. It is also recommended that a dedicated microcontroller be used to manage the IMU sampling and processing.

4.4.6 Global Positioning System Receivers

The NovAtel RT-2 DGPS is available to IARC participants at a special price of US$ 2 700. The high update rate (up to 20 Hz) and position accuracy (2 cm) makes this differential GPS receiver system the system of choice for teams that can afford it.

[5]Rotomotion has made similar changes to its new version of the IMU during the last year [26].

MIT makes use of a NovAtel Superstar GPS receiver (but an extremely high quality IMU) while Rotomotion and CSIRO are making use of the u-Blox TIM-LP GPS receivers. CSIRO is using the u-Blox GPS receiver with WAAS correction [52]. Table 4.8 compares a number of GPS receivers based on manufacturer provided specifications.

Table 4.8: *Comparison of GPS receiver properties*

	Sigtec	u-Blox	NovAtel	NovAtel	Units
Model	MG5001	TIM-LP	Superstar II	RT-2 DGPS	-
CEP (95 %)	5	2.5 (50%)	5	0.002	m
Velocity Accuracy	0.1	n.a.	0.05	0.03	m/s
Maximum update rate	1	4	5	20	Hz
Cost	100	70	200	> 2700	US$

Benjamin Nortier, a previous student, used the Sigtec Navigation MG5001 GPS receiver for his thesis work [45]. The hardware from Nortier's project was used for initial GPS tests.

Sigtec Navigation GPS Receiver Walking Tests

The Sigtec GPS receiver was evaluated by walking known routes while recording the GPS receiver position fixes and velocity measurements. It was found that if the average of the position measurements at the start and finish points of a straight line were recorded over a 30 s period of time, a 100 m distance could typically be measured to within less than ±3 m error.

The length and direction of straight line segments were also measured using the integrated velocity measurements. Typical errors of ±5 m were accumulated over a 100 m distance, when walking at a slow varying pace of between 1 m/s to 3 m/s. Figure 4.12 presents an example of one of the walking tests where the GPS receiver position fixes and integrated velocity measurements were recorded. The tests were performed with the GPS receiver mounted on the helicopter, with all of the other subsystems operational, except the engine. The GPS receiver data was recorded on a laptop via the modified 2.4 GHz RF communication link.

From figure 4.12 it can be seen that the position and integrated velocity measurements matched well if distances in excess of a few metres were covered. The tests do not however provide information regarding the time delay of the measurements. Furthermore, the movement pace and direction was slow varying (accept the direction changes at the

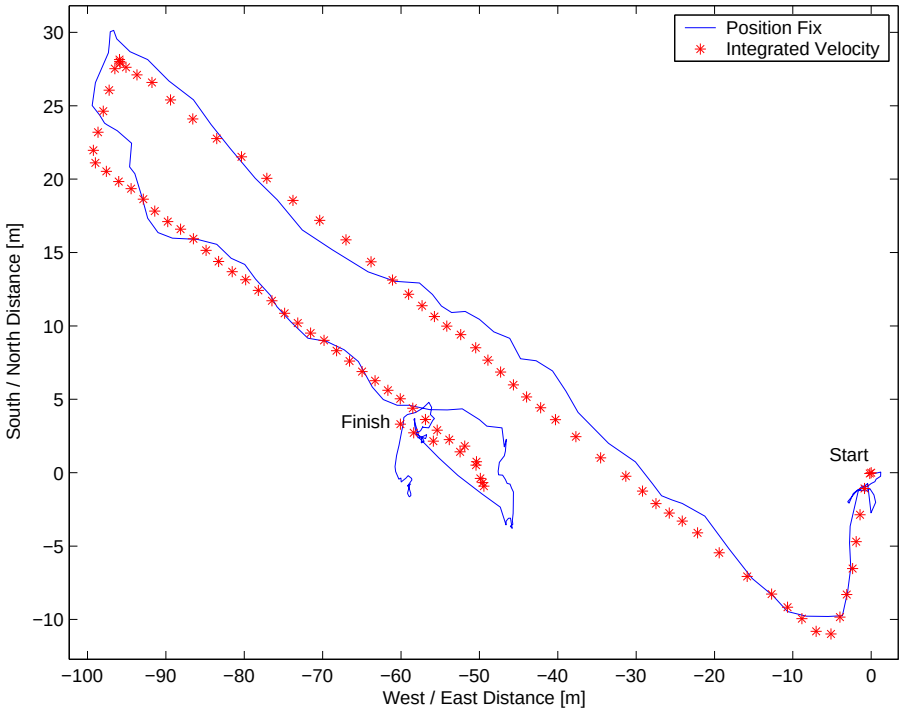

Figure 4.12: *Position fixes and integrated velocity measurements during walking test using Sigtec GPS receiver*

corners) and the walking speed significantly faster than the speed of a hovering helicopter ($< 0.2\,\mathrm{m/s}$).

After these tests were conducted, five months were dedicated to flight tests during which various estimators were tested in realtime and in post-processing. None of the filters succeeded in describing the horizontal motion of the helicopter, using the Sigtec GPS receiver and Rotomotion IMU measurements.

Sigtec Navigation GPS Receiver Pivoting Pole Test

A pivoting pole test bed was constructed to identify the properties of a GPS receiver more accurately. The test is based on work done by Sanghyuk Park [48] at MIT. A GPS receiver antenna was mounted on a 2.7 m long pole that could be swivelled by hand about a fixed axle, while a potentiometer measured the rotation angle of the pole. Knowing the length and the rotation angle of the pole, the velocity of the tip of the pole could be calculated from the potentiometer measurements. Figure 4.13 provides an example of the results obtained using the Sigtec MG5001 GPS receiver during the pivoting pole tests.

The pivoting pole tests provide more information regarding the sensitivity, delay and accuracy of the GPS velocity measurements than the walking tests. If the Sigtec Navi-

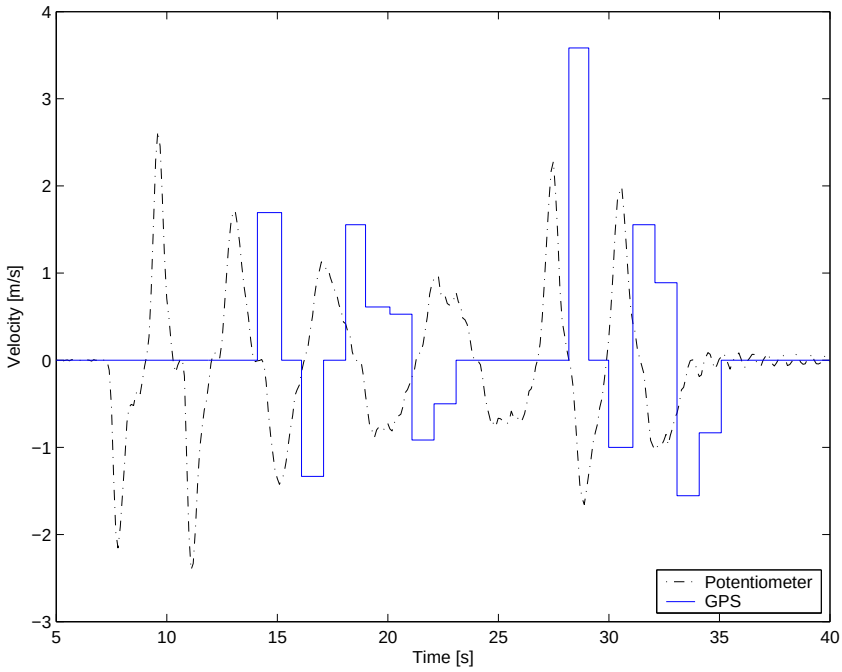

Figure 4.13: *Sigtec MG5001 GPS receiver measured and potentiometer calculated velocity during pivoting pole test*

gation GPS receiver velocity measurements in figure 4.13 are shifted left with one to two seconds, similarities are seen between the potentiometer and GPS measured velocities. A number of the potentiometer measured movements are, however, not visible from the GPS measurements. At time 21 s and 24 s velocities of amplitude ± 0.7 m/s are calculated from the potentiometer measurements. Neither movements are visible from the GPS measurements, even though each movement lasts for approximately two seconds.

After extensive testing of the Sigtec Navigation GPS receiver, a u-Blox GPS receiver was acquired and used during the last five months of the project. The superior quality of the u-Blox has been proved during flight and ground based tests.

u-Blox GPS Receiver

The pivoting pole tests were repeated using the u-Blox GPS receiver. An example of the test results obtained using the u-Blox receiver are presented in figure 4.14.

The velocity measurements from the u-Blox followed the potentiometer measured velocities closely with a delay of approximately 310 ms. The u-Blox GPS receiver provided a more realistic measurement of the GPS antenna velocity than what was obtained using the Sigtec Navigation GPS receiver. Different frequency movements were applied to the

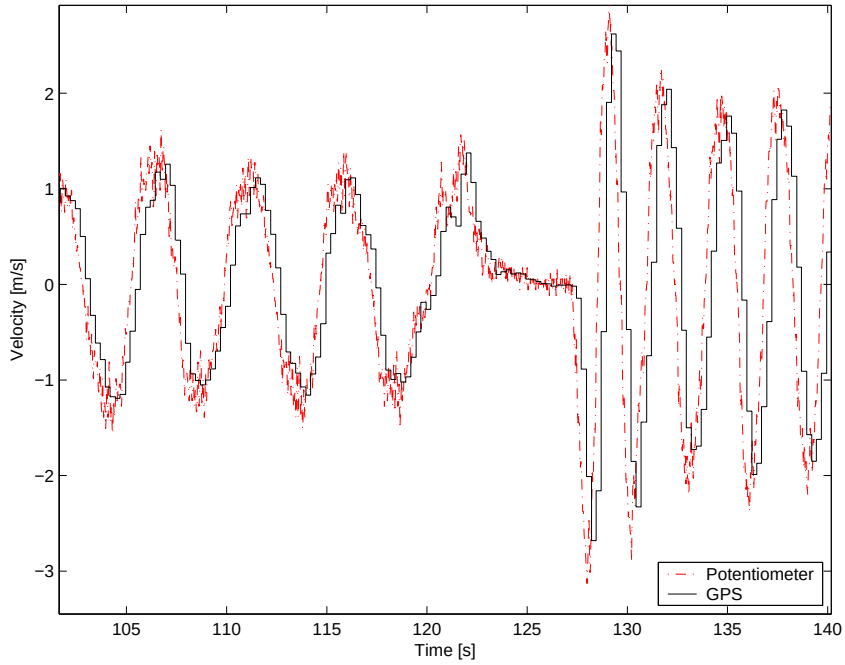

Figure 4.14: *u-Blox GPS receiver measured and potentiometer calculated velocity during pivoting pole test*

pole and were all measured reliably by the u-Blox GPS receiver.

The pivoting pole tests yielded equally poor position measurements for both the Sigtec and the u-Blox GPS receiver units. A simplistic attempt at constructing a DGPS using two receivers was not successful.

In figure 4.15 the integral of the velocity measurements is compared to the position measurements from a u-Blox GPS receiver. The measurements were taken over a three minute time period while the helicopter was switched off and stationary on the ground. The GPS measured West-East movement is approximately 3 m and the North-South movement 8 m. The integrated velocity measurements are contained within a circle with a radius of approximately 0.3 m.

A filter combining the GPS position and integrated velocity measurements was implemented and tested. The filter did not perform better than using only the integrated velocity measurements, because of the small distances covered (flight radius < 20 m) and the short flight length (flight duration < 3 min). The GPS position measurements drift at up to 0.9 m/s within an error radius of 3 to 5 m.

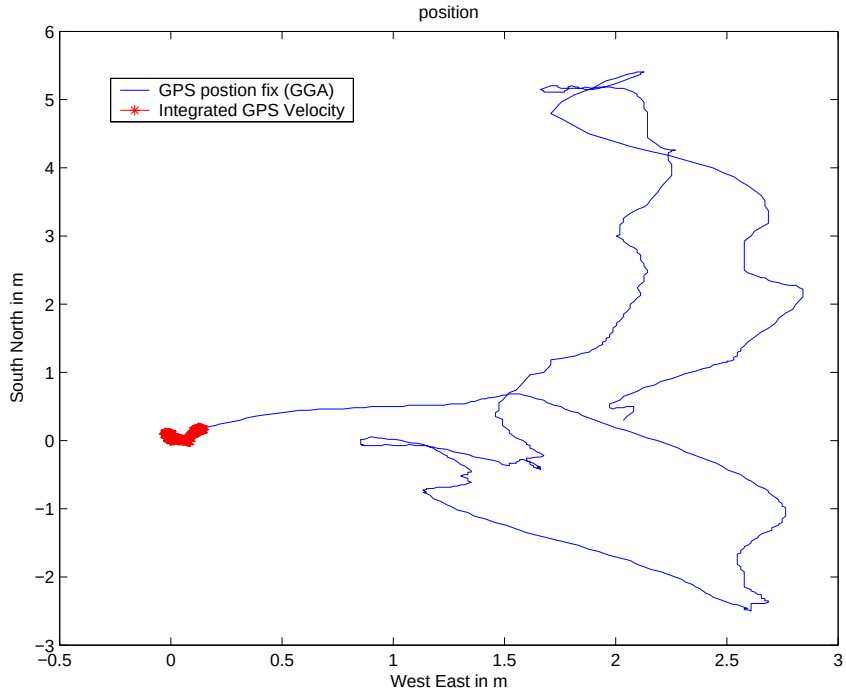

Figure 4.15: *Stationary u-Blox GPS receiver position and integrated velocity measurements*

GPS Antenna Used

The same active antenna was used with both the Sigtec Navigation and the u-Blox GPS receiver. The antennas are sold with three metre long cables. The specific antenna used had two long cables: one from the active GPS antenna and one from the passive GSM antenna. The GPS cable was shortened to 300 mm and the GSM cable to 40 mm. The GPS cable was terminated using a MCX connector. The GPS receiver did however not provide a position fix after the cable was shortened. It was found that reducing the gain by adding losses solved the problem. The necessary losses were added by cutting and removing a section from the cable, and soldering the remaining two ends together. Both the Sigtec and the u-Blox GPS receivers have been able to provide position solutions since losses were added to the shortened GPS receiver antenna cable.

u-Blox warns customers against incorrect shortening of cables and insufficient size antenna ground planes [63]. The antennas used were the only locally available active GPS antennas. Although the GPS receivers provide position fixes using the modified antenna, the quality of the solution might be influenced by the quality of the antenna.

Although the pivoting pole tests have yielded promising results, the antennas used on the helicopter and pole differ. It is possible that the antenna, the size of the ground plane

of the antenna, vibrations or EMI might be degrading the solutions when the helicopter is flying under full load.

The u-Blox GPS receiver was obtained five months before the completion date of the project and limited time could be invested in flight testing using the GPS receiver. The results obtained using the GPS receiver look promising even though the position measurements are poor compared to the differentially corrected GPS position measurement systems used by other research groups.

4.4.7 Position Tracking using a Camera System

Attempts to control the helicopter using the measurements from the Rotomotion IMU and the Sigtec MG5001 GPS receiver were not successful. Before receiving the u-Blox GPS receiver, it was decided to replace the Sigtec GPS receiver with a position measurement system that was developed by Prof. W.H. Steyn.

A high intensity light source was fitted to the helicopter and a stationary camera then aimed in the direction of the helicopter. The position of the helicopter was determined by tracking the high intensity light source using a PC that receives images from the camera.

The camera system was successfully integrated into the helicopter FCS. After some initial flight testing Prof. Steyn adapted the software to increase the maximum velocity that the system is capable of tracking.

However, the u-Blox GPS receiver became available before the updated code was used during test flights. Due to time limitations and the promising results obtained using the u-Blox GPS receiver, the camera system running the updated code was never used to control the helicopter during a flight test. The technology however remains a viable sensor to control the helicopter (indoors and outdoors) within confined space. The absolute position resolution is in the same order of magnitude as what is offered by the best DGPS systems, at an relatively high update frequency of approximately 5.5 Hz.

4.5 Data Communication Links

4.5.1 Helicopter to Ground/Control Station RF Link

A data link was required to send the sensor data from the helicopter to the ground station (see figure 4.1). Size, weight, price, baud rate and availability were the main

factors considered in choosing the transmitter module. The range of operation was not an important consideration in selecting a transmitter since the safety pilot would struggle to fly the small helicopter beyond a range of 70 m.

Most transmitter/receiver pairs were found to be too big and heavy for the application. Due to the small amount of ground clearance, and the rotor blades rotating above the fuselage, mounting a vertical "whip" antenna was not an option.

Reliability and a high baud rate (115 200 baud) were of utmost importance to reduce risks and latency. A 2.4 GHz video transmitter and receiver set was modified and used as a communication link between the helicopter and the ground station.

Table 4.9: *Helicopter to ground station data transmitter*

	Value	Units
Module	2.4 GHz audio/video TX	-
Transmitter Power	100	mW
Size (excluding antenna)	$8 \times 29 \times 41$	mm
Weight (including antenna)	38.2	g
Cost	90	US$
Baudrate	115 200	baud
Range (LOS available)	> 100	m

A signal generator and oscilloscope were used to test the time response of the transmitter/receiver pair.

The data slicer is the component that converts an analog signal into a digital signal: it discriminates between a high and a low bit. Most data slicers require that the number of high and low states are fairly well balanced (a ratio of, for example, no lower than 30 percent to 70 percent), or that a start-up sequence be used to initialise the data slicer. The application required very short data packets, sent as fast as possible, with as little overhead as possible. The packets were padded with the hexadecimal number "A" (binary number "1010"), significantly improving the quality of the results obtained from the data slicer due to the constant stimulation of the slicer. The ground station ignores these padding numbers.

The transmitter was found to be sensitive to vibrations. The frequency selector switch was removed (soldered to a fixed position), a hot silicon glue ("gluegun") was applied to the electrolytic capacitors and tuneable inductors and double sided tape were used to reduce the movement of the antenna. It was also found that the receiver module had to be positioned at least 0.5 m above the ground. Following these modifications and

precautions the data reliability improved notably.

One problem remains unsolved. It has been found that the data link performs poorly if the body of the helicopter obstructs the line-of-sight (LOS) between the transmitter antenna on the helicopter and the receiver antenna on the ground. Unfortunately pilots find it easier to fly model helicopters with the tail boom towards them. A temporary solution has been to move the receiver away from the ground station (which has to be located very close to the pilot) and to the side of the helicopter. The allowed movement of the vehicle is further limited to retain LOS between the data transmitter and receiver antennas.

4.5.2 Ground Control Station to Helicopter Data Link

The control signals are sent from the PC to the helicopter via the JR transmitter. No data, except the PPM signals to control the position of the servos, is sent to the helicopter (see figure 4.1). Section 4.3.4 described the advantages, the limitations and implications of using the DSC plug to control the helicopter from a ground station PC. This section will focus on the implications of communicating only PPM signals.

An interface was designed to receive RS232 UART signals from the PC and transmit commands to the JR transmitter at 45.8 Hz. An AVR microcontroller was used to convert the serial (UART) strings from the PC to a PPM pulse train that is fed into the direct servo control (DSC) plug of the JR transmitter.

The JR transmitter system was not designed to receive input signals that were generated by a computer. The synchronisation between measurement and control is complicated by the closed JR transmitter-receiver-servo system. Due to the system configuration, there is no simple way to ensure a constant delay between measurements and actuator movements. The implication is a time-varying time delay between the sensors and the actuators.

To test the delay through the system (from the IMU sensor inputs to the helicopter actuator response), a digital step was applied to an input of the ADC of the IMU microcontroller. The time delay from the ADC input to the JR receiver output was measured to vary between 31 ms and 75 ms (see figure 4.16 for an example of delay measurements). The majority of delays were approximately 53 ms long.

The time delay can be broken up into the follow dominant components:

- IMU input running at 60 Hz will cause a delay of $0 - 16.7$ ms. The uncertainty

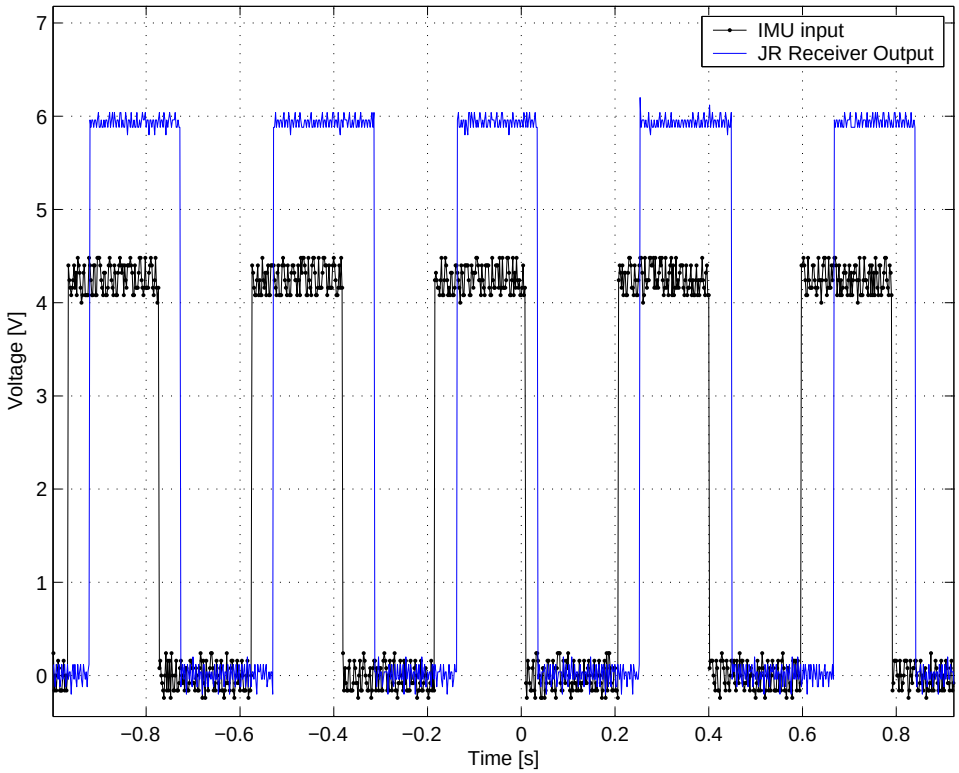

Figure 4.16: *Delay time (time difference between leading edges of pulses) from the IMU ADC input to the JR receiver output*

caused by the microcontroller ADC input could be removed by generating a pulse inside the microcontroller. However, applying the test signal to the ADC inputs ensures that the delay of the microcontroller is included.

- Each of the communication links between the helicopter and ground station PC, and PC to "PC2JR" gray box consume 4.6 ms.
- The "PC2JR" to JR Transmitter and the link from JR Transmitter to servo drivers will each add a $0 - 21.8$ ms delay.

The execution time of the PC and two microcontrollers has been neglected. Little can be done to alter the delays in the system without changing the structure of the system, hardware and software, significantly.

One benefit of using the DSC plug to control the helicopter is that it is simple and reliable to switch between the safety pilot and a computer controller. Even if all developed hardware should fail, there would be no increased risk to the helicopter.

4.6 Conclusion

This chapter has described the hardware purchased and developed for the autonomous RUAV. The circuits are given in appendix D.

The hardware selection was motivated and the results of experimental verification of performance has been given.

The cost and weight restrictions forced selection of many components with performance that is far from ideal, but will be shown in later chapters to be adequate to control the electrically powered helicopter during near-hover flight.

Chapter 5

Software

This chapter describes software that was developed for the onboard microcontrollers, the desktop controller PC and the interface to the RC transmitter. The focus of the chapter will be the structures and methods used to ensure reliable and fast data flow. The Matlab code written to design and test the estimators and controllers can be found on the CD that accompanies the document.

5.1 Onboard Software

The data gathering on the helicopter is distributed between two microcontrollers. The GPS microcontroller handles measurements from sensors with relatively low update frequencies ($\leq 10\,\text{Hz}$). The IMU microcontroller handles other sensors and equipment with higher update rates ($\geq 30\,\text{Hz}$).

The communication between the microcontrollers is one directional - from the GPS microcontroller to the IMU microcontroller. A 115 200 baud UART is used as the communication channel between the microcontrollers. The data is transmitted as ASCII characters with a short header describing the contents of the message, comma separators between values and a carriage return and line feed to indicate the end of a string. The protocol is based on the standard NMEA strings used to transmit data from GPS receivers to other equipment. Although the ASCII characters are on average about double the length required to transmit the data (uncompressed), the protocol has two major advantages over sending raw number values:

- the communication port can be monitored using a simple text terminal which simplifies debugging of modular building blocks; and

- simple, basic error checking: if a number is not within the valid ASCII range of "0" to "F" it has been corrupted, and the string is discarded.

Furthermore, all numbers were transmitted as 16-bit numbers (four hexadecimal ASCII characters) rather than distinguishing between 10-, 12- and 16-bit values. No data compression or error correction was implemented.

All of the AVR software was implemented using the CodeVisionAVR compiler. The CodeWizardAVR application was found to be a very useful tool to fast-track the writing of code for different AVR microcontrollers.

5.1.1 IMU Microcontroller

All data that is gathered onboard the helicopter is transmitted to the ground control station via the IMU microcontroller (see figure 4.4). The main functions of the AVR ATmega128 microcontroller are:

- ADC sample, and transmit the rate gyroscopes, accelerometers and battery voltage at 60 Hz
- Measure the pulse width (PPM signal) from the JR servo driver, and transmit it at 30 Hz
- Receive and transmit magnetometer, GPS and ultrasonic sensor data from the second onboard microcontroller
- Serialise these data strings and feed these to the 2.4 GHz transmitter

The above functions are all interrupt driven. An 8-bit timer generates the interrupts to signal when ADC and servo values have to be transmitted. A rising- and falling edge detection interrupt, coupled to a 16-bit timer, measures the length of the servo pulse widths commanded by the JR receiver. A hardware interrupt is generated every time a byte is transmitted or received and a character (byte) is moved to or from the applicable buffer.

Due to the random data flow to the IMU microcontroller from the GPS microcontroller, a second buffer was added. Data from the GPS microcontroller is captured in the second buffer, and moved to the primary buffer as soon as the complete string has been received and the primary buffer is empty.

The scheme has proved to be simple, reliable and fast, containing minimal overhead. The maximum baudrate at which most standard PC UART Communications ports can transmit and receive data (115 200 baud) was used. The communications time delay between the microcontroller and the PC was found to be small compared to, for example, the time delay between the PC and the servos.

Once again, although the microcontrollers have SPI hardware, neither the speed advantage nor the complexity disadvantage made it worthwhile using SPI to communicate between microcontrollers. A second hardware UART was available on the microcontroller but never used. It would be possible to transmit and receive data to and from a data link via this UART - if the payload constraints permitted it.

5.1.2 GPS Microcontroller

The second AVR (ATmega16) microcontroller controls and processes the data from the sensors operating sampling rates of 10 Hz and lower. The functions of the microcontroller can be summarised as follows:

- ADC sample the magnetometer voltages at 10 Hz
- Command the ultrasonic sensor at 10 Hz and measure the return time of the ultrasonic echo using a 16-bit timer
- Receive the GPS strings from the u-Blox GPS receiver, remove unnecessary information, and transmit the velocity, heading, position and other information at 4 Hz
- Transmit all of this data to the IMU microcontroller

The functions were implemented in a similar fashion to the way the functions on the IMU microcontroller were implemented.

5.2 Ground Control Station Processor and Software

This section provides an overview of the software developed for the ground control station software. A summary of typical processor hardware and operating systems used for the purpose of controlling RC helicopters is also provided.

5.2.1 Processor and Operating System

With the exception of one project, all successful International Aerial Robotics Competition (IARC) participants are making use of 32-bit processors (typically PC-104 stacked Intel or AMD processors, or ARM processors) onboard to perform the control and estimation functions. Furthermore, realtime operating systems (RTOS) such as the very popular QNX are used by many contenders.

The project of the Technical University of Berlin ("MARVIN") is the one exception to the rule. "MARVIN" is flying with an Infineon (formerly Siemens) SAB80C167 16-bit microcontroller as its core processor. The Technical University of Berlin has been one of the few teams not making use of high order (11 or higher) Kalman filters to perform state estimation [43]. Since the team won the 1999 and 2000 IARC competition, they are respected competitors.

Due to the limited payload, a powerful (32-bit) onboard processor board could not be utilised. A standard desktop PC was used to run the controller software on the ground, making it easy to alter the control algorithms and store flight data. Due to the lack of knowledge and experience using realtime operating systems in the ESL, Windows 95 and Windows XP were used even though these are not realtime operating systems. The delays caused by the operating system were found to be negligible compared to the delays caused by the JR transmitter system.

The DevCpp freeware compiler was selected to write the code for the desktop PC due to the project supervisor's preference and experience using the compiler. Since maximum reliability and minimum latency were of utmost importance, no graphics interface was developed to run on the PC that was used to implement the controller difference equations.

5.2.2 PC Software

The majority of the processing power is used to gather data from the helicopter and perform state estimation. A simple set of procedural routines was developed to handle the flow of data and control the helicopter. The code running on the PC was broken up into four files:

main: The main routine is described by the flow chart in figure 5.1.

proc_str: All of the data received from the helicopter and the position tracking camera is captured and decomposed by the `process_str()` routine.

kalman: This contains the Kahn-Hudson EKF code that determines the attitude of the vehicle. All of the EKF code is in the `kalman.cpp` and `kalman.h` files. A separate 'C' structure is used to store the values calculated using the EKF.

control: This contains a routine to write the servo control commands to the UART communications port. The file `control.h` also contains two structures that describe the states of the helicopter and the servo setup (positions, limits, channels).

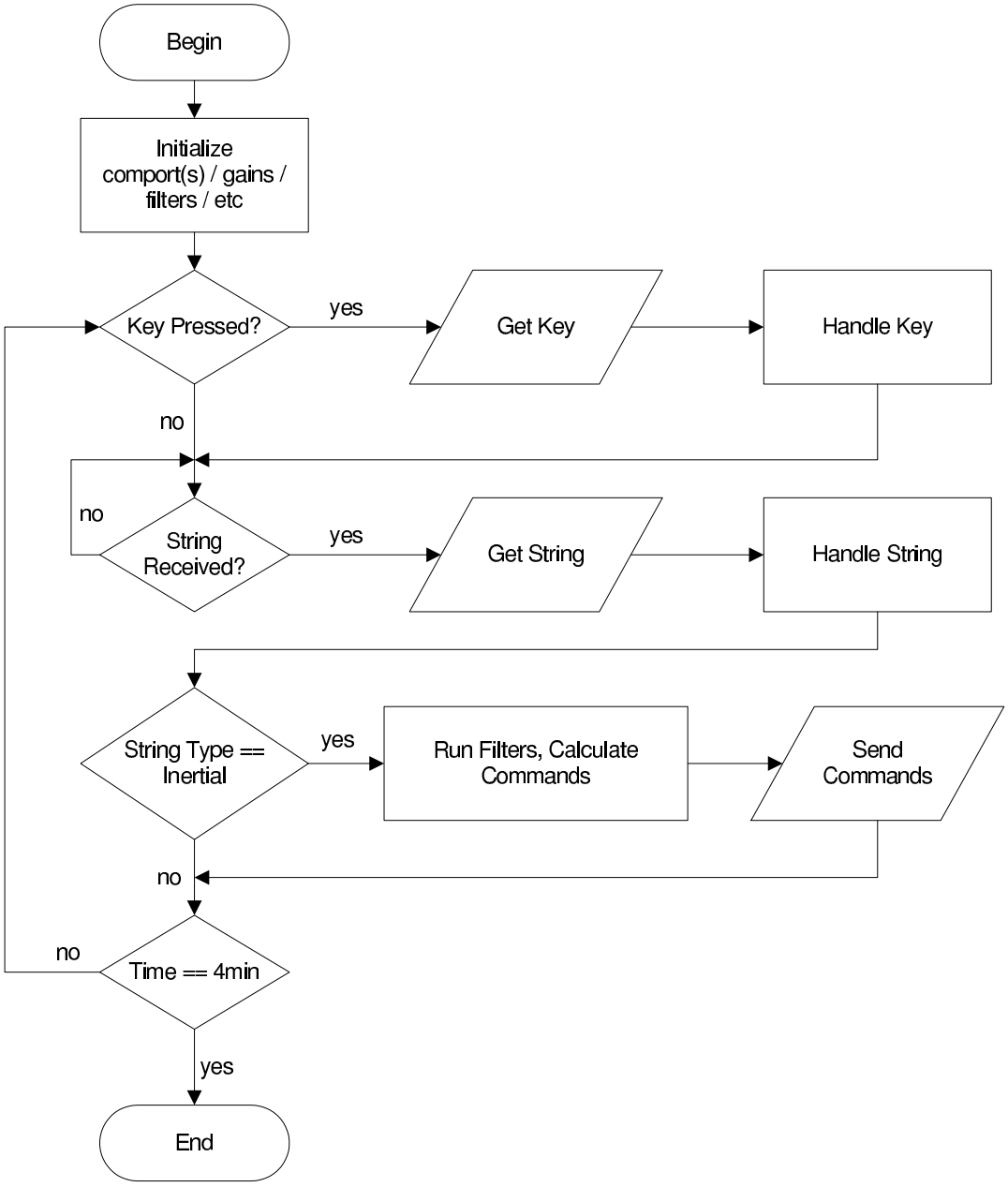

Figure 5.1: *PC software high level flow chart*

5.3 PC to JR Radio-Control Transmitter Interface

An Atmel AVR 90S2313 microcontroller was used to create an interface between the PC running the controller code and the RC transmitter.

The Pentium I (120 MHz) initially used to control the helicopter was equipped with only one communications port, therefore the PC to RC transmitter interface was designed to share a PC UART communications port with the data receiver from the helicopter. Only one PC communications port is required to transmit commands to the helicopter and receive data from the helicopter.

Chapter 6

Control Law Design and Simulation

An RC helicopter is a highly non-linear, multi-input multi-output (MIMO), unstable system, capable of extreme three dimensional aerobatic manoeuvres. However, in spite of the cross coupling existing between the states of the helicopter, a number of projects [1, 6, 11, 35, 41, 56] have demonstrated that RC helicopters can be controlled successfully using multiple classic single-input single-output (SISO) decoupled controllers.

The output states to be controlled are the longitudinal, lateral, and vertical positions, as well as the heading of the helicopter. These are controlled by manipulating the four inputs to the helicopter: longitudinal and lateral cyclic, and main and tail collective blade pitches.

Control and stability derivative identification for RC helicopters has been the topic of numerous research papers, but none cover identification of dynamics of electrically powered, sub-one-metre rotor diameter, free-flying RC model helicopters (without governors).

Due to the similarities between the rotor heads of a Kyosho Concept 60 [54] helicopter (a 0.60-size glow engine helicopter) and the Voyager E helicopter, the eleventh order model presented in [54] will be used for development of a FCS. The model is also extended to include the three position and heading states.

During the design of the controllers, some of the cross coupling will be ignored. The full eleven state model will however be used to demonstrate that the designed controllers can effectively control the helicopter in spite of the cross coupling that was ignored during the design phase.

The initial design and analysis will be performed in the continuous domain, but the influence of the sampling rates and delays of the sensors used will also be investigated. It will be demonstrated that it is possible to control a small RC helicopter in spite of the

limited update rates and delays of the sensors and communication links used.

6.1 Heading Control

A pilot controls the heading (ψ) of a model helicopter using the tail rotor collective pitch (δ_r) during near-hover flight. The yaw rate dynamics of a model helicopter is well damped due to the active yaw rate damping subsystem. Using the model structure presented in section 2.4.2, Shim *et al.* [54] identified the control and stability derivatives for their Concept 60 helicopter. The yaw dynamics are described by the following equations:

$$\dot{r} = -0.02p + 1.19w - 3.00r - 22.13r_{fb} + 4.49\delta_c - 103.34\delta_r \tag{6.1}$$

$$\dot{r_{fb}} = 3.15r - 9.50r_{fb} \tag{6.2}$$

$$\dot{\psi} = r \tag{6.3}$$

The yaw angle (ψ) and yaw rate (r) are dominated by the response to the yaw rate reference command (δ_r) and the active yaw rate damping feedback (r_{fb}). The influence of p, w and δ_c is neglected during the controller design, but will be included during the simulations. Some manipulation of 6.1 and 6.2 yields the transfer function

$$\frac{\psi(s)}{\delta_r(s)} = \frac{-103.3(s+9.5)}{s(s^2+2(0.63)(9.9)s+(9.9)^2)} \tag{6.4}$$

The root locus, assuming feedback from ψ to δ_r, and open loop bode plot is presented in figure 6.1.

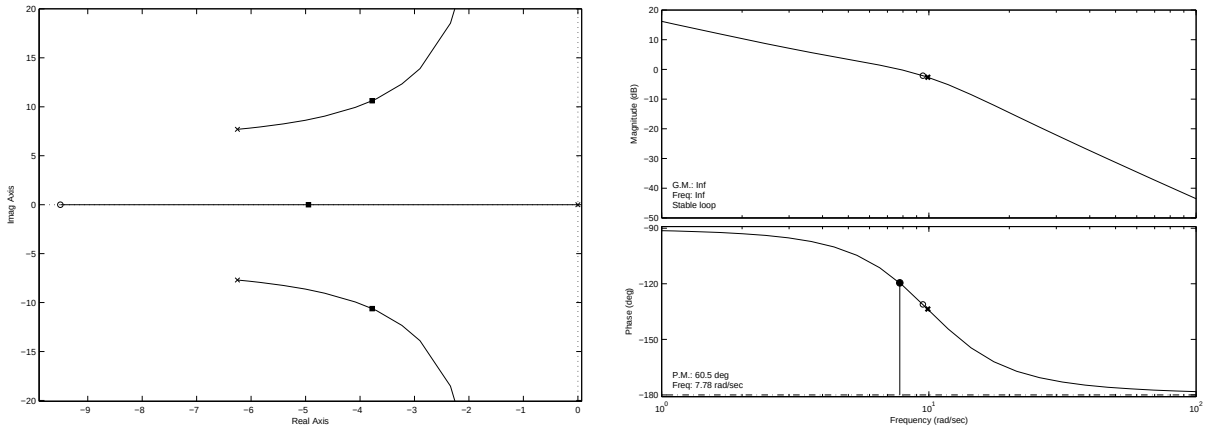

Figure 6.1: *Root locus of $\frac{\psi(s)}{\delta_r(s)}$ with ψ feedback to δ_r, and open loop bode plot*

The pole at the origin is from integration of yaw rate (r) to yaw angle (ψ). Figure 6.1 shows that there is no risk that the system will be unstable if the loop is closed. Selecting a feedback gain will determine the bandwidth of the system.

The controller is however implemented in a digital computer and the heading sensor (the magnetometer) only measures the heading at 10 Hz. A delay of up to 70 ms is introduced due to interfaces and communication links between the heading measuring sensor and the servo actuator.

Figure 6.2 presents the root locus for the digital controller and a step response of the closed loop system, in which a 100 ms delay was added between the time of measurement and the actuator. It can be seen from the figure that in spite of the added phase due to the delay and the fairly low sampling rate, using a feedback gain of $K_{\phi_d} = 0.3$, a phase margin of 56.7° and a gain margin of 6.03 dB is achieved. The gain margin and phase margin can be increased at the cost of lower closed loop bandwidth by decreasing the feedback gain.

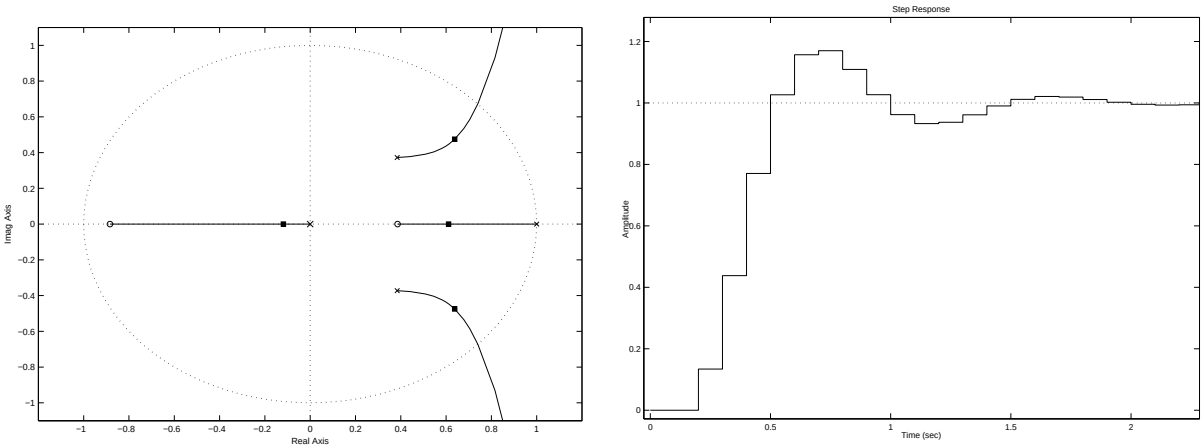

Figure 6.2: *Root locus and yaw angle step response using digital controller with* 100 *ms delay*

From the above it is clear that the yaw dynamics can be controlled accurately by mere selection of a single gain. The results obtained using the real helicopter will be presented in section 7.1.

6.2 Altitude Control

The altitude of the Concept 60 is described by the following set of equations:

$$\dot{w} = -3.05a_1 - 15.06b_1 - 1.35w + 0.22r + 10.64\delta_c \tag{6.5}$$

$$\dot{z} = w \tag{6.6}$$

The influence of a_1, b_1, w and r is neglected during the design of the controller. The transfer function from main rotor collective command to altitude simplifies to a second order function:

$$\frac{z(s)}{\delta_c(s)} = \frac{10.6}{s(s+1.34)} \tag{6.7}$$

The altitude is controlled using velocity and position feedback:

$$\delta_c = K_z z_{ref} - K_w w - K_z z \tag{6.8}$$

Using feedback gains of $K_w = 1$ and $K_z = 1$, an infinite gain margin and a phase margin of 85° is obtained.

The controller is implemented in a digital computer as a set of difference equations, and the ultrasonic range sensor measures the distance to the ground at 10 Hz. The altitude measurement is delayed with an amount of time that is proportional to the distance being measured. At two metres from the ground the delay is approximately 12 ms. A delay of 100 ms is included in the digital control analysis to simulate the time delay introduced by the sensor, communication and other interface devices. A climb rate measurement is required to be able to close the inner climb rate loop, providing lead compensation (derivative feedback control). The climb rate is calculated using the difference between consecutive ultrasonic range measurements.

Figure 6.3 presents the root locus for the digital controller and a step response of the closed loop system. The effect of the sensor delay has been taken into account for closing both the rate and the position loops. The results have been verified using a Simulink simulation (see figure 6.4). Using a feedback gain of $K_{w_d} = 0.2$ and $K_{z_d} = 0.8$ a phase margin of 45.4° and a gain margin of 6.9 dB is achieved.

An additional complication that had to be dealt with in the real system is the noise of the altitude measurement. If the noise levels are too high, the helicopter reacts violently to the false climb rate changes. The output of the sensor needs to be smoothed, which introduces additional phase delay. One solution would be to introduce an estimator.

Low frequency errors (offsets) can be minimised by the introduction of an integral control term (lag compensator). However, the lag compensator will not contribute to the stability of the vehicle, it will only assist in rejecting steady-state errors.

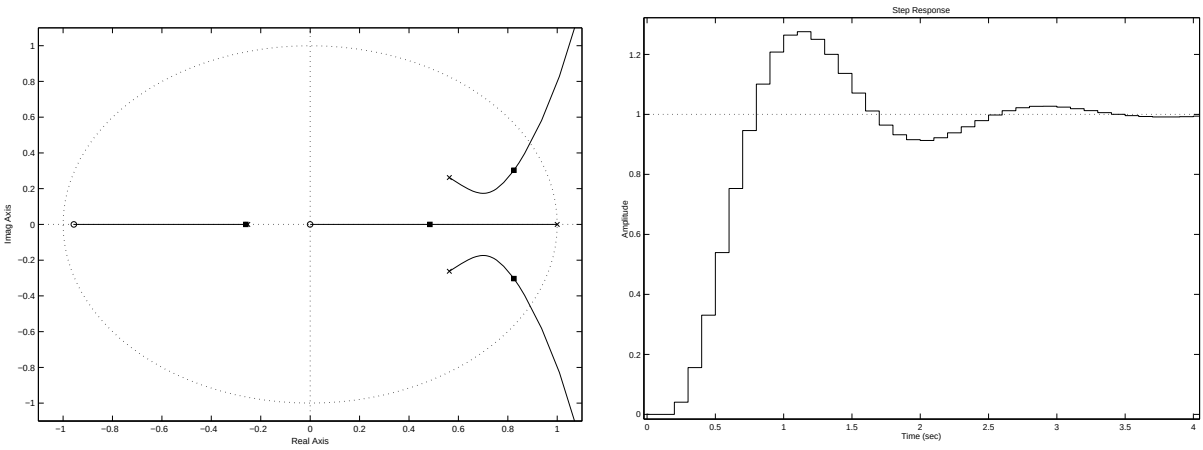

Figure 6.3: *Root locus and altitude step response using digital controller*

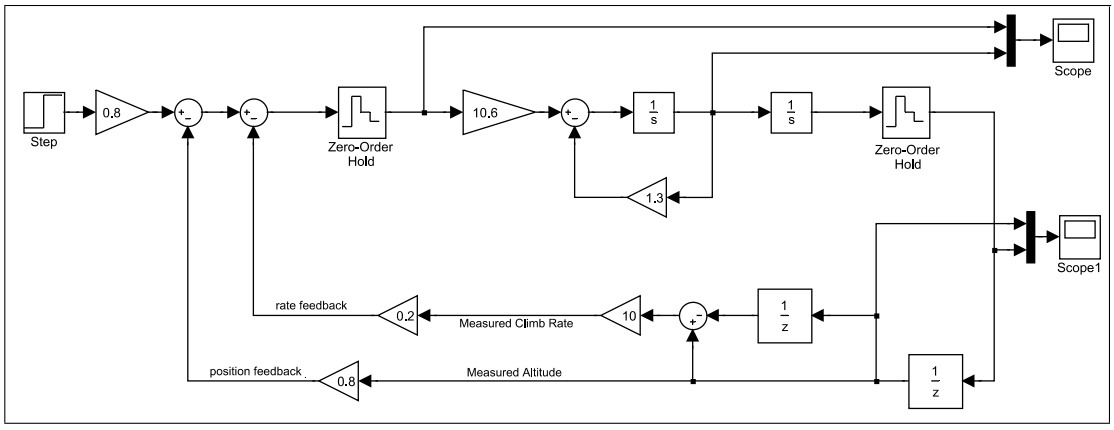

Figure 6.4: *Altitude control simulation in Simulink*

6.3 Horizontal Control

The horizontal position and velocity of an RC model helicopter can be controlled using feedback of the attitude, velocity and position state variables [11, 35, 41, 56]. The cross-coupling between the longitudinal and lateral degrees of freedom is sufficiently low to enable the design of separate longitudinal and lateral gains.

Kim *et al.* [29] used a simple control law design to control the longitudinal and lateral positions of their Yamaha R-50. The regulator control law is described by the following equations:

$$\delta_a = -K_\phi \phi - K_v v - K_y e_y - K_{Iy} \int e_y dt \tag{6.9}$$

$$\delta_b = -K_\theta \theta - K_u u - K_x e_x - K_{Ix} \int e_x dt \tag{6.10}$$

where e_x and e_y denote the position errors. Each of these control equations contain a feedback term proportional to the angle of the vehicle and PID position feedback terms.

The control law will be designed using successive loop closure. First the pitch and roll angle loops will be closed, then the velocity and then the position loops. The design of the control laws will be presented as follows:

- Subsection 6.3.1 illustrates an attempt to control the velocity of the helicopter using only proportional velocity feedback.
- Subsection 6.3.2 presents the design of the attitude controller. It is shown that the attitude can be controlled without angular rate feedback
- Subsection 6.3.3 treats the selection of the velocity and position feedback gains.

6.3.1 Velocity Control without Angle Feedback

This subsection illustrates the results obtained if only velocity feedback is used in an attempt to control the velocity of the helicopter. The analysis will be performed using a simplified six state model. It will then be shown that a fourth order model describes the system very effectively. The results obtained using the simplified models will then be compared to the results obtained using the full eleventh order model.

Equation 6.11 describes the longitudinal velocity (u) response of a model helicopter

to longitudinal cyclic (δ_b) perturbations, assuming that the lateral velocity equals zero.

$$\begin{bmatrix} \dot{u} \\ \dot{p} \\ \dot{q} \\ \dot{\theta} \\ \dot{a_1} \\ \dot{b_1} \end{bmatrix} = \begin{bmatrix} X_u & 0 & 0 & -g & X_{a_1} & 0 \\ L_u & 0 & 0 & 0 & L_{a_1} & L_{b_1} \\ M_u & 0 & 0 & 0 & M_{a_1} & M_{b_1} \\ 0 & 0 & 1 & 0 & 0 & 0 \\ 0 & 0 & -1 & 0 & \frac{-1}{\tau_e} & A_{b_1} \\ 0 & -1 & 0 & 0 & B_{a_1} & \frac{-1}{\tau_e} \end{bmatrix} \begin{bmatrix} u \\ p \\ q \\ \theta \\ a_1 \\ b_1 \end{bmatrix} + \begin{bmatrix} 0 \\ 0 \\ 0 \\ 0 \\ A_{\delta_b} \\ B_{\delta_b} \end{bmatrix} \begin{bmatrix} \delta_b \end{bmatrix} \tag{6.11}$$

Since the roll angle (ϕ) only influences the lateral acceleration ($\dot{v}$), which has been assumed a constant zero, the roll angle (ϕ) has also been omitted. The climb rate and yaw rate is also assumed to be zero so as not to have a significant influence on the longitudinal dynamics. The states included are: u, p, q θ, a_1 and b_1.

Shim *et al.* [54] have identified and published the parameters for their Concept 60 to be:

$$\begin{bmatrix} \dot{u} \\ \dot{p} \\ \dot{q} \\ \dot{\theta} \\ \dot{a_1} \\ \dot{b_1} \end{bmatrix} = \begin{bmatrix} -0.06 & 0 & 0 & -9.81 & -9.81 & 0 \\ 0.30 & 0 & 0 & 0 & 40.36 & 237.42 \\ 1.31 & 0 & 0 & 0 & 220.18 & -11.44 \\ 0 & 0 & 1 & 0 & 0 & 0 \\ 0 & 0 & -1 & 0 & -4.35 & 1.45 \\ 0 & -1 & 0 & 0 & -1.59 & -4.35 \end{bmatrix} \begin{bmatrix} u \\ p \\ q \\ \theta \\ a_1 \\ b_1 \end{bmatrix} + \begin{bmatrix} 0 \\ 0 \\ 0 \\ 0 \\ 2.19 \\ -0.09 \end{bmatrix} \begin{bmatrix} \delta_b \end{bmatrix} \tag{6.12}$$

The root locus of the transfer function $\frac{u}{\delta_b}$ with velocity feedback to longitudinal cyclic, and the open loop bode response of the transfer function, is provided in figure 6.5. From figure 6.5 it can be seen that the system is unstable, and that it can not be stabilised by mere proportional velocity feedback to δ_b.

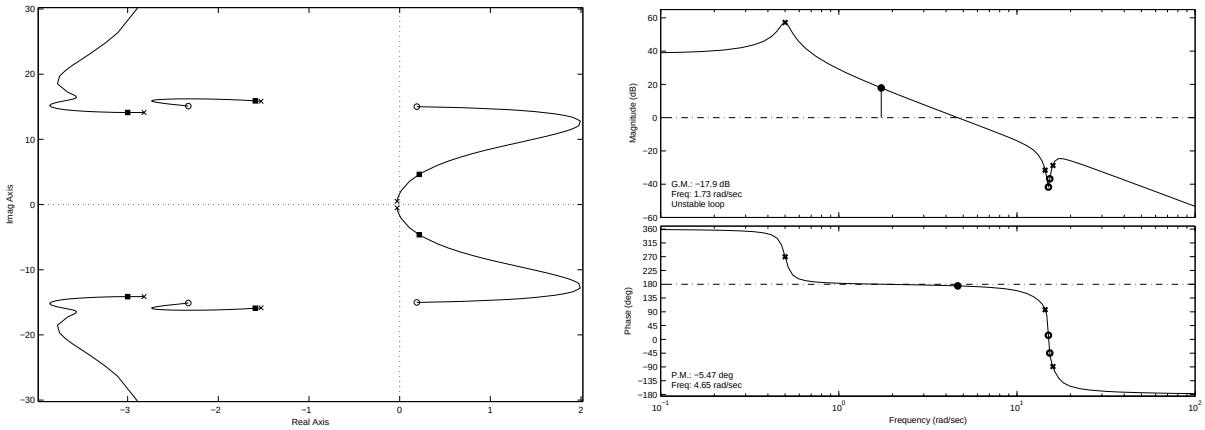

Figure 6.5: *Root locus with only u feedback to δ_b, and open loop bode response*

If the roll rate (p) and the lateral flapping angle (b_1) are removed from the model, the set of complex zeroes (near $-2.4 \pm 15j$) and set of complex poles (near $-1.5 \pm 15j$) disappear. The rest of the roots remain very close to where they are located with the roll

rate and flapping angle states included. The remaining set of stable complex poles are the body pitch rate and longitudinal blade flapping dynamics dominated by the interaction between the Bell-Hiller stabiliser bar, main rotor and the fuselage. The last two slower unstable complex poles are due to the pitch angle and longitudinal velocity dynamics.

The root locus controlling the lateral velocity using only lateral velocity feedback to the lateral blade flapping is seen in figure 6.6. The full eleven state identified model from [54] for the Concept 60 was used. Figure 6.6 also presents the resulting root locus if only longitudinal velocity feedback to the longitudinal cyclic is used to control the longtitudinal velocity.

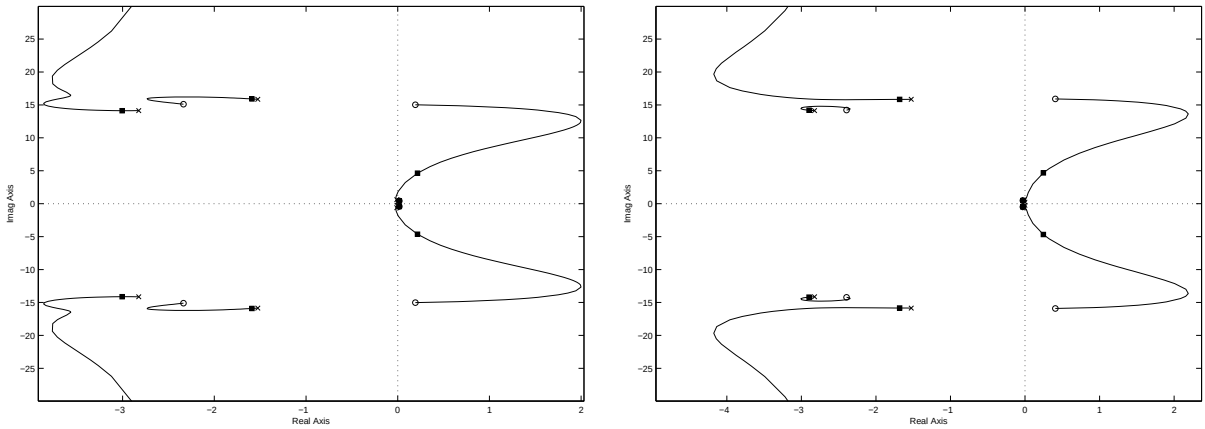

Figure 6.6: *Root loci for control of u using only u feedback to δ_b (left) and v control with only v feedback to δ_a, using 11 state model*

A number of similarities are noted between the two root loci of the longitudinal and lateral systems in figure 6.6:

- The four pairs of open loop complex poles are located at exactly the same locations ($-1.53 \pm 15.85j$, $-2.82 \pm 14.13j$, $-0.01 \pm 0.60j$ and $0.00 \pm 0.24j$).
- The three open loop complex zero pairs are located at approximately the same locations ($0 \pm 0.5j$, $0.4 \pm 15j$ and $-2.4 \pm 15j$).

Looking at the symmetry in the model, the findings are not surprising. Two complex zeros approximately cancel two complex poles in each of the loci, and the model for each can be reduced to a fourth order system by ignoring the cross coupling (the approximately cancelled poles), which yields equation 6.20 that will be discussed later.

6.3.2 Pitch and Roll Angle Control

The attitude control section will be divided into two sections: the effect of pitch and roll rate feedback, and the selection of pitch and roll angle feedback gains.

Pitch and Roll Rate Feedback

Figure 6.7 shows the pitch rate response of the Concept 60 to a longitudinal cyclic command step, using the simplified model described by equation 2.23. For the Concept 60:

$$\frac{q}{\delta_b} = \frac{482.7}{s^2 + 4.346s + 220.2} \approx \frac{2.19(14.84)^2}{s^2 + 2(0.15)(14.84)s + (14.84)^2} \tag{6.13}$$

The step response from figure 6.7 can be compared to the measurements that were performed using the Voyager E, seen in figure 2.3. The step response in both figure 6.7 and 2.3 is seen to be dominated by a second order, lightly damped behaviour. The simple second order model describes the high frequency behaviour of the real helicopter accurately. Two differences are noted: the measured response contains high frequency noise that the theoretical plot does not contain, and the natural frequency and damping ratio differs for the Concept 60 ($\omega_n = 14.84$ and $\zeta = 0.15$) and the Voyager E ($\omega_n \approx 18.4$ and $\zeta \approx 0.09$). The theoretical prediction of the natural frequencies was described in section 2.4.3.

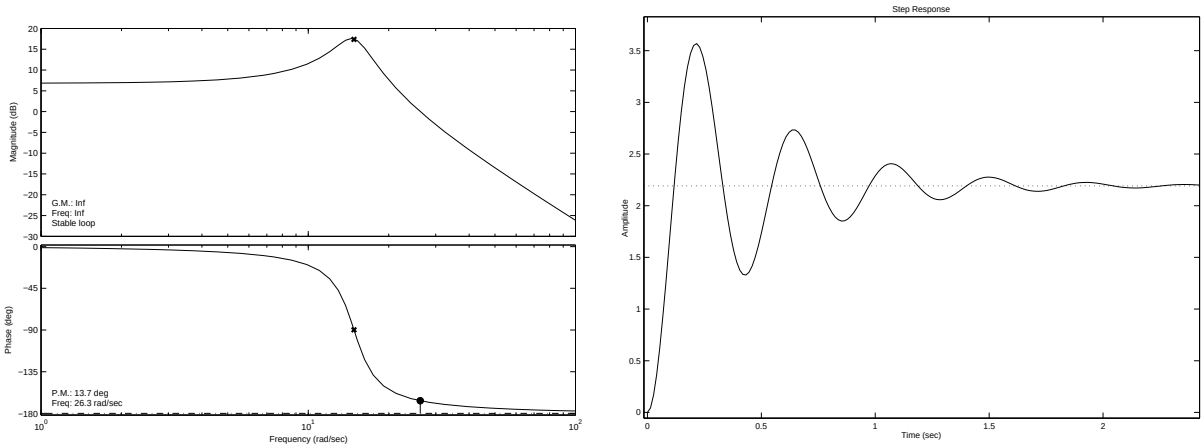

Figure 6.7: *Bode plot and step response of* $\frac{q}{\delta_b}$

From equations 6.9 and 6.10 it can be seen that Kim *et al.* did not include pitch or roll rate feedback terms to control their R-50 helicopter. It has become common practice not to use pitch- or roll rate feedback. The Bell-Hiller stabiliser bar acts as a lagged rate feedback system. Due to the Bell-Hiller stabiliser bar, the rotor/stabiliser bar/fuselage mode is lightly damped, as can be seen in figure 6.7 and was discussed in section 2.4.3.

Although rate feedback would help to reduce the gust response of the helicopter, it has been found that additional rate feedback is not essential [35]: the mode is lightly damped, yet fast and stable. The fact that it is lightly damped is of little concern except for the relatively small decrease in the phase margin due to the resonant peak.

Mettler *et al.* [35] suggest using a notch filter to improve the gain margin when closing the pitch and roll angle loops using pitch and roll angle feedback - no rate feedback used. Mettler *et al.* compare the results obtained using a baseline controller using only pitch and roll angle feedback to a controller utilising a notch filter to increase the closed loop control bandwidth. The resonant peak is located at the 180° critical phase frequency (see Bode plot in figure 6.8). The gain margin, and consequently the robustness and bandwidth, can be significantly increased if notch filters are used at the correct frequencies. In figure 6.8 the results obtained for the Concept 60 can be seen: the gain margin is increased by 16 dB, while the phase margin is reduced from 87° to 72°.

The risk of using the notch filter is that if the open loop poles shift, or the frequency is incorrectly identified, the strategy will lose effectiveness. The frequencies are, amongst others, dependant on the properties of the Bell-Hiller stabiliser bar, the main rotor RPM, the fuselage moment of inertia and the main rotor blade properties. Although Mettler *et al.* argue that the filter is of value even if the natural frequency of the fuselage-rotor-stabiliser bar changes by 10%, the notch filter poses a threat to a helicopter of which the dynamics are ill-described and highly variant. It was decided to design conservatively for lower bandwidth. Other helicopters are flying successfully without notch filters. The natural frequency of the Voyager E has been identified using a step function and theoretical prediction, but the dynamics of the helicopter have not been identified extensively and a number of mechanical failures have required frequent changes to the the helicopter setup.

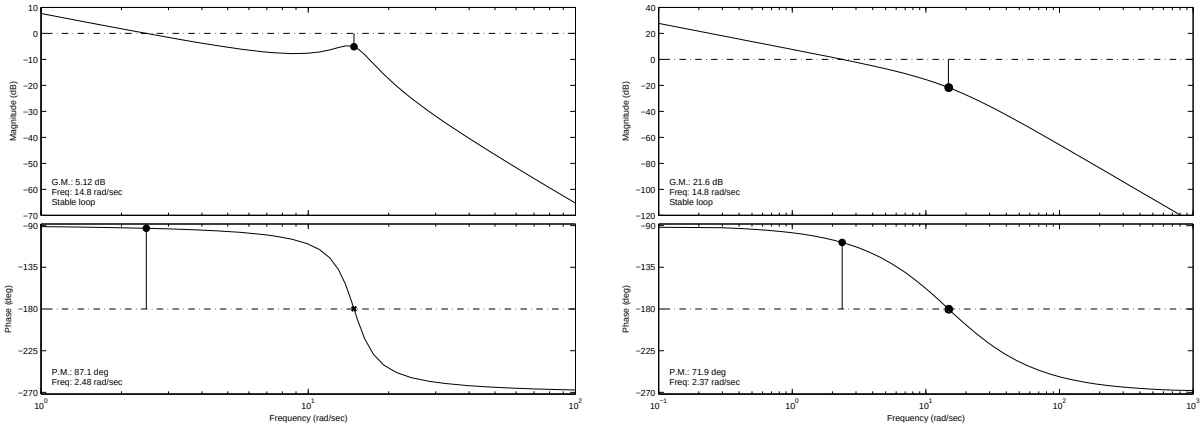

Figure 6.8: *Open loop bode of $\frac{\theta}{\delta_b}$ without (left) and with (right) a notch filter*

Pitch and Roll Angle Feedback

Using the full eleventh order model, the root locus of θ with only θ feedback to δ_b and the open loop bode response $\frac{\theta}{\delta_b}$ is presented in figure 6.9, which includes the longitudinal velocity dynamics.

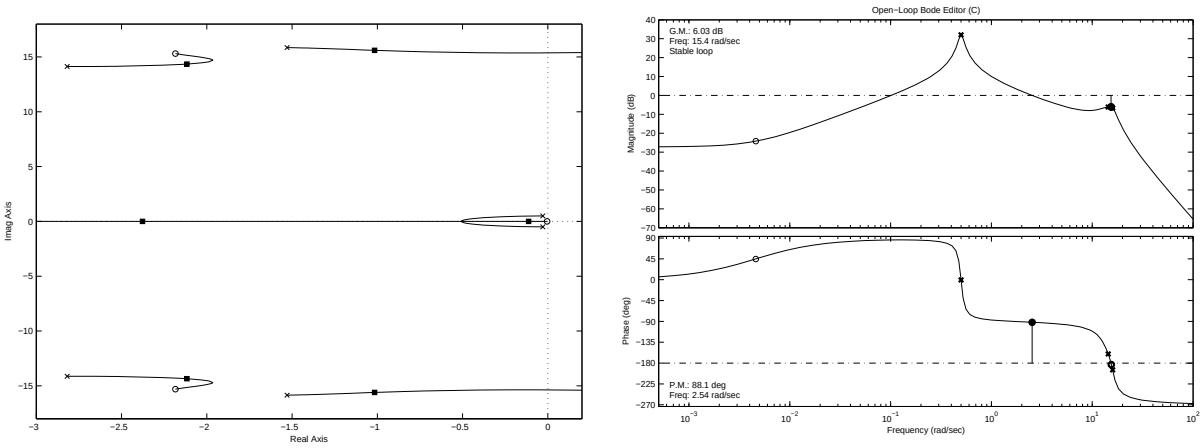

Figure 6.9: *Root locus with θ as output using only θ feedback to δ_b, and open loop bode response*

Two resonant peaks can be seen in figure 6.9: one at a higher frequency ($\omega \approx 15\,\text{rad/s}$) and one at a lower frequency ($\omega \approx 0.5\,\text{rad/s}$). The higher frequency is dominated by the interaction between the fuselage, the Bell-Hiller stabiliser bar and the main rotor blades, while the lower resonant frequency is dominated by the flap-back of the main rotor TPP [18] (M_u for longitudinal and L_v for lateral). The stability derivatives M_u, M_v, L_v, L_u have a destabilising influence on the phugoid motion of the helicopter [37].

Figure 6.9 shows that the attitude and position dynamics modes are separated by approximately a factor of 30 in frequency, which makes it possible to largely separate the control of attitude and position by means of successive loop closure. The goal is to close the higher frequency inner attitude control loop by means of attitude feedback. The short to medium ($0 - 5\,\text{s}$) term response to reference pitch and roll angle commands is evaluated when testing the pitch and roll angle controllers. The resonant peak, located at approximately 15 Hz, is where the gain and phase margin is low, while the low frequency response essentially remains open loop.

Mettler *et al.* [35] and Shim [56] ignored the influence of the velocity dynamics while designing their respective attitude controllers. The motivation was that the bandwidth of the closed attitude loop is much higher than the other outer loops.

The pitch and roll angle loops are closed using pitch and roll angle feedback to δ_b and

δ_a respectively:

$$\delta_a = K_\phi(\phi_{ref} - \phi) \tag{6.14}$$
$$\delta_b = K_\theta(\theta_{ref} - \theta) \tag{6.15}$$

The gains K_ϕ and K_θ have to be found. The gain selection is based on maximising the gains while maintaining adequate gain margin (6 dB) and phase margin (45°). With $K_\theta = 1.1$, a gain margin of 6 dB and a phase margin of 88° are obtained (see figure 6.9).

In figures 6.9 and 6.10 it can be seen that at low frequencies the closed loop pitch angle response remains essentially open loop due to the low open loop gain at low frequencies.

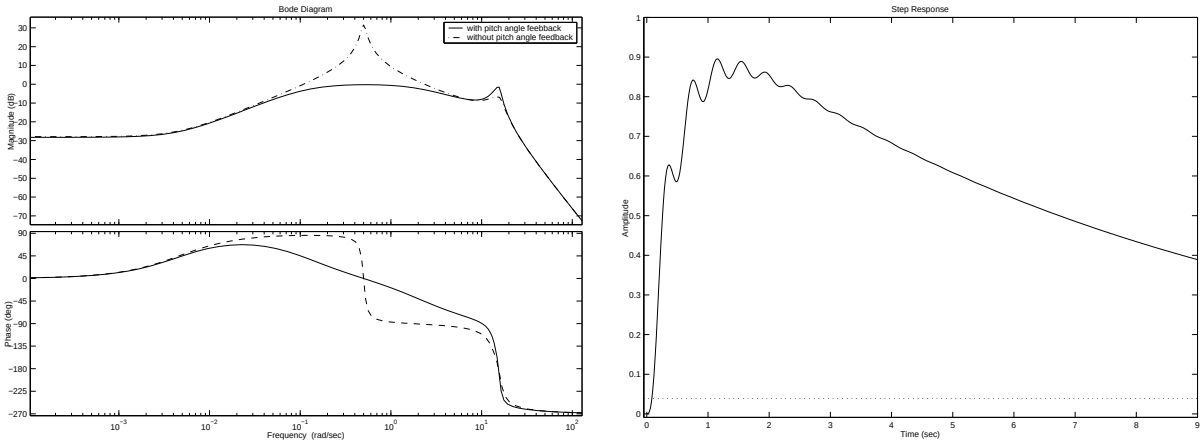

Figure 6.10: *Bode plot of pitch angle response to δ_b with and without pitch angle feedback, and step response with pitch angle feedback*

6.3.3 Velocity and Position Control

Adding position and velocity states to the model adds two more integrators to the model. The goal is now to close the velocity and position loops, which are viewed as outer loops.

The velocity feedback loops are closed using the following gains, assuming that the pitch and roll angle feedback gains (K_θ and K_ϕ) have been determined:

$$\delta_a = K_\phi(-\phi + K_v(v_{ref} - v)) \tag{6.16}$$
$$\delta_b = K_\theta(-\theta + K_u(u_{ref} - u)) \tag{6.17}$$

The root locus of the transfer function $\frac{u}{\theta_{ref}}$ with u feedback to the pitch angle reference, with pitch angle feedback designed in the previous section, is presented in figure 6.11. A bode plot of the transfer function $\frac{u}{\theta_{ref}}$ is also presented in figure 6.11.

Unless the goal is to achieve very high bandwidth, the loop can be closed without complications. Selecting $K_u = 0.36$ yields a gain margin of 22.4 dB and a phase margin of 45°. The process is repeated for the closure of the lateral velocity loop.

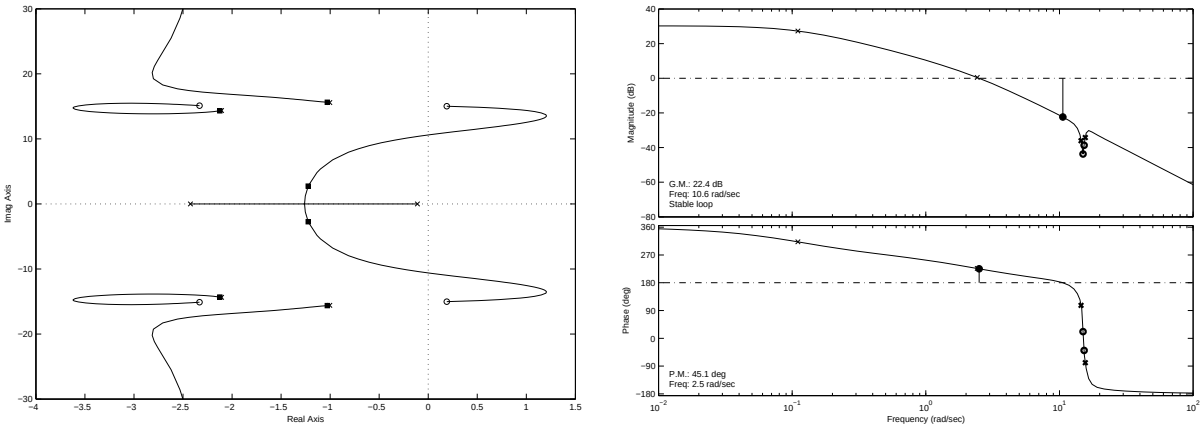

Figure 6.11: *Root locus and open loop bode response of* $\frac{u}{\theta_{ref}}$ *with pitch angle controller*

Now position feedback will be added. The position loops are closed as follows:

$$\delta_a = K_\phi(-\phi + K_v(-v + K_y(y_{ref} - y))) \tag{6.18}$$

$$\delta_b = K_\theta(-\theta + K_u(-u + K_x(x_{ref} - x))) \tag{6.19}$$

The closed loop pole locations from figure 6.11 become the open loop pole locations in figure 6.12, with the addition of a pole at the origin: the integration of velocity (u and v) to position (x and y). Selecting a feedback gain $K_x = 1.22$ a gain margin of 6 dB and a phase margin of 64° is obtained (see figure 6.12).

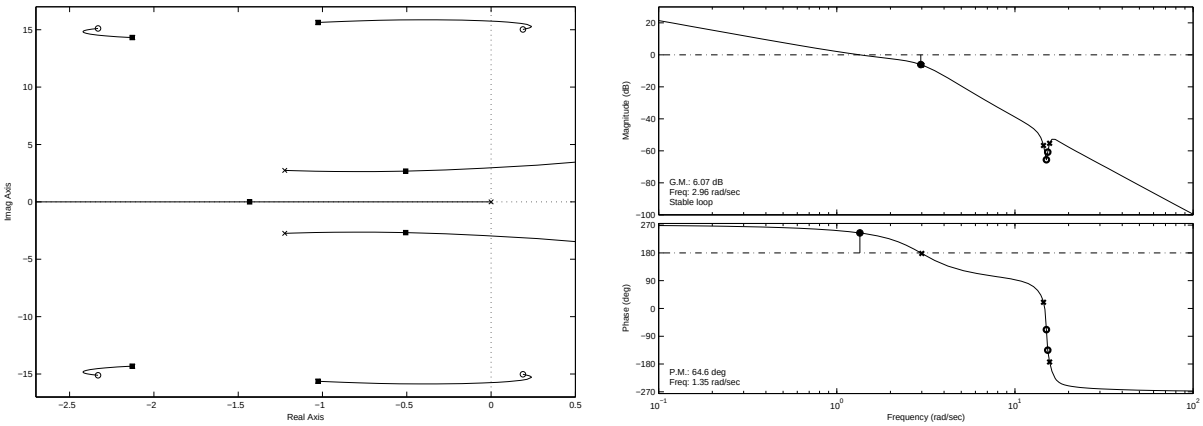

Figure 6.12: *Root locus and open loop bode response of* $\frac{x}{u_{ref}}$ *with attitude controller*

6.4 Testing all controllers simultaneously

The next step is to analyse the response of the system when the heading, altitude, longitudinal and lateral position loops are closed simultaneously. The designed control law was simulated using both Simulink and a Matlab `m-file` describing the closed loop system using a state space model. The results obtained using the fifteenth order state space representation and the Simulink block diagram (see figure 6.13) were exact matches.

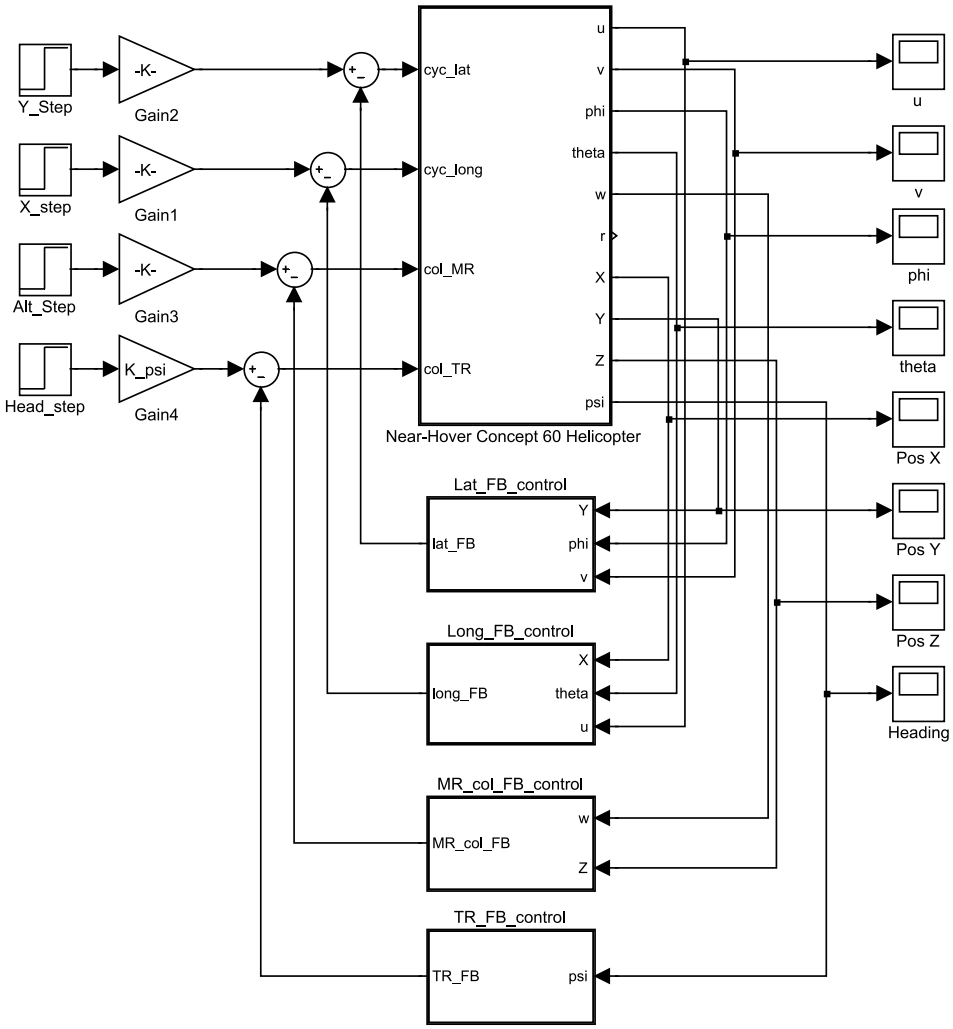

Figure 6.13: *Simulink block diagram implementation of the 15th order model used to test the digital controllers*

Up to this point it has been assumed that it is possible to measure all the states continuously and accurately. Controlling the helicopter becomes more difficult if the controller needs to be implemented in a digital computer and the states required to control

the helicopter have to be estimated. The pitch and roll angles are estimated at 60 Hz sampling rate. The closed loop bandwidth of the horizontal velocity and position loops is much slower than for the pitch and roll angles. The horizontal velocity is measured at a sample rate of 4 Hz, but the states are estimated at 60 Hz clock rate using the inertial sensors and GPS receiver.

Originally a seven state model (using equation 6.11 and adding the position state) was used in section 6.3.3 to design the longitudinal velocity and position feedback controllers. A fifth order model was later used to simulate the response obtained using the designed longitudinal position controller. The fifth order model was obtained by reducing the order of the model presented in equation 6.11 by neglecting the states p and b_1, and adding an integrator to model the longitudinal position x:

$$\begin{bmatrix} \dot{x} \\ \dot{u} \\ \dot{q} \\ \dot{\theta} \\ \dot{a_1} \end{bmatrix} = \begin{bmatrix} 0 & 1 & 0 & 0 & 0 \\ 0 & -0.06 & 0 & -9.81 & -9.81 \\ 0 & 1.31 & 0 & 0 & 220.18 \\ 0 & 0 & 1 & 0 & 0 \\ 0 & 0 & -1 & 0 & -4.35 \end{bmatrix} \begin{bmatrix} x \\ u \\ q \\ \theta \\ a_1 \end{bmatrix} + \begin{bmatrix} 0 \\ 0 \\ 0 \\ 0 \\ 2.19 \end{bmatrix} \begin{bmatrix} \delta_b \end{bmatrix} \tag{6.20}$$

The results obtained using the fifth order continuous model were compared to the results obtained using the fifteenth order digital implementation of the model. The pitch angle, longitudinal velocity and position results obtained were near perfect matches. In figure 6.14 the fifth order continuous longitudinal position controller design is compared to the Simulink discrete controller without sensor delays modelled.

The Simulink simulation was then extended to include a 60 ms delay caused by the communication and interface devices. The gains from the lower order, decoupled model, continuous domain design were used. The damping was lower than what was the case in the continuous domain simulations, but performed well (see figure 6.15) in spite of the introduced delays. The `m-file` fifth order simulation was not changed, and used as a reference. The simulation highlights the performance differences between the system with and without sensors delays, not the differences between a digital and continuous, or a higher or a lower order model.

The Simulink simulation was also adapted to test a worst-case scenario. A 60 ms delay was included for the pitch and roll angle feedback values, with the pitch and roll angle estimators' update rate of 60 Hz. The position and velocity were measured at a 4 Hz rate with a 500 ms delay added to the horizontal velocity and position measurements. The horizontal velocity and position feedback gains were each reduced. The changes resulted in a reduction in the closed loop bandwidth of the system, less overshoot, but most importantly: the system could be controlled accurately.

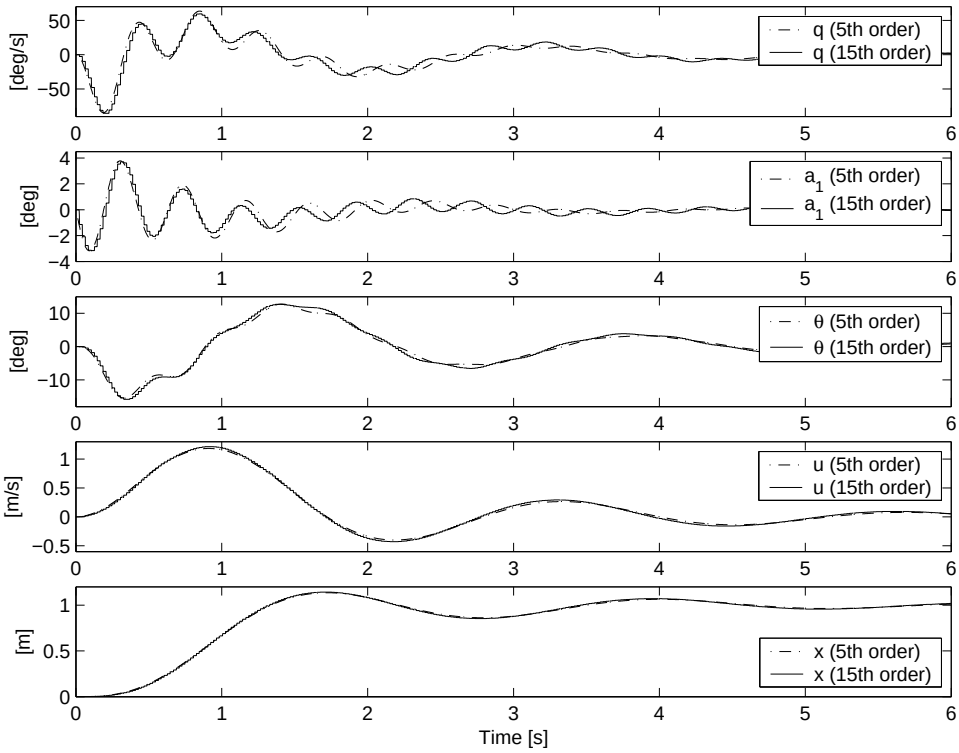

Figure 6.14: *Comparing 5th order continuous with 15th order digital position control simulation, using same gains*

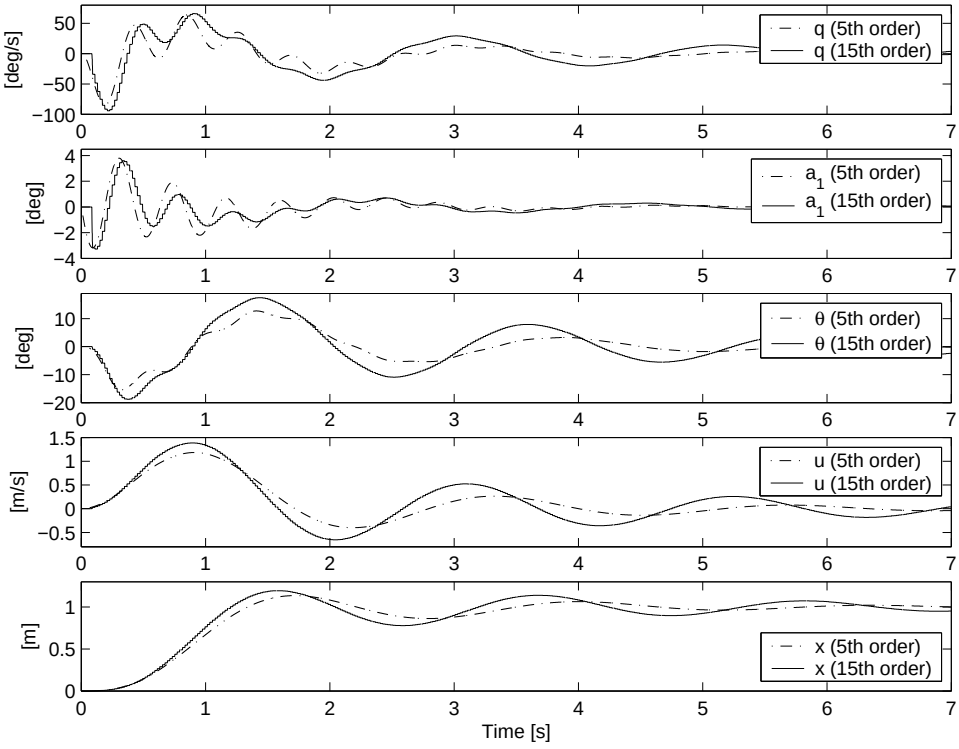

Figure 6.15: *Comparing 5th order m-file control design with 15th order Simulink Digital control, using same gains,* 60 *ms delay*

Care was taken to ensure that the limits of the actuators were not reached. For example: some glow powered helicopters might be able to climb at 4 m/s. The Voyager E cannot; neither can it pitch at 200°/s.

It is important to remember that the eleven state model used is a linearisation around the hover condition. Control and stability derivatives might change sign and values during cruise conditions. Furthermore, the assumption of near-hover manoeuvres has been made throughout the system analysis. The model and analysis is only valid for low velocities (horizontal and vertical) and small pitch and roll angles. During all longitudinal and lateral movements it has been assumed that the heading is kept constant - which is a limitation that can be overcome (but acceptable for this analysis).

The analysis has shown that a controller can be designed using consecutive loop closure. If we now assume that the Voyager E helicopter has similar characteristics to the Concept 60, we can expect to obtain a satisfactory controller if we experimentally close the loops successively, adjusting feedback gains for satisfactory response of the pitch and roll angles, then velocities, and finally positions.

By this process, we can expect obtain a controller that works satisfactorily without having an exact dynamic model for the Voyager E. A number of projects have successfully used a similar strategy to control their RC helicopters [1, 7, 11, 26, 28, 33, 56].

6.5 GUI Simulations

Aaron Kahn developed an OpenGL based flight simulator (figure 6.16) as part of the work he did for his MSc(Eng) degree [28]. The author obtained the source code and permission to modify and use the code from Kahn. A hardware and software interface was developed to enable a human pilot to control the helicopter.

Although it would be possible to use the code that was developed by Kahn as the foundation for a hardware-in-the-loop simulation (HILS), as was done by Rotomotion [26] and the University of Southern California [24], this was not done due to time limitations. The helicopter dynamic model used by Kahn is based on the properties of an X-Cell, but can be adapted to simulate the response of any well identified model helicopter.

The flight simulator Realflight G2 (figure 6.17) was acquired and used as a training tool for potential safety pilots. In spite of the author's extensive RC fixed wing model flying experience, the level of competence required to act as a safety pilot was found to be much higher than anticipated. Performing the function of safety pilot is a task better

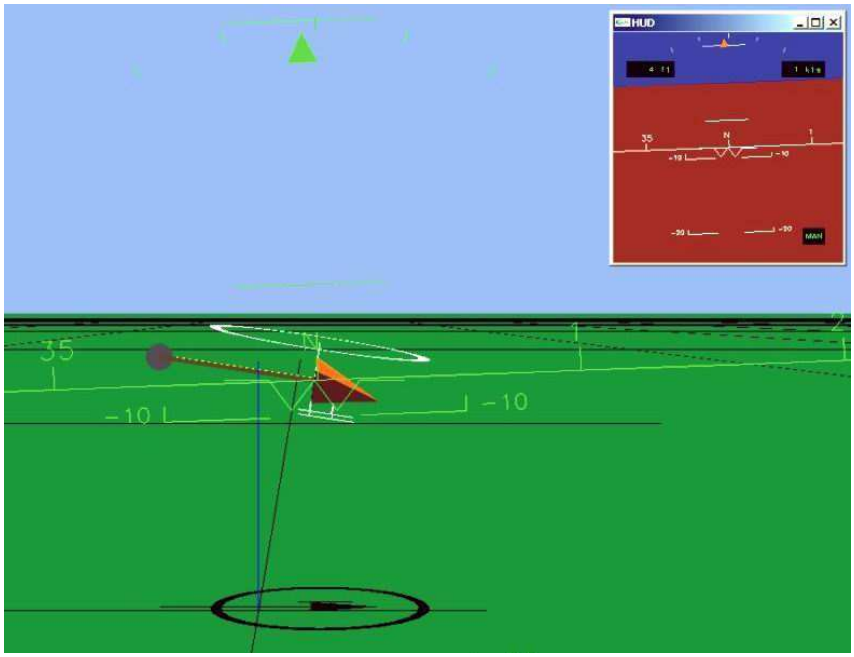

Figure 6.16: *Screenshot from Aaron Kahn's simulation*

Figure 6.17: *Screenshot from Realflight G2*

left for a person with years of helicopter flying experience.

The simulator nevertheless proved valuable to understanding and experiencing the level of control and sensory accuracy required to hover an RC helicopter accurately.

6.6 Conclusion

> *"Everybody's simulation model is guilty until proved innocent."*
> Thomas H. Lawrence at the 50th Annual Forum of the AHS, [47].

Although the control and stability derivatives of the Voyager E differ from the values for the Concept 60, the two helicopters have very similar actuators and stability augmentation systems. Rather than presenting a full analysis of a poorly identified model, the author has chosen to present a thorough analysis of a well described helicopter with very similar properties to the helicopter that was used during this project.

The goal of this chapter has been to present and justify a simple approach to developing control laws for a model helicopter. The model that was used has been proposed by Mettler *et al.* [35] and used successfully by Mettler *et al.* and Shim *et al.* [54, 56] to describe glow and gasoline powered helicopters.

The focus has been on demonstrating that a set of control laws can be designed using simple, successive loop closure of decoupled systems. The chapter also provided insight into why simple empirically tuned classical SISO controllers have proved to be so successful amongst researchers [1, 7, 11, 26, 28, 33, 56]. These research groups have all been investing significant effort (or money) in sensor development, without applying similar effort to the control system design based on a model of their helicopters.

The control laws were designed with knowledge about the available sensors in mind. The influence of the sensor limitations on the system have been investigated and simulated.

Chapter 7

Control Law Implementation and Results Obtained

Developing and identifying a full mathematical model of the Voyager E is a difficult and time consuming task, and was not the goal of this project. No published model of a small electrically powered RC helicopter was available.

The work presented in chapter 6 shows that successive loop closure produced a suitable controller for a Concept 60 RC helicopter. Due to the similarities between the actuators and stability augmentation systems of the larger glow and the smaller electrically powered helicopters, it is reasonable to assume that the same strategy used to design a control system for the larger helicopter would also succeed if applied to the JR Voyager E.

Instead of selecting the gains theoretically, the loops were closed successively through empirical selection of the gains during flight tests. A number of successful helicopter FCS have been designed using empirically tuned classical SISO feedback controllers [1, 7, 11, 26, 28, 33, 56] . The main reason why each of these projects resorted to empirical tuning was the same: the lack of an accurate model of the specific helicopter, with all of its non-linear behaviour and changes in configurations and loads. The lack of an accurate model is regarded as one of the primary reasons why limited success has been achieved by groups using model-based techniques like H_∞ and LQ controller design [33, 56].

The focus of this chapter is to present the implemented control laws and the results that were obtained using the designed controllers.

7.1 Heading Control

The heading controller was chosen as the first loop to close for the following reasons:

- The primary sensor (three axis magnetometer) works very well indoors.
- Minimal translational movement results from yaw perturbations and therefore it is safe to pass control over to the controller within a confined space.
- The yaw rate is well damped due to the active yaw rate damping subsystem.

Since the active yaw rate damping subsystem was retained, no additional lead compensation (derivative feedback) was included to control the heading of the helicopter. The yaw rate damping subsystem was set up using the same criteria as would have been used by any other model helicopter pilot:

1. Before the helicopter is flown, the pilot ensures that the rate damping system provides negative and not positive rate feedback.
2. A number of short hover flights are then flown in low wind speed conditions. The feedback gain is increased until the closed loop system starts oscillating (the tail starts "wagging"). The feedback gain is then reduced to provide some gain and phase margin.
3. The helicopter is finally flown in windy conditions and the gain reduced if any oscillations are noticed.

The results obtained during a test flight with heading angle feedback can be seen in figure 7.1. During the flight described in figure 7.1, the other feedback loops were under pilot control. The author used the keyboard of the ground control station PC to command heading steps in increments of 20°.

Figure 7.2 presents a flight during which the pilot controlled the horizontal movement (indoors), while both the altitude and heading were under computer control. Unfortunately the heading reference commands were not recorded during this flight. However, the 20° incremental steps are visible between times 110 s and 130 s. Figure 7.2 will be discussed in more detail in section 7.2.

It is difficult to examine the accuracy of the heading estimate during flight since the pitch and roll angles together with magnetometer measurements are used to calculate the

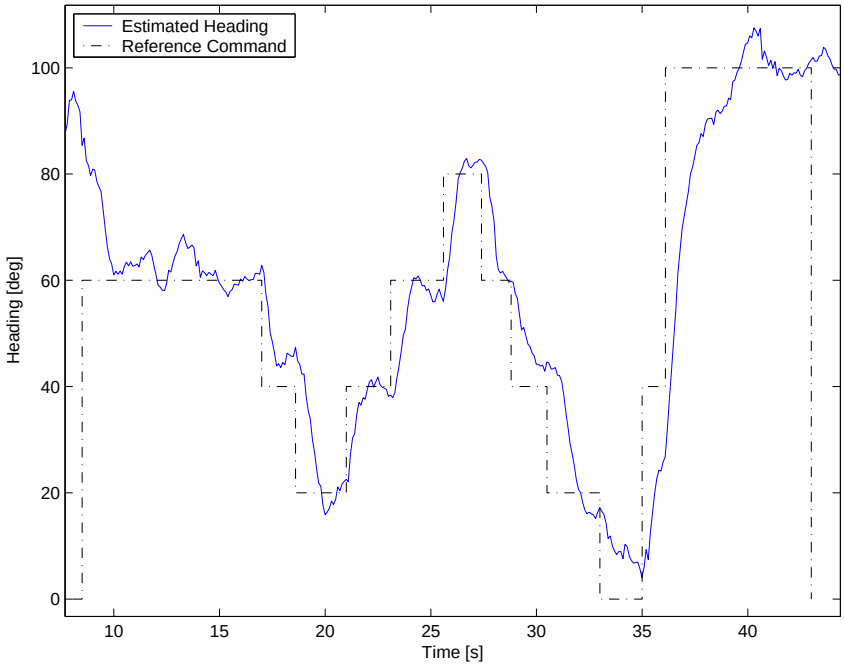

Figure 7.1: *Flight demonstration of yaw angle response under PC control to commanded yaw angle step changes*

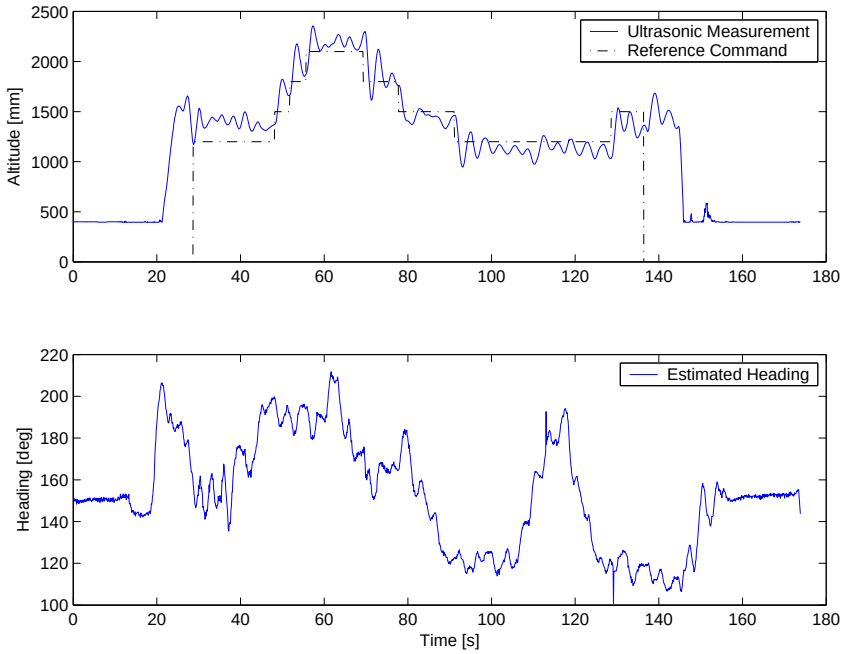

Figure 7.2: *Measured altitude and estimated heading during flight testing with altitude and heading simultaneous under PC control*

heading. Combining the magnetometer readings with yaw rate gyroscope measurements would be a sensible next iteration at refining the estimates - assuming once again that small pitch and roll angles are maintained.

Controlling the heading was not too difficult. Although the controller only succeeds in keeping the heading within $\pm 10^\circ$ of the commanded reference, the performance is sufficient as a first iteration controller for near-hover flight.

7.2 Altitude Control

The second control loop that was successfully closed indoors was the altitude control loop. The Polaroid ultrasonic range sensor was used to measure the climb rate and the altitude. Both the climb rate and the altitude were fed back to close the altitude control loop, as was described in section 6.2. The strategy can be viewed as proportional-derivative control of the altitude.

During initial flight testing no lead compensation (derivative control) was used due to intermittently experienced ultrasonic range measurement problems. The results obtained during one of the first altitude control flight tests can be seen in figure 7.3. The ultrasonic sensor performed very well during this particular flight test. Due to too high proportional gain the system began oscillating. The oscillations were growing at a very slow rate.

One of the biggest risks during the testing of the altitude control loop is that the FCS will decrease the collective-throttle too much while the helicopter is flying at "eye-level". If the command to the collective-throttle was found to be lower than the hover trim setting, the feedback gain was reduced to limit the rate of downward acceleration to prevent the helicopter from responding too fast to noisy, intermittently failing ultrasonic range measurements.

The vertical response of the Voyager E was simulated using the simplified model with the parameters identified in section 2.4.1, $Z_{\delta_c} \approx 13.5$ and $Z_w \approx -1.1$. The results obtained can be seen in figure 7.4. The frequency and amplitude of the simulated response (figure 7.4) and the last 20 s of the flight test (figure 7.3) correspond well.

Once the intermittently experienced ultrasonic range measurement problems were solved, only safety limitations were placed on the collective-throttle control. During all of the flight tests, the controller never reached these safety limitations. Engine failures and battery failures did however cause a number of hard, unexpected landings and hair-raising moments.

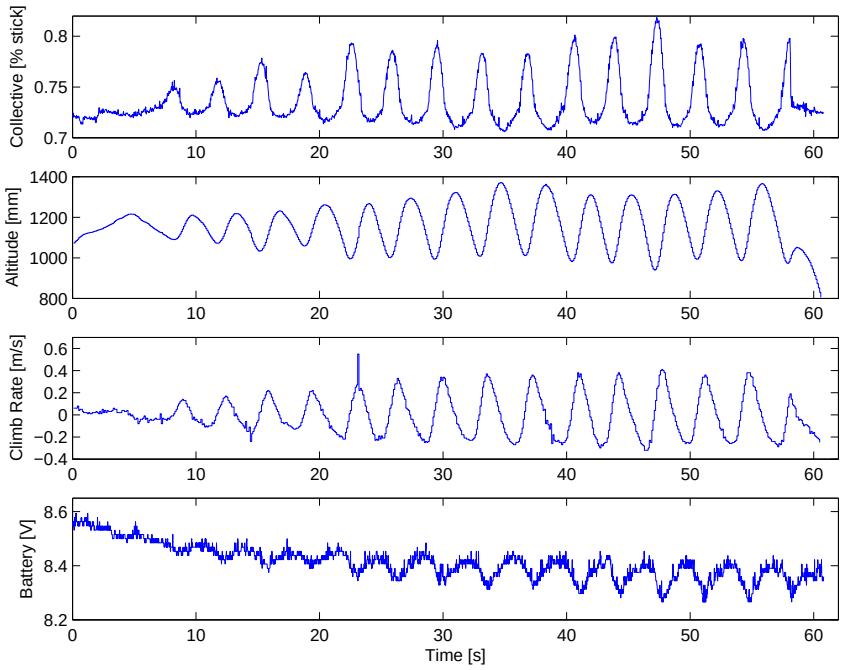

Figure 7.3: *Altitude oscillations measured during flight tests under PC control with too high proportional feedback gain*

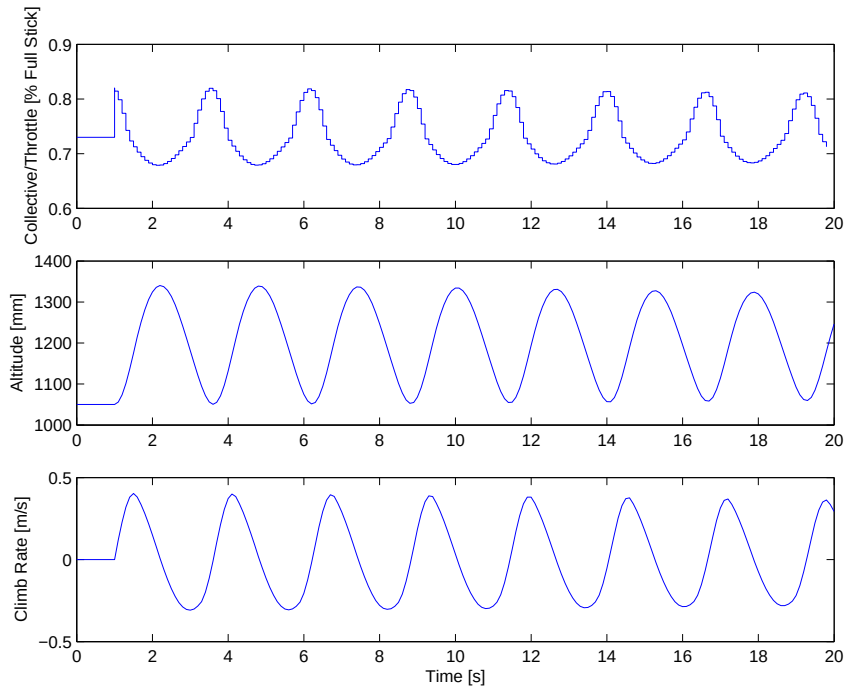

Figure 7.4: *Simulated altitude oscillations under PC control with too high, non-linear proportional feedback gain*

As has been described in section 2.4.1: the accuracy of the heave model could not be tested thoroughly. Both Z_{δ_c} and Z_w were identified using a single set of positive step commands. A number of higher order effects and/or differences between ascent and descent might be the cause of the anomalies between the simulated and measured flight test results. The influence of the battery voltage and electronic speed controller (ESC), lack of main rotor RPM regulation and differences between descending and climbing flight have not been investigated.

Another interesting phenomenon seen in figure 7.2 is the small disturbance on the altitude that coincides with a significant change in heading at time 110 s. The altitude oscillations are dying when there is a sudden increase in the altitude oscillations, as the heading is changed. The heading reference commands were unfortunately not recorded, but were once again applied in steps of 20°. Mettler *et al.* acknowledges the coupling between yaw rate and climb rate in their eleventh order model, while Gavrilets *et al.* [19, 20] have neglected the coupling.

Figure 7.5 shows the results obtained while the pilot was flying longitudinal and lateral movements (indoors) with the altitude under PC control. The helicopter was moved around within a 15 m radius. Due to the lack of indoor position measurements and reliable attitude estimates, the translational "disturbances" and cross coupling between states could not be investigated. However, it can be seen that the helicopter follows the reference height command within less than ±0.3 m during the majority of the flight.

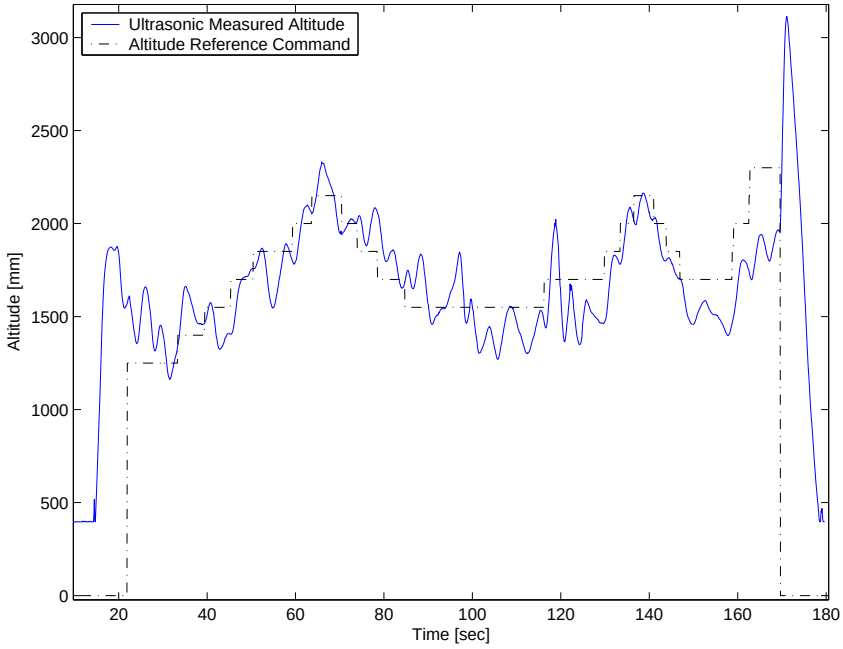

Figure 7.5: *148 second flight testing of altitude controller, with longitudinal and lateral movements performed by the pilot*

Notice that as the pilot takes over control at the end of the flight, he has the collective-throttle command stick at 100% of the stick movement. The safety pilot continues to move his control sticks while the helicopter is under computer control. With time the safety pilot learned to adjust the position of the control sticks to minimise transients when switching from autonomous to manual control. However, during the flight the required hover collective-throttle command bias moved from 73% to 84%, which is very difficult for the pilot to anticipate. Eleven percent stick movement is significant since an eight percent collective-throttle step command resulted in 1.1 m/s climb (see figure 2.2). The low frequency disturbance can also be noticed in figure 7.5.

The altitude controller works well as long as the ultrasonic range sensor is providing measurements with low noise levels. Due to high noise levels measured by the ultrasonic range sensors during some flights, the lead feedback could not be increased without degrading the overall performance of the system. No filter was required to smooth the measurements from the ultrasonic range sensor during the flights portrayed in figures 7.2 and 7.5.

Simulation has shown that significantly better damping can be achieved by increasing the derivative feedback gain. The low frequency disturbance rejection can be improved through the addition of integral control (lag compensation) or a main rotor speed governor.

Probably the most valuable change to the altitude control system would be to design and implement an estimator to reduce the effect the ultrasonic range sensor noise has on the performance of the altitude controller. The inertial sensors, or other sensors like a high resolution DGPS or vision system could be used to create a complementary filter to measure the altitude.

Figure 7.6 shows vertical accelerations and velocities measured during aggressive pilot-controlled climbs and descents. Since the helicopter was flying at low pitch and roll angles the vertical accelerations can be measured using the vertically mounted accelerometer. Assuming that low pitch and roll angles are maintained, it would be possible to construct an estimator that combines the accelerometer and ultrasonic range sensor measurements to obtain a better estimate of the helicopter climb rate.

Figure 7.6 also shows that the battery voltage increases while the helicopter is descending, while during most of the ascents it does not drop significantly below the hover value. With the aid of a model that describes the relationship between heave, the battery voltage and the main rotor RPM, more valuable simulation tests can be performed.

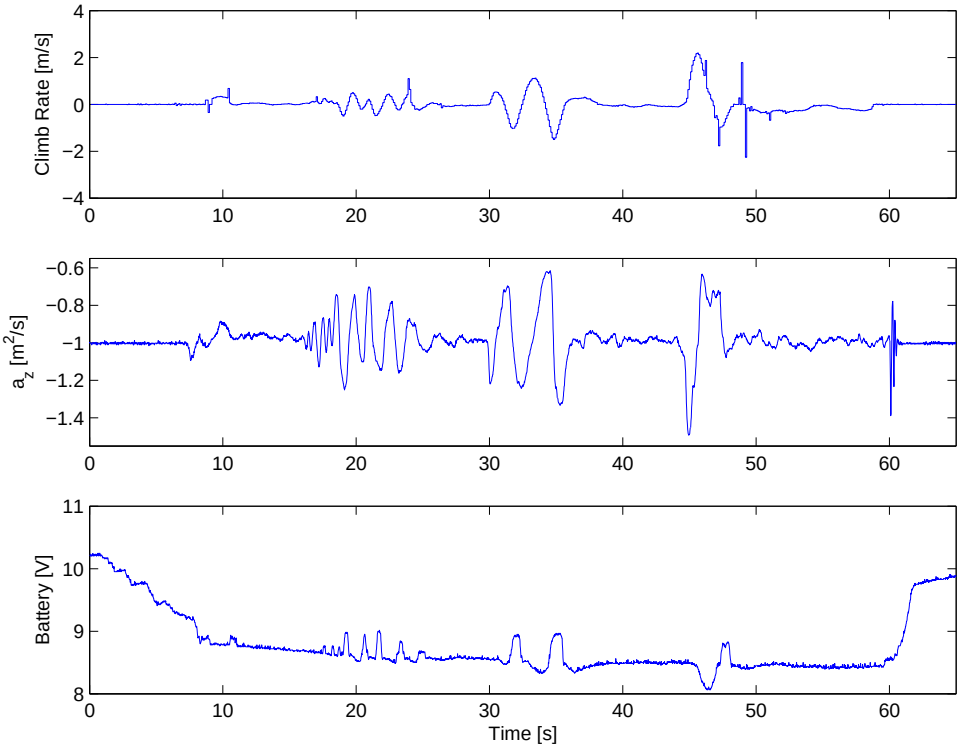

Figure 7.6: *Ultrasonic, accelerometer and battery voltage measurements during aggressive climbing manoeuvres under pilot control*

7.3 Horizontal Control

7.3.1 Pitch Angle Control

The initial pitch angle controller tests were conducted indoors using the Kahn-Hudson EKF to estimate the pitch angle. Due to the lack of sensors providing velocity and position measurements indoors, the pitch angle had to be determined using only inertial sensor measurements. After the u-Blox GPS receiver was acquired and tested, all indoor tests were stopped and the focus shifted to demonstrating position control outdoors.

Two methods were used to test the pitch angle controller indoors:

1. The PC operator could command reference pitch angles for the FCS to follow.
2. Starting in hover, the safety pilot would command a pitch angle before passing control over to the FCS. The FCS then had to correct the pitch angle to the initial hover pitch angle.

PC Keyboard Reference Pitch Angle Commands

Figure D.1 shows the results obtained using keyboard reference pitch angle commands to test the pitch angle controller. During this flight test the author succeeded in keeping the helicopter within a three metre radius from the take-off point for over 30 s using the keyboard to command reference pitch angles.

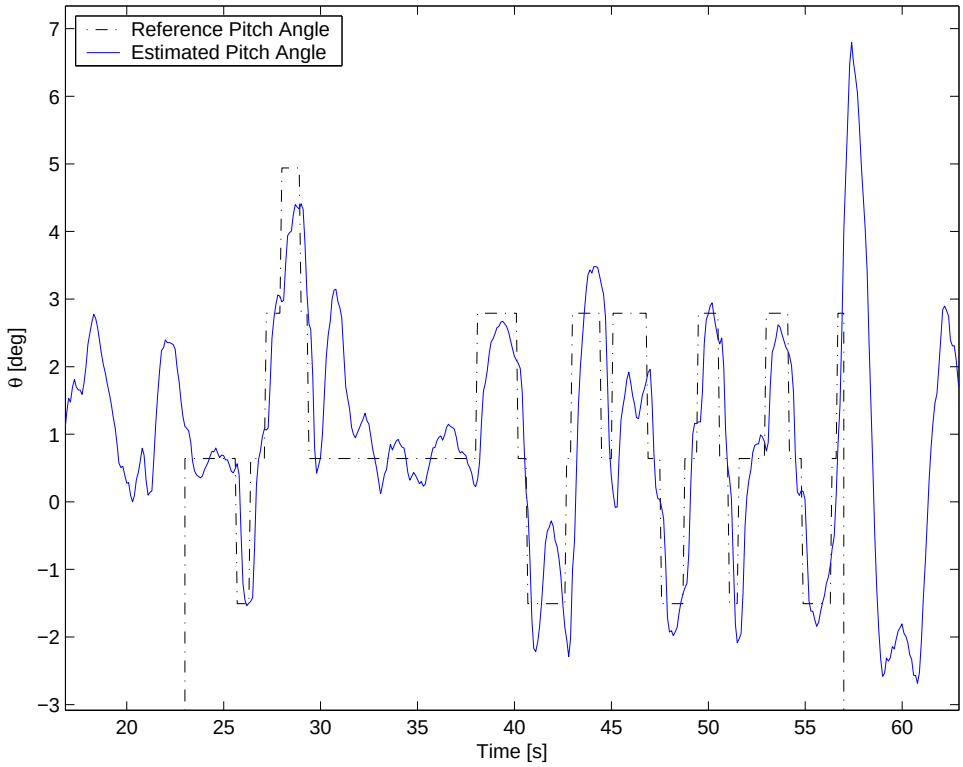

Figure 7.7: *Pitch angle controller flight test using PC keyboard to input reference pitch angle commands*

It is difficult to qualify the nature of the anomalies between the reference commands and the estimated pitch angle response since no velocity or position measurements were available indoors at the time that these experiments were conducted. However, from the figure it is clear that the controller succeeds in stabilising the pitch angle. It can be seen that the helicopter follows the reference pitch angles to within approximately $\pm 1^\circ$ during the majority of the flight.

Using a simplified helicopter model, it can be shown that if a pitch angle error of 1° is maintained for one second, the resultant position error would be approximately 9 cm - assuming no position or velocity feedback is used to control the helicopter. The accuracy of the pitch angle estimate can however not be judged based only on the information provided in figure D.1.

Failure to Restore the Hover Pitch Angle

Figure 7.8 presents an example of the second set of experiments performed. The safety pilot gave a nose down (negative pitch rate) command (starting at time 23.7 s) before passing control to the FCS at time 24.5 s.

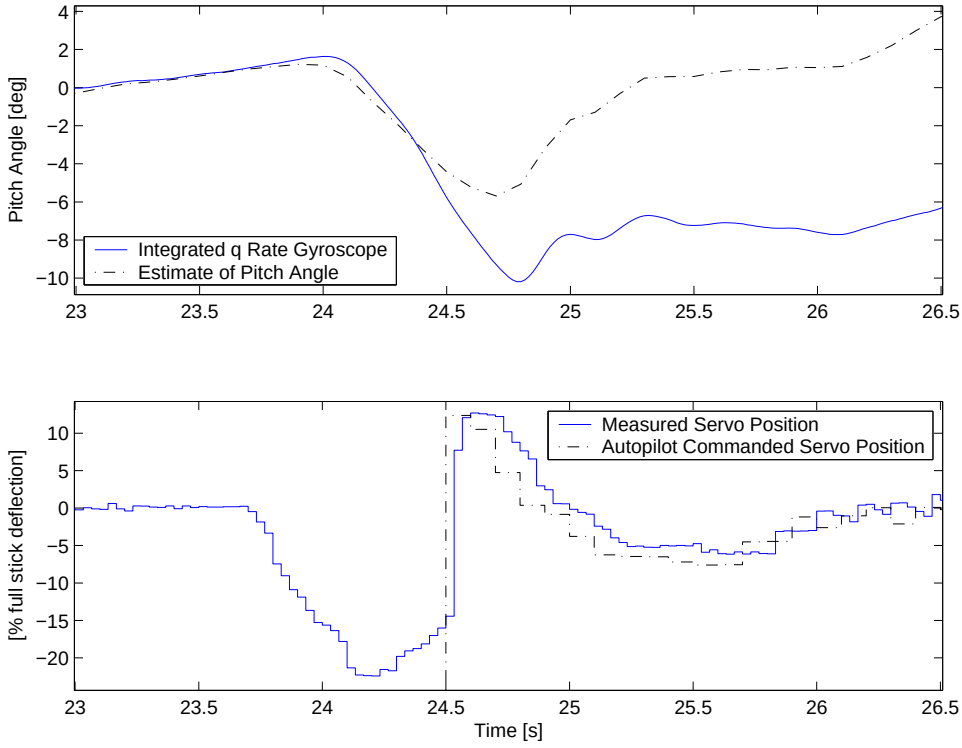

Figure 7.8: *Testing ability of pitch angle controller to correct helicopter pitch angle after pilot induced disturbance*

The pilot ensures that the helicopter body maintains a near zero roll angle during the pitching manoeuvres. The measurements from the body pitch rate gyroscope can therefore be integrated over a short period of time to determine the change in Euler pitch angle.

It was found that although the pitch angle controller did restore the helicopter pitch angle to the Kahn-Hudson EKF estimated hover pitch angle, the EKF estimated pitch angle was wrong. The change in the EKF estimated pitch angle was not the same as was measured using the integrated pitch rate gyroscope measurements. Figure 7.8 compares the pitch angle estimate from the Kahn-Hudson filter with the change in angle measured by the pitch rate gyroscope. At time 26.5 s the nose down attitude and acceleration of the helicopter was physically visible during the test flight, confirming the integrated rate gyroscope measurements. The pilot switches back to manual control after time 26.5 s.

At time 25.5 s the angular rate is zero. The EKF output indicates that the hover pitch angle has beeen restored, while the integrated rate gyroscope indicates a 7° angle difference between the pitch angles at time 23.5 s and 25.5 s. A pitch angle error of 7° will result in an initial acceleration of 1.2 m/s^2. The position error will be approximately 2.4 m after two seconds if no or highly delayed velocity and position measurements are fed back to control the position of the helicopter.

One of the contributing reasons for the incorrect estimator outputs might be the selected values of $\mathbf{Q}_k$ and $\mathbf{R}_k$, as was described in section 3.3.4. Placing too much weight on the pitch and roll angles calculated using the accelerometer measurements will falsely correct the outputs of the filter too fast for bias drift of the rate gyroscopes. However, if the time constant is increased to make the angle estimates less dependant on the accelerometer measurements, the influence of the rate gyroscope biases on the angle estimates reaches unacceptably high levels.

The EKF requires three rate gyroscope, three accelerometer and three magnetometer measurements to estimate the Euler angles of the helicopter. Debugging the filter is not an easy task if the sensors contain random walk and noise.

Alternative filters and estimators were investigated, for example the filter described in section 3.3.3. No significant, reliable improvements were found through changing only the filter without using different sensors.

After initial tests using the u-Blox GPS receiver and the Analog Devices ADXRS150 rate gyroscope, the Rotomotion IMU and Kahn-Hudson EKF were no longer used to estimate the pitch and roll angles. The vehicle kinematics based estimator that was described in section 3.3.5 was successfully used to control the pitch angle of the helicopter.

7.3.2 Longitudinal Position Control

Within a few hours from beginning the flight tests using the vehicle kinematics based pitch angle estimator, the longitudinal velocity and pitch angle were stabilised and the position controller tests begun.

Figure 7.9 shows one of the tests that was performed. The pilot took the helicopter off, flew 5 m forward (guided by tape markings on the ground), and gave control of the longitudinal position over to the FCS at time 28 s. Within seven seconds the helicopter settled within half a metre from the cross marking the take-off position, before moving further back for an unknown reason. Due to the space confinement the pilot could not allow the helicopter to drift further back and had to take over control at time 45 s.

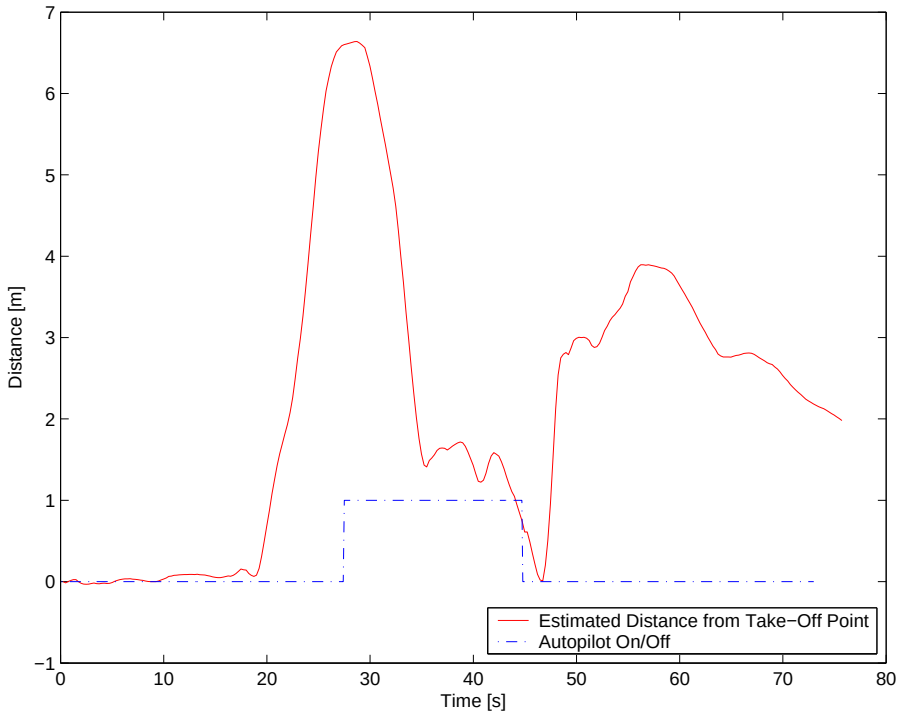

Figure 7.9: *Testing ability of longitudinal position controller to correct 5 m position offset*

The following day the first successful 104 s long PC controlled longitudinal position flight was completed. The FCS kept the longitudinal position of the helicopter within a 4 m radius from the commanded zero reference position. The pilot controlled the heading, altitude and lateral motion of the helicopter.

The flight is described in figures 3.3, 3.4, 3.5 and 7.10. The safety pilot passes control of the longitudinal motion over to the FCS at time 27 s, and reclaims control at time 131 s, landing the helicopter at time 146 s, within 0.2 m from the take-off position.

Although figures 7.9 and 7.10 provide relatively good indications of the position of the helicopter during the longitudinal position controller flight testing, the position estimates also contain errors. The error in the estimated position in figure 7.10 is 2.2 m at the time of landing (time 146 s). Similarly, the point at which the pilot gave control to the FCS in figure 7.9 was not at 6.5 m (as indicated by the estimated position values) but within less than 0.5 m from the 5 m mark. The factors contributing to the errors in the estimated position, obtained through integration of the velocity estimates, have not yet been quantified. The heading estimation errors, velocity estimation errors and the inability of the pilot to maintain a constant heading are most likely three of the main contributing factors.

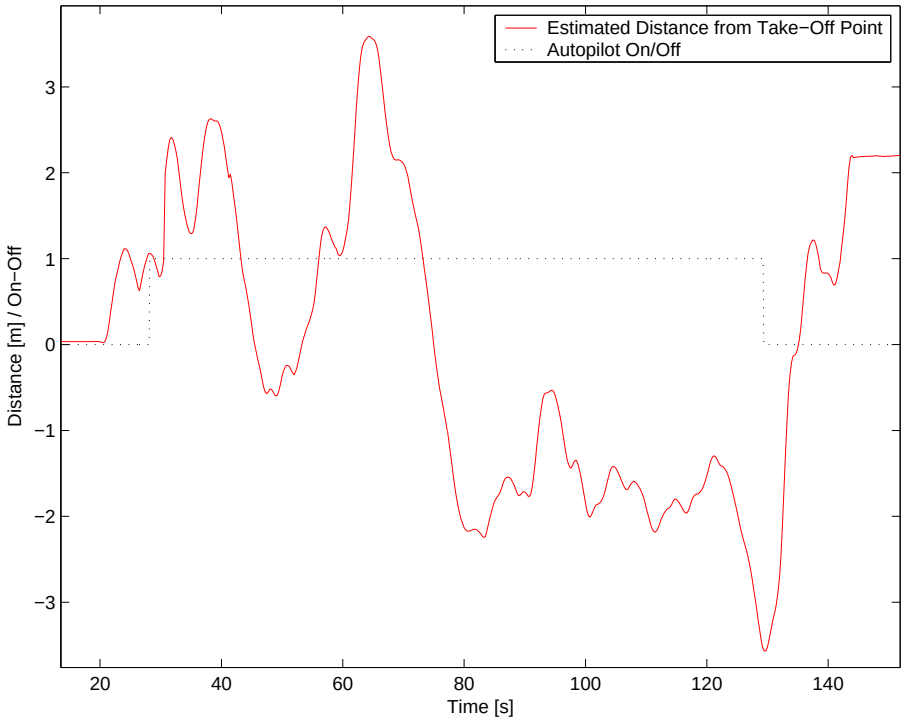

Figure 7.10: *Position estimate during* 104 *s longitudinal PC control*

The random walk of the position measurements from the GPS receiver was found to be too fast (up to 0.9 m/s) and large and therefore no GPS position measurements were used to estimate the position of the helicopter.

The next day the motor stopped working in mid-air, a few hours before a demonstration flight was to be conducted. After a very hard landing, the motor was replaced and the preparations for the demonstration continued. However, after the incident and motor replacement, neither the heading nor the altitude control loops worked reliably. During the following weeks of testing it was found that high vibration levels were being measured, which influenced the majority of the sensors. The problem progressively worsened.

The project was concluded due to time limitations and mechanical complications of the vehicle.

7.4 Conclusion

This chapter presented the results obtained using the implemented flight control system. The heading, altitude and longitudinal position loops were closed successfully, although none of the controllers have proved to be robust.

System integration complications, vibrations, payload restrictions and non-ideal low cost sensors make controlling a real model helicopter significantly more challenging than predicted by simulation. After thorough investigation it has been found that limited success has been achieved using low cost sensors. Even projects using larger glow or gasoline powered helicopters struggle to perform autonomous take-off and landing without the aid of a high quality DGPS, a high quality IMU or vision aiding.

During the development of all of the controllers, one problem has dominated: state measurement and estimation. The majority of time and effort invested in this project has been dedicated to the development of hardware and algorithms to improve the state measurements and estimates.

These efforts have paid off and a number of problems have been identified. The final results obtained look promising, but more time and effort will have to be invested in testing the proposed solutions.

Chapter 8

Conclusion

This document has outlined the progress made towards the development of a low cost, low weight FCS for a RC model helicopter. A basic FCS has been designed, implemented and tested. The system modelling, state estimation, hardware selection, system simulation, control law analysis and flight test results have been presented.

8.1 Project Overview

8.1.1 Selected Helicopter

The two properties of the JR Voyager E helicopter that distinguish it from most other RC helicopters that have been used as platforms to create autonomously flying RUAV systems are:

- The rotor diameter of the helicopter is sub-one-metre.
- It is an electrically powered helicopter.

The movement of most other electrically powered helicopters has been restricted using a variety of support structures. To the knowledge of the writer, at the time of writing, no other research group has demonstrated a more mature autonomous RUAV system using an electrically powered helicopter with a sub-one-metre rotor diameter. The success using un-tethered, small, electrically powered rotary-wing vehicles has been limited.

Due to the marginal payload, decreased stability and frequent mechanical failures (see appendix B), the Voyager E has been a frustrating vehicle to operate. Payload restrictions

influence every component of the system: vibration isolation, electromagnetic shielding and selection of sensors, communication devices and processors. The vehicle was found to have low immunity against even mild wind speeds and lacks general mechanical reliability.

The author's conclusion is that this small electrically powered helicopter is neither a low cost nor a mechanically simple or reliable alternative to glow and gasoline powered helicopters. When the maintenance costs, like motor replacements and brushes, and expenses like chargers and batteries are taken into account, it is as expensive to operate as a larger glow powered helicopter.

8.1.2 Hardware and System Integration

A variety of sensors were acquired, tested and integrated.

A Honeywell three-axis magnetometer was used to measure the magnetic field of the earth. Although it is not the cheapest magnetic field sensor available on the market, the work done by previous students has proved that it is a reliable, small and high quality sensor. A printed circuit board carrying the sensor, set/reset and signal conditioning electronics was designed to fit onto the tail boom of the helicopter. The location of the sensor provided sufficient clearance between the sensor and magnetic noise sources. The heading of the helicopter was successfully controlled using the measurements from the Honeywell sensor.

A Polaroid ultrasonic range sensor was successfully integrated and used to control the altitude of the helicopter. Mounting the ultrasonic range sensor requires careful consideration and testing of vibration isolation and electromagnetic compatibility with the rest of the system.

Two sets of rate gyroscopes were used: the Tokin CG-16D and Analog Devices ADXRS150 sensors. The bias of the Tokin rate gyroscopes was found to be very sensitive to temperature changes. Bias stability and scaling were the primary factors making the Analog Devices ADXRS150 rate gyroscopes superior sensors for this project. Vibration isolation and filtering of the rate gyroscopes and accelerometers have proved to be important to obtain high accuracy attitude estimates and prevent saturation of the sensors.

Static ground based tests, dynamic ground based tests and flight tests were conducted to compare two different GPS receivers. The u-Blox GPS receiver replaced the Sigtec Navigation GPS receiver due to the lower delays, higher update rates and more accurate velocity measurements obtained from the u-Blox GPS receiver.

A small, lightweight 2.4 GHz video transmitter and receiver was used to develop a data communication link to transmit data from the helicopter to the ground control station.

8.1.3 State Estimation

Various filtering techniques were investigated during the development of the system. The source code for the Kahn-Hudson EKF was tested and theoretically investigated. The filter utilises three rate gyroscope, three accelerometer and three magnetometer measurements to estimate the attitude of the vehicle. Due to the complexity of the filter it is difficult to isolate the sources of errors in the filter.

A simpler vehicle kinematics based estimator proved sufficiently accurate to control the longitudinal position of the helicopter within ± 4 m from the launch point under low dynamic conditions.

8.1.4 Helicopter Model and Flight Control

The models that have been published by other authors have been investigated. The properties of the Voyager E were compared to the properties of other helicopters that have been used and characterised by others for use in similar projects.

Based on the published models, simulations were performed to show that a model helicopter can be controlled near-hover using simple PID controllers. These findings are supported by numerous demonstrations of helicopters that are flying autonomously using simple SISO PID controllers.

8.2 Achievements

8.2.1 Literature Study

This project was the first project in the Computer and Control group of the University of Stellenbosch utilising a RC helicopter. In an effort to further strengthen the knowledge foundation within the group, a significant amount of time was spent studying the works that have been published by other authors. The publications of more than seventeen academic research institutions and other commercial projects have been investigated.

For more information regarding the thesis documents, technical reports, articles and

other publications used, refer to Appendix A and the compact disc that accompanies this document.

8.2.2 Hover Control

Yaw angle, height and longitudinal position controllers were implemented and demonstrated.

The yaw angle of the helicopter was commanded in reference increments of 20° and controlled to within less than ±10°. Higher accuracy and resolution magnetometer measurements and pitch and roll angle estimates are required to further improve the accuracy of the controller.

The height was controlled to within ±0.4 m. Using simulations and tests performed it has been shown that the performance of the altitude controller can be improved if the climb rate damping can be increased. This objective can be achieved through implementation of an estimator that combines the ultrasonic range sensor measurements with measurements from other sensors. The low frequency errors can be reduced by adding a lag compensator (integral control) and/or a main rotor RPM governor.

The longitudinal position of the helicopter was controlled to within less than ±4 m from the launch point for more than one and a half minutes. The lack of an accurate position measurement remains the primary factor limiting the performance of the controller.

8.2.3 Cost and Weight

The total component cost of the system, including every subsystem required, except a desktop or notebook PC, the helicopter and standard RC transmitter and receiver equipment, is approximately US$ 1000. The price includes a three-axis magnetometer worth approximately US$ 300, which was selected due to the availability of knowledge and experience of people who have worked with the sensor. The sensor can be replaced with an alternative low cost sensor [26], or bought as a non-integrated set of individual sensors at a fraction of the cost [31].

The total weight of the components that were added to the helicopter is less than 0.4 kg. The additional weight of the larger battery pack is not included in the specified 0.4 kg since the battery pack has been added to improve the endurance of the vehicle.

8.3 Recommendations for Future Work

8.3.1 Sensors

The majority of complications experienced in the development of the FCS were related to sensor inadequacies. The performance of the controller is directly related to the accuracy, delay and update rate of the attitude, velocity and position state estimates. To the knowledge of the author, no group has published results indicating successful autonomous landing or sub-one-metre accurate hover without using either DGPS or a vision aiding sensor system. These position sensors typically have update rates of 5 Hz or higher, and position measurement accuracies in the order of $2-5$ cm. The first step toward improving the horizontal position control accuracy would be to improve the accuracy of the position measurements.

The accuracy of the raw IMU measurements can be improved, which would lower the dependance on filters and other sensors to estimate the states of the vehicle. Using higher sampling rates, external 12- or 16-bit ADC and improved mounting of the rate gyroscopes would improve the accuracy of the attitude estimates.

8.3.2 Main Rotor RPM Governor

It would simplify the task of describing the dynamics and controlling the helicopter if the main rotor blade speed was measured and regulated. Due to variations in battery voltage it is even more important than in the case of a gasoline and glow powered helicopter to be able to control the main rotor blade speed independent of the main rotor collective pitch angle.

8.3.3 Data Communication Links

The current configuration requires a reliable communication link transmitting data from the helicopter to the ground control station in order to control the helicopter using the DSC plug. The poor reliability of the current communication link limits the operational range of the vehicle.

The dependency on this communication link can be removed by shifting all of the computation to the helicopter. The control laws are simple and should not be difficult to implement using the existing microcontrollers. The state estimation algorithms will

determine the additional processing power required onboard the helicopter.

Being able to operate without the data communication link would not only increase the operational range and reliability of the system, but decrease and make it possible to identify the exact magnitudes of the delays between measurements and control signals. This change would make it possible to describe and design the controllers more accurately.

8.3.4 Weight of Subsystems and Helicopter Size

Reducing the weight of PCBs, sensors, mountings, replacing the standard motor with a brushless motor, switching to low weight Lithium batteries and replacing some plastic components with aluminium components will improve the endurance, performance and reliability of the current system. The helicopter will however remain a small vehicle with minimal payload-carrying capability.

Larger gasoline and glow powered helicopters offer significantly better power to weight ratios, are more stable and mechanically reliable than smaller electrically powered model helicopters. For these reasons a glow powered Miniature Aircraft X-Cell Fury helicopter has been purchased for future work at the ESL.

8.4 Conclusion

The goal of the project was to investigate and demonstrate near-hover manoeuvres performed by a small electrically powered rotary-wing vehicle.

To date, most RUAV projects have solved the measurement and estimation problems using expensive, heavy measurement and processing equipment. Due to the vehicle chosen and the goal of keeping the costs low, alternative solutions had to be sought.

In spite of the time, cost and weight constraints, a solid foundation has been prepared for future work. An extensive literature study has been completed, the problem has been investigated theoretically and the heading, altitude and longitudinal position of a real electrically powered RC helicopter have been controlled successfully.

> "*Hovering over a spot is a precision manoeuvre comparable to landing an airplane, and it doesn't come easy.*" - R. W. Prouty [50]

Bibliography

[1] AMIDI, O., *An Autonomous Vision-Guided Helicopter*. PhD thesis, Carnegie Mellon University, August 1996.

[2] ARMS, S., "Microstrain." http://www.microstrain.com/inclino.htm.

[3] BAERVELDT, A.-J. and KLANG, R., "A Low-cost and Low-Weight Attitude Estimation System for an Autonomous Helicopter."

[4] BRYSON, A. E., *Control of Spacecraft and Aircraft*. Princeton University Press, 1994.

[5] BUSKEY, G., ROBERTS, J., CORKE, P., RIDLEY, P., and WYETH, G., "Sensing and Control for a Small-Size Helicopter." *International Symposium on Experimental Robotics, Sant' Angelo d' Ischia, Italy*, July 2002.

[6] BUSKEY, G., ROBERTS, J., CORKE, P., and WYETH, G., "Helicopter Automation Using a Low-Cost Sensing System." *Australasian Conference on Robotics and Automation*, 2003.

[7] BUSKEY, G., ROBERTS, J., and WYETH, G., "A helicopter named Dolly - Behavioural cloning for autonomous helicopter control." *Australasian Conference on Robotics and Automation*, 2003.

[8] CALITZ, P. C., "HOPTUS: Elektries-Aangedrewe Helikopter Platform." tech. rep., University of Stellenbosch, 1998.

[9] CARUSO, M. J., "Applications of Magnetic Sensors for Low Cost Compass Systems." tech. rep., Honeywell.

[10] CHEN, M. and HUZMEZAN, M., "A Combined MBPC/2DOF H infinity Controller for a Quad Rotor UAV." *AIAA Atmospheric Flight Mechanics Conference and Exhibit, Austin, Texas, USA*, August 11-14 2003.

[11] CONWAY, A. R., *Autonomous Control of an Unstable Model Helicopter Using Carrier Phase GPS Only*. PhD thesis, Stanford University, March 1995.

[12] CORKE, P., SIKKA, P., and ROBERTS, J., "Height estimation for an autonomous helicopter." *International Symposium on Experimental Robotics*, 2000.

[13] DRAGAN, Z., "RC Toys: Dragan Flyers." http://www.rctoys.com.

[14] DUINE, A., "Paparazzi Quick and Dirty UAV." http://www.nongnu.org/paparazzi/.

[15] ECK, C., *Navigation Algorithms with Applications to Unmanned Helicopters*. PhD thesis, Swiss Federal Institute of Technology Zurich, 2001.

[16] ETTINGER, S. M., NECHYBA, M. C., IFJU, P. G., and WASZAK, M., "Vision-Guided Flight Stability and Control for Micro Air Vehicles." *Proc. IEEE Int. Conference on Intelligent Robots and Systems*, October 2002.

[17] FRAZZOLI, E., *Robust Hybrid Control for Autonomous Vehicle Motion Planning*. PhD thesis, Massachusetts Institute of Technology, June 2001.

[18] GAVRILETS, V., METTLER, B., and FERON, E., "Dynamic Model for X-Cell 60 Helicopter in Low Advance Ratio Flight." *Laboratory of Information and Decision Systems Technical Report P-2543*.

[19] GAVRILETS, V., METTLER, B., and FERON, E., "Nonlinear Model for a Small-Size Acrobatic Helicopter." *AIAA Guidance, Navigation, and Control Conference, Montreal, Canada*, August 2001.

[20] GAVRILETS, V., METTLER, B., and FERON, E., "Control Logic for Automated Aerobatic Flight of a Miniature Helicopter." *AIAA Guidance, Navigation and Control Conference, Monterey*, August 2002.

[21] GAVRILETS, V., SHTERENBERG, A., DAHLEH, M. A., and FERON, E., "Avionics system for a small unmanned helicopter performing aggressive maneuvers." *Digital Avionics Systems Conference*, 2000.

[22] HAMEL, T., MAHONY, R., LOZANO, R., and OSTROWSKI, J., "Dynamic Modelling and Configuration Stabilization for an X4-Flyer." *IFAC 15th Triennial World Congress*, 2002.

[23] HONEYWELL. *Set/Reset Pulse Circuits for Magnetic Sensors*. Application Note 201.

[24] HRABAR, S., "University of South California." http://www-robotics.usc.edu/~avatar/projects.htm.

[25] HUBBARD, A., "Intelligent 3-Axis Magnetometer." tech. rep., University of Stellenbosch, November 2002.

[26] HUDSON, T., "Rotomotion." http://rotomotion.com/index.htm.

[27] HUDSON, T., "Source Forge Autopilot group." http://autopilot.sf.net.

[28] KAHN, A. D., "The Design and Development of a Modular Avionics System." Master's thesis, Georgia Institute of Technology, April 2001.

[29] KIM, H. J., SHIM, D. H., and SASTRY, S., "A Flight Control System for Aerial Robots: Algorithms and Experiments." *Control Engineering Practice*, April 2003.

[30] KINGSTON, B. D. and BEARD, R. W., "Real-Time Attitude and Position Estimation for Small UAVs." *IEEE American Control Conference*, 2004.

[31] LAMERS, R., "MGL Avionics." http://www.mglavionics.co.za/.

[32] MCRUER, ASHKENAS, and GRAHAM, *Aircraft Dynamics and Automatic Control*. Princeton University Press, 1973.

[33] METTLER, B., DEVER, C., and FERON, E., "Scaling Effects and Dynamic Characteristics of Miniature Rotorcraft." *AIAA Journal of Guidance, Control and Dynamics*, May - June 2004, Vol. 27, pp. 466–478.

[34] METTLER, B., GAVRILETS, V., FERON, E., and KANADE, T., "Dynamic Compensation for High-Bandwidth Control of Small-Scale Helicopter." *American Helicopter Society Aerodynamics, Acoustics and Test and Evaluation Technical Specialist Meeting. San-Francisco*, January 2002.

[35] METTLER, B., KANADE, T., TISCHLER, M. B., and MESSNER, W., "Attitude Control Optimization for a Small-Scale Unmanned Helicopter." *AIAA Guidance, Navigation and Control Conference, Denver, Colorado*, 2000.

[36] METTLER, B., TISCHLER, M. B., and KANADE, T., "System Identification of Small-Size Unmanned Helicopter Dynamics." *55th Forum of the American Helicopter Society, Montreal, Canada*, May 1999.

[37] METTLER, B., TISCHLER, M. B., and KANADE, T., "System Identification Modeling of a Small-Scale Unmanned Rotorcraft for Flight Control Design." *American Helicopter Society Journal*, 2002.

[38] MICROPILOT, "MicroPilot." http://www.micropilot.com.

[39] MOOREN, F., "Practical Work Experience Period - HOPTUS Prestudy." tech. rep., Delft University of Technology, 1996.

[40] MUNZINGER, C., "Development of a Real-Time Flight Simulator for an Experimental Model Helicopter." Master's thesis, Georgia Institute of Technology School of Aerospace Engineering, Atlanta, December 1998.

[41] MUSIAL, M., BRANDENBURG, U. W., and HOMMEL, G., "Success of an Inexpensive System Design: The Flying Robot MARVIN." tech. rep., Berlin University of Technology.

[42] MUSIAL, M., BRANDENBURG, U. W., and HOMMEL, G., "MARVIN: Technische Universitat Berlins Flying Robot for the IARC Millennial Event." tech. rep., Berlin University of Technology, 2000.

[43] MUSIAL, M., DEEG, C., REMUB, V., and HOMMEL, G., "Orientation Sensing for Helicopter UAVs under Strict Resource Constraints." tech. rep., Berlin University of Technology.

[44] NAFFIN, D. J. and SUKHATME, G. S., "A Test Bed for Autonomous Formation Flying." *Institute for Robotics and Intelligent Systems Technical Report IRIS-02-412*, 2002.

[45] NORTIER, B., "A Spaceborne GPS receiver." Master's thesis, University of Stellenbosch, 2003.

[46] O-NAVI, "O-Navi." `http://www.o-navi.com`.

[47] PADFIELD, G. D., *Helicopter Flight Dynamics: The Theory and Application of Flying Qualities and Simulation Modeling*. AIAA Education Series, 1996.

[48] PARK, S., *Avionics and Control System Development for Mid-Air Rendezvous of Two Unmanned Aerial Vehicles*. PhD thesis, Massachusetts Institute of Technology, February 2004.

[49] POUNDS, P., MAHONY, R., HYNES, P., and ROBERTS, J., "Design of a Four-Rotor Aerial Robot." *Proc. 2002 Australasian Conference on Robotics and Automation*, November 2002.

[50] PROUTY, R., *Practical helicopter aerodynamics*. PJS Publications, 1982.

[51] RÖNNBÄCK, S., "Development of an INS/GPS navigation loop for an UAV." Master's thesis, Luleå University of Technology, February 2000.

[52] SARIPALLI, S., ROBERTS, J. M., CORKE, P. I., BUSKEY, G., and SUKHATME, G., "A Tale of Two Helicopters." *Proceedings of IEEE/RSJ International Conference on Intelligent Robots and Systems*, October 2003, pp. 805–810.

[53] SARIPALLI, S., SUKHATME, G. S., and MONTGOMERY, J. F., "An Experimental Study of the Autonomous Helicopter Landing Problem." *Eighth International Symposium on Experimental Robotics*, July 2002.

[54] SHIM, D. H., KIM, H. J., and SASTRY, S., "Control System Design for Rotorcraft-based Unmanned Aerial Vehicles using Time-domain System Identification." *IEEE International Conference on Control Applications*, September 2000, pp. 808–813.

[55] SHIM, D. H., KIM, H. J., and SASTRY, S., "System Identification and Control Synthesis for Rotorcraft-based Unmanned Aerial Vehicles." *IEEE International Conference on Control Applications, Anchorage*, 2000.

[56] SHIM, H., *Hierarchical Flight Control System Synthesis for Rotorcraft-based Unmanned Aerial Vehicles*. PhD thesis, University of California, Berkeley, March 2000.

[57] SINDLE, T., "Design of an Orientation Sensor for Borehole Radar." tech. rep., University of Stellenbosch, November 2002.

[58] SPRAGUE, K., GAVRILETS, V., DUGAIL, D., METTLER, B., FERON, E., and MARTINOS, I., "Design and Application of an Avionics System for a Miniature Acrobatic Helicopter." *AIAA Digital Avionics Systems Conference, Daytona Beach*, October 2001.

[59] STEPNIEWSKI, W. Z. and KEYS, C. N., *Rotary-Wing Aerodnamics*, vol. One and Two. Dover Publications, New York, 1978.

[60] TANNER, O., *Modeling, Identification, and Control of Autonomous Helicopters*. PhD thesis, Swiss Federal Institute of Technology Zurich, 2003.

[61] TAYLOR, B., BIL, C., WATKINS, S., and EGAN, G., "Horizon Sensing Attitude Stabilisation: A VMC Autopilot." *18th International UAV Systems Conference*, 2003.

[62] TITTERTON, D. H. and WESTON, J. L., *Strapdown inertial navigation technology*. Peter Peregrinus Ltd. on behalf of the IEE, 1997.

[63] U-BLOX. *TIM-LC, TIM-LF, TIM-LP System Integration Manual*. GPS.G3-MS3-01001-A.

[64] VAGLIENTI, B. and HOAG, R., "Cloud Cap Technology." `http://www.cloudcaptech.com`.

[65] VAN DER MERWE, R. and WAN, E. A., "Sigma-Point Kalman Filters for Integrated Navigation." *60th Annual Meeting of The Institute of Navigation (ION), Dayton, Ohio*, June 2004.

[66] VENTER, D. W., "HOPTUS: A Case Study." tech. rep., University of Stellenbosch, 1996.

[67] WOODLEY, B., JENNINGS, C., CONWAY, A., and ROCK, S., "A Contestant in the 1995 Aerial Robotics Competition." tech. rep., Aerospace Robotics Laboratory, Stanford University, May 1995.

[68] ZARCHAN, P. and MUSOFF, H., *Fundamentals of Kalman Filtering - A Practical Approach*. American Institute of Aeronautics and Astronautics, 2000.

[69] ZHU, X. and VAN NIEUWSTADT, M., "The Caltech Helicopter Control Experiment." tech. rep., California Institute of Technology, June 1996.

Appendix A

References to Related Projects

The list of RC helicopter and RUAV projects to be presented in this appendix was inspired by a survey that was compiled by Christoph Eck in 2001 and presented in his PhD thesis document [15], as well as the vast amount of projects investigated by the author himself. A number of sites on the internet offer similar lists of references. Links to these sites have also been included.

A number of projects were not included due to a lack of information available on the projects or vehicles. The author decided not to include fixed wing projects due to the large number of fixed wing projects under development and the limited value these projects offer to researchers in the field of low cost RUAV systems.

The majority of references used in this project are digitally available from the web pages listed in this section. These and many more thesis documents, articles, technical reports and conference papers can also be found on the compact disk that accompanies this document.

Table A.1: *Academic Autonomous RC Helicopter Projects*

Institution:	Georgia Institute of Technology
URL:	`http://controls.ae.gatech.edu/gtar/`
	`http://avdil.gtri.gatech.edu/AUVS/IARCLaunchPoint.html`
Leadership:	Prof. Robert Michelson, Prof. Eric N. Johnson
Platform:	Yamaha R-50, Yamaha R-Max
Description:	Initiated IARC; first autonomous take-off and landing
Institution:	Stanford University ("Hummingbird")
URL:	`http://sun-valley.stanford.edu/~heli`
Leadership:	Dr Andrew Richard Conway (1995)
Platform	X-Cell 60
Description:	First autonomous RC helicopter flight; Attitude, velocity and position measurement using only four GPS antennas
Institution:	Massachusetts Institute of Technology
URL:	`http://gewurtz.lids.mit.edu/research/heli.htm`
	`http://gewurtz.lids.mit.edu/publications.htm`
Leadership:	Prof. Eric Feron, Dr Bernard Mettler
Platform:	X-Cell 60
Description:	First to perform aerobatic manoeuvres; Significant system identification and control research
Institution:	Carnegie Mellon University
URL:	`http://www.cs.cmu.edu/afs/cs/project/chopper/www`
Leadership:	Dr Omead Amidi (1996)
Platforms	Yamaha RMAX, Yamaha R-50
Description:	Won 1997 IARC; vision aiding; initial experiments conducted using a constrained electrically powered RC helicopter;
Institution:	ETH Zürich, Measurement and Control Lab
URL:	`http://www.heli.ethz.ch`
Leadership:	Prof. H.P. Geering, Dr C. Eck (2001), Dr O. Tanner (2003)
Description:	2nd in 1996 IARC; founded weControl; Initial experiments conducted using electrically powered RC helicopter on robot arm.
Institution:	University of California at Berkeley
URL:	`http://robotics.eecs.berkeley.edu/bear/`
Leadership:	Prof. S. Shankar Sastry, Dr David Shim (2000)
Platforms:	Concept 60, Bergen Industrial Twin, Yamaha R-50, Yamaha RMAX

Table A.2: *Academic Autonomous RC Helicopter Projects (continued)*

Institution:	University of Berlin ("MARVIN")
URL:	`http://pdv.cs.tu-berlin.de/MARVIN/`
Leadership:	Prof. G. Hommel
Platform:	SSM (German manufacturer), 23 cc gasoline egine, 1.88 m rotor diameter
Description:	Won 1999 and 2000 IARC; low cost inertial sensors; using 16-bit microcontroller onboard as main processor
Institution:	University of Southern California ("AVATAR")
URL:	`http://www-robotics.usc.edu/~avatar/`
Leadership:	Prof. Gaurav S. Sukhatme; Srikanth Saripalli
Platform:	Bergen Industrial Twin, Lite Machines LMH-110
Description:	Working towards formation flight of electrically powered RC helicopters omnidirectional vision aiding; collaboration with CSIRO
Institution:	University of Waterloo ("WARG")
URL:	`http://ece.uwaterloo.ca/~warg`
Description:	Developing a ducted fan vehicle
Institution:	Linköping University, Wallenberg Laboratory
URL:	`http://www.ida.liu.se/ext/witas/`
Institution:	Simon Fraser University Aerial Robotics Group
URL:	`http://www.sfu.ca/~arg/heli/`
Institution:	Rose-Hulman Institute of Technology
URL:	`http://www.rose-hulman.edu/arc/`
Institution:	Southern Polytechnic State University Aerial Robotics Team
URL:	`http://a-robotics.spsu.edu/`
Description:	Working with Rotomotion
Institution:	University of Texas at Austin Aerial Robotics
URL:	`http://iarc1.ece.utexas.edu/`
Institution:	North Carolina State University Aerial Robotics Club
URL:	`http://www.ncsu.edu/stud_orgs/ar/`
Institution:	University of Arizona Aerial Robotics Club
URL:	`http://clubs.engr.arizona.edu/arc/0405site/index.htm`
Institution:	South Dakota School of Mines and Technology
URL:	`http://uav.sdsmt.edu/Default.htm`

Table A.3: *Commercial RC Helicopter Autopilot Development Projects*

Company:	CSIRO (in collaboration with University of Queensland)
URL:	`http://www.cat.csiro.au/cmst/automation/expertise/heli/`
Platform:	X-Cell 60
Description:	Stereo vision aiding; Low cost IMU and GPS receiver sensors
Company:	Rotomotion
URL:	`http://rotomotion.com/index.htm`
Leadership:	Trammell Hudson; Aaron Kahn (Gatech)
Description:	Using low cost IMU and GPS receiver sensors
Company:	weControl (spin-off of ETH Zürich)
URL:	`http://www.wecontrol.ch`
Company:	Guided Systems Technologies, Inc.
URL:	`http://www.mindspring.com/~guided/`

Table A.4: *RC Helicopter Manufacturers*

Project:	Miniature Aircraft USA (X-Cell)
URL:	`http://www.miniatureaircraftusa.com/index.asp`
Project:	Bergen RC Helicopter
URL:	`http://www.bergenrc.com`
Project:	Yamaha, "RMAX Aero Robot"
URL:	`http://www.yamaha-motor.co.jp/global/business/sky/index.html`
Description:	Equipped with an attitude control system (YACS)

Table A.5: *Small Rotary-Wing Vehicles*

Company:	RC-Toys
URL:	`http://www.rctoys.com`
Products:	Dragan Flyer IV, X-Pro
Description:	Electrically powered, quad rotors
Company:	AirScooter
URL:	`http://www.airscooter.com`
	`http://www.airscooter.net`
Description:	Coaxial electrically and glow powered helicopters
Company:	Pixel Heliocpters
URL:	`http://pixelito.reference.be/`
Description:	For years the lightest RC helicopter in the world

Table A.6: *Industrial and military RUAV projects*

Project:	Schiebel, "Camcopter"
URL:	`http://www.schiebel.net/`
Description:	Two-bladed autonomous helicopter, 3.1 m rotor diameter
Project:	SAIC, "Vigilante"
URL:	`http://www.vtol.org/uavpaper/NavyUAV.htm`
Project:	Orion Aviation, "Seabat"
URL:	`http://uav.wff.nasa.gov/`
Project:	North Grumman, "Fire Scout"
URL:	`http://www.northgrum.com`
Project:	Thrope Seeop Corporation, "Spinwing"
URL:	`http://www.seeop.com`
Project:	Scandicraft, APID
URL:	`http://www.scandicraft.se`
Project:	ONERA, Dépt. Commande des Systèmes et Dynamique du vol
URL:	`http://www.cert.fr/dcsd/VIGILANT`
Description:	Surveillance and area monitoring
Project:	Bombardier Aerospace CL-327 "Guardian"
URL:	`http://fas.org/man/dod-101/sys/ac/row/cl-327.htm`
Description:	Co-Axial Counter rotating RUAV
Project:	Sikorsky "Cypher" and "Cypher II" (Dragon Warrior)
URL:	`http://avia.russian.ee/vertigo/sik_cypher2-r.html`
Description:	Shrouded counter rotating RUAV
Project:	Bell Eagle Eye
URL:	`http://www.bellhelicopter.com`
Description:	Tilt-rotor UAV
Project:	Moller Aerobot
URL:	`http://www.moller.com/aerobot/`
Description:	Variety of unconventional VTOL research vehicles
Project:	Dragon Warrior, "Stalker"
URL:	`http://avdil.gtri.gatech.edu/RCM/RCM/DroneProject.html`

Table A.7: *Commercial RC Helicopter systems customized for photography applications*

Project:	Coptervision RC Helicopter
URL:	`http://www.coptervision.com`
Project:	Dragonfly Pictures Inc.
URL:	`http://www.dragonflypictures.com`
Project:	Hover Cam Ltd.
URL:	`http://www.hovercam.com`
Project:	Survey-Copter
URL:	`http://www.survey-copter.com`
Project:	CARVEC Remote Vehicle Control System
URL:	`http://www.carvec.co.uk/index.htm`

Table A.8: *RUAV sites*

Site:	International Aerial Robotics Competition
URL:	`http://avdil.gtri.gatech.edu/AUVS/IARCLaunchPoint.html`
Site:	Association for Unmanned Vehicle Systems International
URL:	`http://www.auvsi.org`
Site:	UAV Forum
URL:	`http://www.uavforum.com/vehicles/overview.htm`
Site:	Federation of American Scientists
URL:	`http://fas.org/irp/program/collect/uav.htm`
	`http://fas.org/man/dod-101/sys/ac/row/`
	`http://fas.org/irp/program/collect/`
Site:	American Helicopter Society (AHS) International
URL:	`http://www.vtol.org/uavpaper/`
Site:	NASA Wallops Flight Facility
URL:	`http://uav.wff.nasa.gov/`
Site:	Unmanned Aerial Vehicle Blog
URL:	`http://www.livingroom.org.au/uavblog/`
Site:	Joint Robotics Program
URL:	`http://robot.spawar.navy.mil/`

Appendix B

Voyager E Modifications, Maintenance and Failures

Helicopters require maintenance and frequent inspections to ensure that all of the components are working correctly. If maintenance is neglected accidents will inevitably occur.

Unfortunately, however, not all problems stem from negligence of maintenance checks. Very few RC helicopters are manufactured to carry a payload. Pilots will spend in excess of what they paid for a standard helicopter to reduce the weight and increase the strength of the mechanics of the helicopter. These upgrades are usually performed to ensure better performance under high aerobatic loads.

The helicopter used in this project is a standard JR Voyager E, except for the 8-cell batteries and the relocation of the tail rotor collective pitch servo. The standard brushed motor, electronic speed controller (ESC), wooden blades, a tail rotor "gyro" and other standard subsystems were used.

B.1 Modifications Made

Trail Rotor Collective Pitch Servo

A number of helicopter frames are designed with the the tail rotor servo located at the front (nose) of the helicopter, requiring long control push rods. It is fairly common to move the servo onto a mounting that clamps onto the tail boom. The location of the servo on the tail boom opens up space in the Voyager E and has allowed us to use a very

stiff, short tail rotor push rod (allowing more accurate control authority). Although the modification has definitely improved the control authority, there is still a large amount of dead-band between the servo and the trail rotor pitch angle.

Yaw Rate Augmentation System

The yaw rate augmentation system was relocated from being mounted in the fuselage to a small piece of plastic next to the main rotor head. Relocating the active yaw rate damping subsystem has not deteriorated the performance, but provided more space in the frame for the mounting of other electronics. The new location is once again a fairly standard location for the yaw rate damping subsystem.

B.2 Maintenance Required and Mechanical Failures

Motor Replacement

During the last year of flight testing, the motor had to be replaced twice. It is not always easy to distinguish between a motor that is nearing the end of its lifetime and problems with the brushes or electronic speed controller. However, once a fully changed 3300 mAh battery pack only provides power for one minute under flight load, it is a clear sign that the motor needs to be replaced.

The replacement cost of a standard JR brushed 540 motor for the Voyager E is approximately US$ 60.

The failure of the motor has lead to two very hard landings, the last of which the impact of is not yet clear. A number of problems not previously encountered are being experienced since the motor replacement.

Brushes

The performance of the motor is a function of the state of the brushes. Furthermore, the two brushes do not usually wear off at the same rate.

Twenty four sets of brushes have been used during the last year of flight operation. A set of brushes lasts for between ten and twenty flights - depending on the length of the flights, the weight of the helicopter and at what point the decision is made to replace

the brushes. At US$ 6 a set and four minutes a flight, the running costs of an electrically powered helicopter become significant.

Brushless motors offer great efficiency, reduced maintenance costs and more reliable operation. Converting to a brushless motor is not a low cost option, but neither is the cost of two standard motors and twenty four sets of brushes.

Flight times of ten to fifteen minutes are commonly achieved using a brushless motor and a ten cell battery pack (without the payload carried for the purposes of this project).

Battery Packs

The original 7-cell battery pack was destroyed due to operator error in an attempt to charge the battery pack too fast.

The pack was replaced with a 8-cell pack constructed from eight Sanyo SCR 2400 mAh NiCd cells. Since it was the only pack available for flight testing, it lasted about three months. It was replaced with two sets of 8-cell GP 3300 mAh NiMH cells. The author later personally acquired two more of these battery packs. These four battery packs have not yet showed any signs of fatigue during six months of flight testing. Three SuperNova 250S chargers were used to charge the batteries.

The endurance and performance of the helicopter can be significantly enhanced by reducing the weight of the helicopter and the onboard electronics. A quarter of the weight of the complete system is accounted for by the 8-cell battery packs. The NiCd and NiMH battery packs weigh approximately 500 g each. Although somewhat notoriously dangerous to use at the moment, Lithium battery packs that are capable of providing sufficient current are becoming available at affordable prices. Although somewhat expensive at the moment, Lithium battery packs offer greater capacity at reduced weight.

Electronic Speed Controller

In general, the ESC has performed well, in spite of the fact that it is rated for use with an 8.4 V and not a 9.6 V battery pack.

However, there have been a number of instances where the motor would not run. Sometimes recalibration of the ESC has solved the problem, while sometimes the brushes were at fault. The problem is difficult to find since it seldom happens.

Tail Rotor Pitch Link

The tail rotor pitch link has melted and jammed at three different occasions. The lack of a bearing or other friction prevention device is a classic example of low cost, low weight electrically powered model helicopter workmanship. All bigger glow or gasoline powered helicopters have at least a bearing in the tail rotor collective pitch adjustment mechanism.

It seems as if the two washers that have been added have solved the problem. However, little flying has been conducted since the last occurrence of the problem.

Main Rotor Flapping Damper Rubbers

It is common model helicopter pilot knowledge that the main rotor flapping damper rubbers should be replaced after a period of aggressive aerobatic flying. However, it was somewhat unexpected to find it necessary to replace the rubbers after a year of flying only near-hover manoeuvres. Judging the extent of the problem is difficult, but since excessive low frequency vibrations were still present after replacement of all the rotor head parts except the rubbers, it was deemed worthwhile replacing the rubbers. Replacing the rubbers was found to reduce the problem.

JR R700 Receiver

During one of the first test flights the safety pilot lost complete control of the helicopter. The helicopter was flying about 15 m from the pilot when it rolled over and plummeted 4 m to the ground. No other electronics, except for the standard JR gear, were onboard the helicopter.

The exact cause is still a bit of a mystery. At the time a JR R700 receiver was used. It was replaced with a JR NER-549X receiver.

Servo Control Electronics

After a year of regular flying, the electronic control circuit of the tail rotor collective pitch servo failed during a test flight. The helicopter was about one metre above ground level at the time of the event, and the safety pilot could land the helicopter without incident. If it was any of the other servos it could have endangered the pilot and would

almost certainly have resulted in a helicopter-destroying accident.

The incident highlights two important facts:

- Unexpected accidents will happen and can cause damage to equipment and endanger lives.
- Over-engineering might limit performance and cost money, but might prevent even more expensive and time consuming accidents from happening.

Servo Gears

Seventeen sets of servo gears were used to repair servos with "stripped" gears. The first three servos were damaged during a crash. The others sets were all used to fix servos of which the same gear in the chain stripped frequently.

Appendix C

Longitudinal and Lateral FCS Design

```
% Lateral and Longitudinal control law design for a RC model helicopter
% Version 3
%------------------------------------------------------------------------
%
% Model structure based on work by Mettler, Tischler, Kanade
% "System Identification of Small-Size Unmanned Helicopter Dynamics"
% 11 state model, extended later in this code to include positions
% 13 state model not used cause it yields insight, not better fitts
% file: Tischler_R50.pdf
%
% Model used taken from D H Sim, H J Kim and S Sastry :
% "Control Systems Design for Rotorcraft-based Unmanned Aerial Vehicles
%  using Time-domain System Identification"
% Model is for URSA Minor, '60' size helocopter - Concept 60
% file: cca2000.ps and Hsdiss.pdf
%
% Also see: MTKM00.pdf, helimodel.pdf, MGFK02.pdf
%
%------------------------------------------------------------------------
%
% States are :    u, v, p, q, phi, theta, A1s, B1s, w, r,  rgyro
%          X =  [ 1  2  3  4  5    6      7    8    9  10  11   ]
%
% Xdot = AX + BU
%
% u      : longitudinal velocity
% v      : lateral velocity
% p      : roll rate
% q      : pitch rate
% phi    : angle of roll
% theta  : angle of pitch
% A1s    : longitudinal blade flapping (also refer to as a1, or a)
% B1s    : lateral blade flapping (also refer to as b1, or b)
% w      : climb rate
% r      : yaw rate
% rgyro  : active yaw rate damper state (model yaw as second order system)
%
% This model does not include states c and d (flapping angle of flybar)
% that Mettler loves and presents in his 13 state model.
%
% Longitudinal blade flapping (A1s) is controlled (primary) by
% input 2 which is refered to as \delta_b or u_b1s
% Similarly, Lateral blade flapping (B1s) is controlled (primary) by
% input 1 which is refered to as \delta_a or u_a1s
%
%------------------------------------------------------------------------
%
% Author    : Nicol Carstens
% Date      : Saturday 08/02/2003
% Work Done : Basic model used for Simulink based control design
%
% Author    : G W Milne & Nicol Carstens
% Date      : Wednesday  23/06/2004
% Work Done : Model used for rltool() long and lat control design
%
% Author    : Nicol Carstens
% Date      : Friday 03/09/2004
% Work Done : Clean up code
%
%------------------------------------------------------------------------

close all; clear all; clc;

g = 9.81;
A = zeros(11);

A(1,1) = -0.0629;          % Xu
A(1,7) = -g;               % Xa1s
A(1,6) = -g;

A(2,2) = 0.0305;           % Yv
A(2,8) = g;                % Yb1s
A(2,5) = g;

A(3,1) = 0.2978;           % Lu
A(3,2) = -0.7061;          % Lv
A(3,7) = 40.361;           % La1s
A(3,8) = 237.42;           % Lb1s => wnp = 15.40
```

```
A(4,1) = 1.3057;           % Mu
A(4,2) = -1.2199;          % Mv
A(4,7) = 220.18;           % Ma1s => wnq = 14.83
A(4,8) = -11.438;          % Mb1s

A(5,3) = 1;

A(6,4) = 1;

A(7,7) = -4.3459;          % -1/thau_f
A(7,8) = 1.4487;           % Ab1s
A(7,4) = -1;

A(8,7) = -1.5915;          % Ba1s
A(8,8) = -4.3459;          % -1/thau_f
A(8,3) = -1;

A(9,7) =  -3.0523;         % Za1s
A(9,8) =  -15.063;         % Zb1s
A(9,9) =  -1.3453;         % Zw
A(9,10) =  0.2222;         % Zr

A(10,3) =  -0.0178;        % Np
A(10,9) =  1.1860;         % Nw
A(10,10) = -2.9986;        % Nr
A(10,11) = -22.126;        % Nrff

A(11,10) = 3.1541;         % Kr
A(11,11) = -9.5035;        % Krfb

B = zeros(11,4);

B(7,1) = 0.5259;
B(7,2) = 2.1922;
B(8,1) = 2.2333;
B(8,2) = -0.0917;
B(9,3) = 10.6446;
B(10,3) = 4.4911;
B(10,4) = -103.335;

C = zeros(3,11);
C(1,1) = 1;                % u => x velocity
C(2,4) = 1;                % q => pitch rate
C(3,6) = 1;                % theta => pitch

D = zeros(3,4);

%--------------------------------------------
% Can stop here if only the model is required
%--------------------------------------------

%--------------------------------------------
% This code is old code by GWM to design LQR controller
%
% % Now angular units are in radians and rad/s. ! rad pitch is a hell of a pitch angle
% % and is more likely comparable to 100m/s than 1m/s. This scale units so 1.0 = 100m/s
% % Thus let Xold = T Xnew, so
% %  dot T Xnew = A  T Xnew + B u
% % and   dot Xnew = inv(T) A T    Xnew    +   inv(T) B   u
% T = diag([ 100 100 1 1 1 1 1 1 100 1 1]);
% T = diag([ 1 1 1 1 1 1 1 1 1 1 1]);
%
% Aold=A;Bold=B;
% A=T\Aold*T;   B=T\Bold;
%--------------------------------------------

% Check Eigen vectors and values
[vec,val]=eig(A);

design_long = 1;
design_lat  = 0;

if design_long == 1

   % eigen_values = val*[ 1 1 1 1 1 1 1 1 1 1 1]'
   % C = [ 0 0 0 0 0 1 0 0 0 0 0 ];
   % D = 0;
   % Along=A(Longstates, Longstates);
   % Blong=B(:,2);
```

```
% AlongThetaFB=A-Blong*C*1;
% clc
% [vec,val]=eig(AlongThetaFB);
% eigen_values = val*[ 1 1 1 1 1 1 1 1 1 1 1]'

% B=B(:,2);
% C = [ 0 0 0 0 0 1 0 0 0 0 0 ];
% D = 0;
% Xfull=ss(A,B,C,D);
% rltool(Xfull)
% %

% %States are  u, v, p, q, phi, theta, A1s, B1s, w, r, rgyro
% %           1  2  3  4   5     6     7     8  9  10  11
% % Yaw =                                       *   *   *
% % Lateral =     *  *  *    *                              === u = 0
% % Longit =   *     *  *         *     *     *              === v = 0
% Longstates=[1 2 3 4 5 6 7 8 9 10 11];
Longstates=[1 3 4 6 7 8];

D=0;
%Ctheta=[1 0 0 0 0 0 0 0 0 0 0];   % Pitch angle output.
Ctheta=[ 0 0 0 1 0 0];   % Pitch angle output.

Along=A(Longstates, Longstates);
Blong=B(Longstates,2); % 2 => long, 1 => lateral
%
% [vec,val]=eig(Along)
% % disp('States = u, q,  theta, A1s, B1s');
% absvec=abs(vec);
% val=diag(val);
%
% Xtheta=ss(Along,Blong,Ctheta,D);
% % set(Xtheta,'OutputName',[{'Theta'}]);set(Xtheta,'InputName',[{'LonStick'}]);
% %
%Ctheta=[ 1 0 0 0 0 0];   % Pitch angle output.
%Ctheta=[1 0 0 0 0 0 0 0 0 0 0];   % Pitch angle output.
Ctheta=[ 0 0 0 1 0 0];   % Pitch angle output.
Xtheta=ss(Along,Blong,Ctheta,D);

Ktheta = 1.1;

if Ktheta == 0
   rltool(Xtheta); % enables one to apply feedback gain of 1 from theta to LongStick to
   % stabilise all but the speed mode.
else

   AlongThetaFB = Along-Blong*Ctheta*Ktheta   % Pitch angle feedback max gain of 1.6
   BlongThetaFB = Blong*Ktheta;
   Cu=[1 0 0 0 0 0];
   Xu=ss(AlongThetaFB,BlongThetaFB,Cu,D);
   % % set(Xu,'OutputName',[{'Theta'}]);set(Xu,'InputName',[{'LonStick'}]);
   % step(Xu,10)
   % % %
   % Cu=[1 0 0 0 0 0];
   % Xu=ss(AlongThetaFB,BlongThetaFB,Cu,D);
   %Xu=ss(Along,Blong,Cu,D);

   Ku = -0.36;
   if Ku== 0
      % NB: MINUS SIGN!!!
      % positive angle causes negative acceleration! just for
      % longitudinal case!
      rltool(Xu)
   else

      % % % NB: MINUS SIGN!!!
      % % % Velocity feedback 0.36 => 45 deg fase grens
      AlongTheta_u_FB=AlongThetaFB-BlongThetaFB*Cu*Ku;
      BlongTheta_u_FB = BlongThetaFB*Ku;
      % %
      % Xu_FB=ss(AlongTheta_u_FB,BlongTheta_u_FB,Cu,D);
      % set(Xu_FB,'OutputName',[{'u'}]);
      % % set(Xu_FB,'InputName',[{'LonStick'}]);
      % % figure
      % % step(Xu_FB)
      % % rltool(Xu_FB)
      %
      % Now need to add the position state (augment matrix), and add
```

```
        % the position feedback.
        AlongTheta_u_North_FB= [AlongTheta_u_FB [0;0;0;0;0;0];[1 0 0 0 0 0 0]];
        Blong_North=[BlongTheta_u_FB;0];
        C_North=[0 0 0 0 0 0 1];

        North_FB=ss(AlongTheta_u_North_FB,Blong_North,C_North,0);
        set(North_FB,'OutputName',[{'North'}]);
        set(North_FB,'InputName',[{'LonStick'}]);
        figure
        % step(North_FB)

        Knorth = 0 ;%1.22;

        if Knorth == 0
           rltool(North_FB) %  Used to select POs FB gain=25 =>> 1.23 rad/s 0.73 damping
        else

           NorthFeedback= Knorth*Blong_North*C_North;
           North_FB=ss(AlongTheta_u_North_FB + NorthFeedback ,Blong_North*Knorth,C_North,0);
           step(North_FB);
        end
     end
  end
end

if design_lat == 1
  % => design lateral loop gains

  % States are  u, v, p, q, phi, theta, A1s, B1s, w, r, rgyro
  %             1  2  3  4   5     6     7     8  9  10  11
  % Yaw =                                        *   *   *
  % Lateral =     *  *  *    *                                 === u = 0
  % Longit =   *     *  *         *     *     *              === v = 0
  % Latstates=[1 2 3 4 5 6 7 8 9 10 11];
  Latstates=[2 3 4 5 7 8];

  D=0;
  %Ctheta=[1 0 0 0 0 0 0 0 0 0 0];
  Cphi=[ 0 0 0 1 0 0];                % Roll angle output.

  Alat=A(Latstates, Latstates);
  Blat=B(Latstates,1);                 % 2 => long, 1 => lateral
  %
  % [vec,val]=eig(Along)
  % % disp('States = u, q,  theta, A1s, B1s');
  % absvec=abs(vec);
  % val=diag(val);
  %
  % Xtheta=ss(Along,Blong,Ctheta,D);
  % % set(Xtheta,'OutputName',[{'Theta'}]);set(Xtheta,'InputName',[{'LonStick'}]);
  % %
  %Ctheta=[ 1 0 0 0 0 0];   % Pitch angle output.
  %Ctheta=[1 0 0 0 0 0 0 0 0 0 0];   % Pitch angle output.

  Xphi=ss(Alat,Blat,Cphi,D);

  % set K_phi = 0 to stop rest of design process, and use rltool to select
  % K_phi...
  Kphi = 0.77;

  if Kphi == 0
     rltool(Xphi);   % enables one to apply feedback gain from LatStick to theta
     % stabilise all but the speed mode.
  else
     AlatPhiFB = Alat-Blat*Cphi*Kphi   % Roll angle feedback max gain of ??
     BlatPhiFB = Blat*Kphi;               % before going unstable
     Cv=[1 0 0 0 0 0];
     XphiFB=ss(AlatPhiFB,BlatPhiFB,Cv,D);
     % % set(Xu,'OutputName',[{'Theta'}]);set(Xu,'InputName',[{'LonStick'}]);
     % step(XphiFB,10)
     % % %
     % Cu=[1 0 0 0 0 0];
     Xv=ss(AlatPhiFB,BlatPhiFB,Cv,D);
     %Xu=ss(Along,Blong,Cu,D);

     % set K_v = 0 to stop rest of design process, and use rltool to select
     % K_v...
     Kv = 0.23;
```

```
      if Kv == 0
         rltool(Xv);   % enables one to apply feedback gain from LatStick to v
      else

         % % % NB: NO EXTRA MINUS SIGN!!!
         % % % Velocity feedback  =>  deg fase grens
         AlatPhi_v_FB = AlatPhiFB-BlatPhiFB*Cv*Kv;
         BlatPhi_v_FB = BlatPhiFB*Kv;
         %
         Xv_FB=ss(AlatPhi_v_FB,BlatPhi_v_FB,Cv,D);
         set(Xv_FB,'OutputName',[{'v'}]);
         set(Xv_FB,'InputName',[{'LatStick'}]);
         figure
         step(Xv_FB)
         % % rltool(Xu_FB)

         % Now need to add the position state (augment matrix), and add
         % the position feedback.
         AlatPhi_v_East= [AlatPhi_v_FB [0;0;0;0;0;0];[1 0 0 0 0 0 0]];
         Blat_East=[BlatPhi_v_FB;0];
         C_East=[0 0 0 0 0 0 1];

         Xeast=ss(AlatPhi_v_East,Blat_East,C_East,0);
         %set(East_FB,'OutputName',[{'East'}]);
         %set(East_FB,'InputName',[{'LatStick'}]);
         %figure
         % step(East_FB)

         % set Keast = 0 to stop rest of design process, and use rltool to select
         % Keast...
         Keast = 0.83;

         if Keast == 0
            rltool(Xeast)
         else
            % NB: NO extra MINUS SIGN!!!
            EastFeedback= Keast*Blat_East*C_East;
            East_FB=ss(AlatPhi_v_East - EastFeedback,Blat_East*Keast,C_East,0);
            step(East_FB);
         end
      end
   end
end
```

Appendix D

Schematics

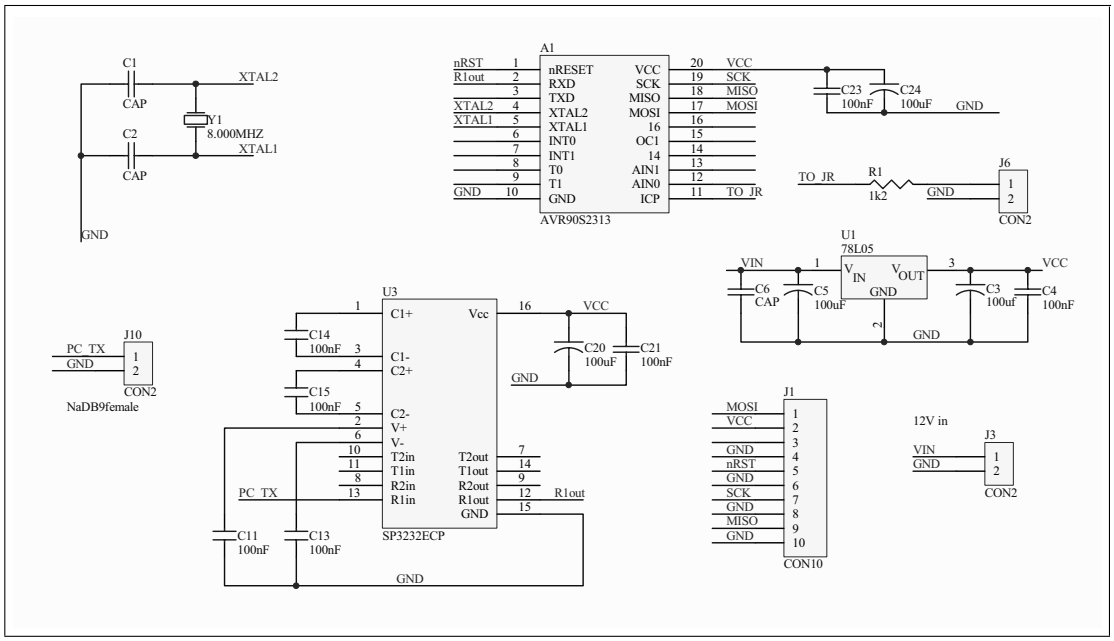

Figure D.1: *Designed PC RS-232 to JR interface circuit*

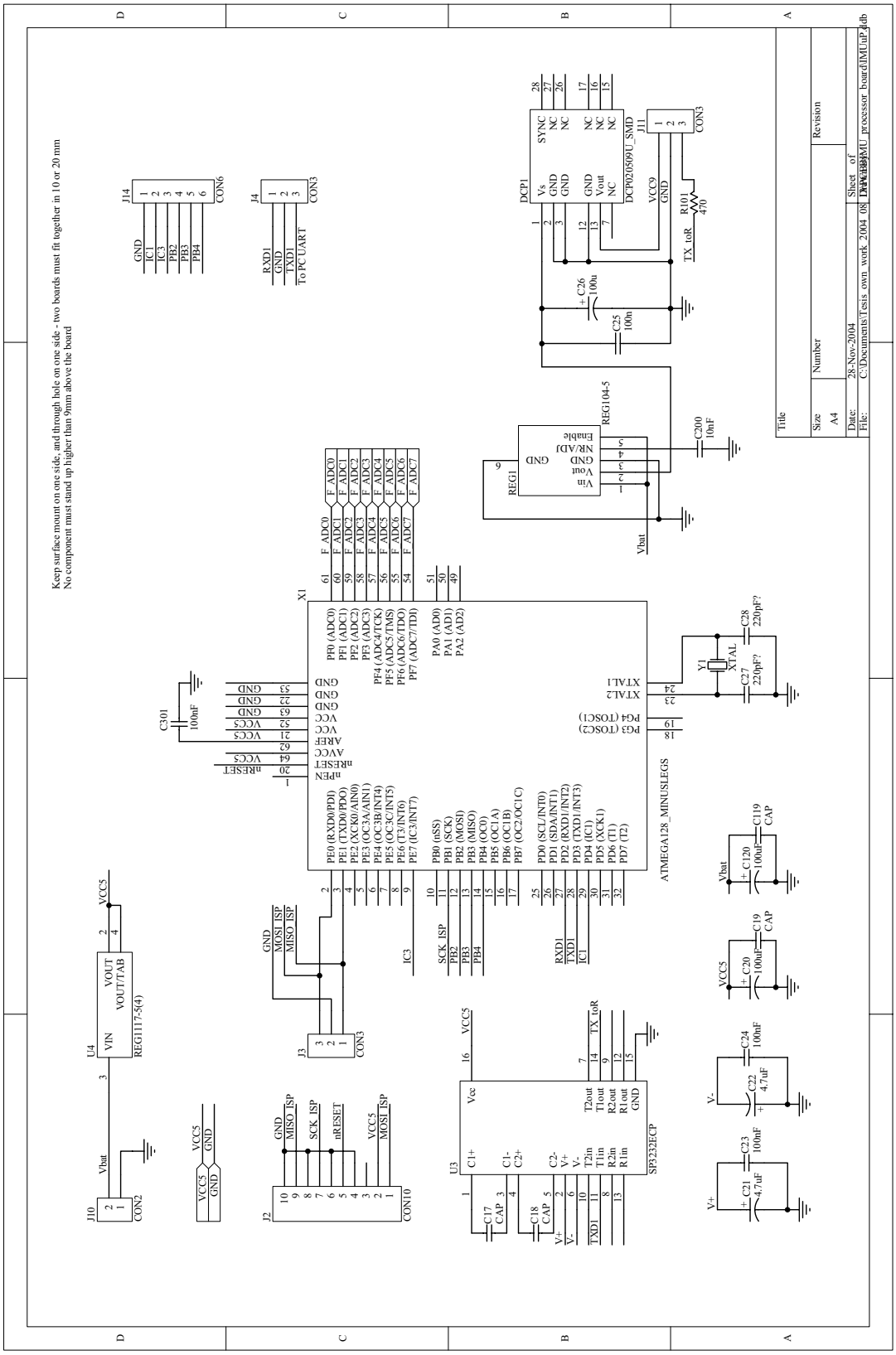

Figure D.2: *Designed RF transmitter interface, power supply and IMU microcontroller circuit*

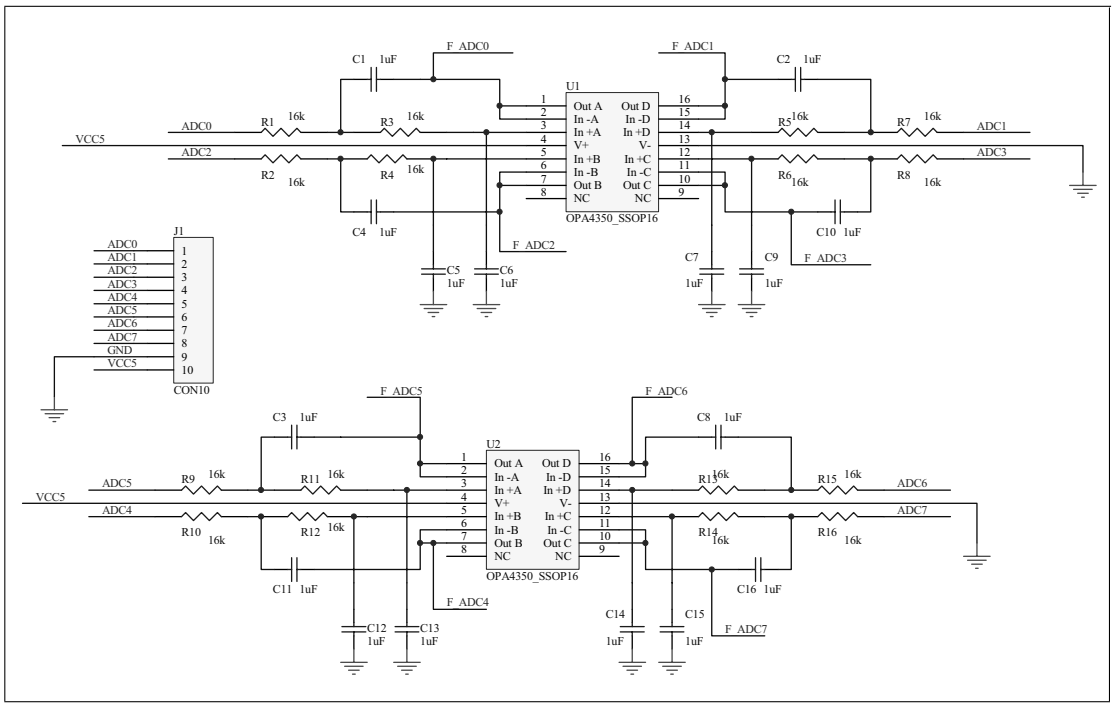

Figure D.3: *Low pass filters added to IMU microcontroller board*

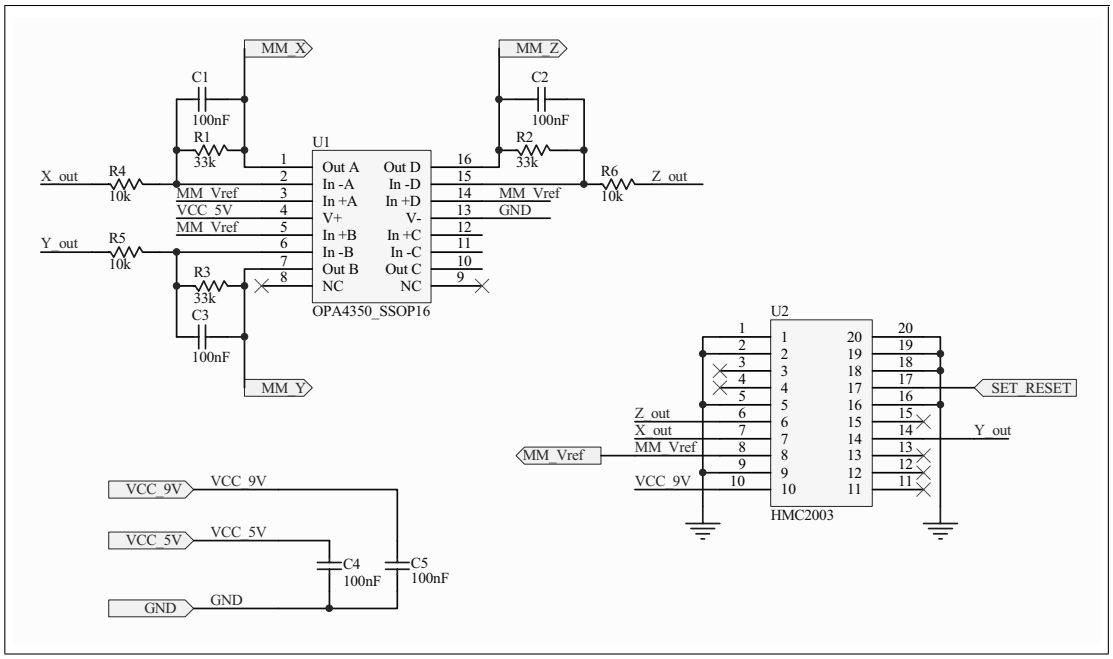

Figure D.4: *Circuit for HMC2003 magnetometer sensor with designed signal conditioning*

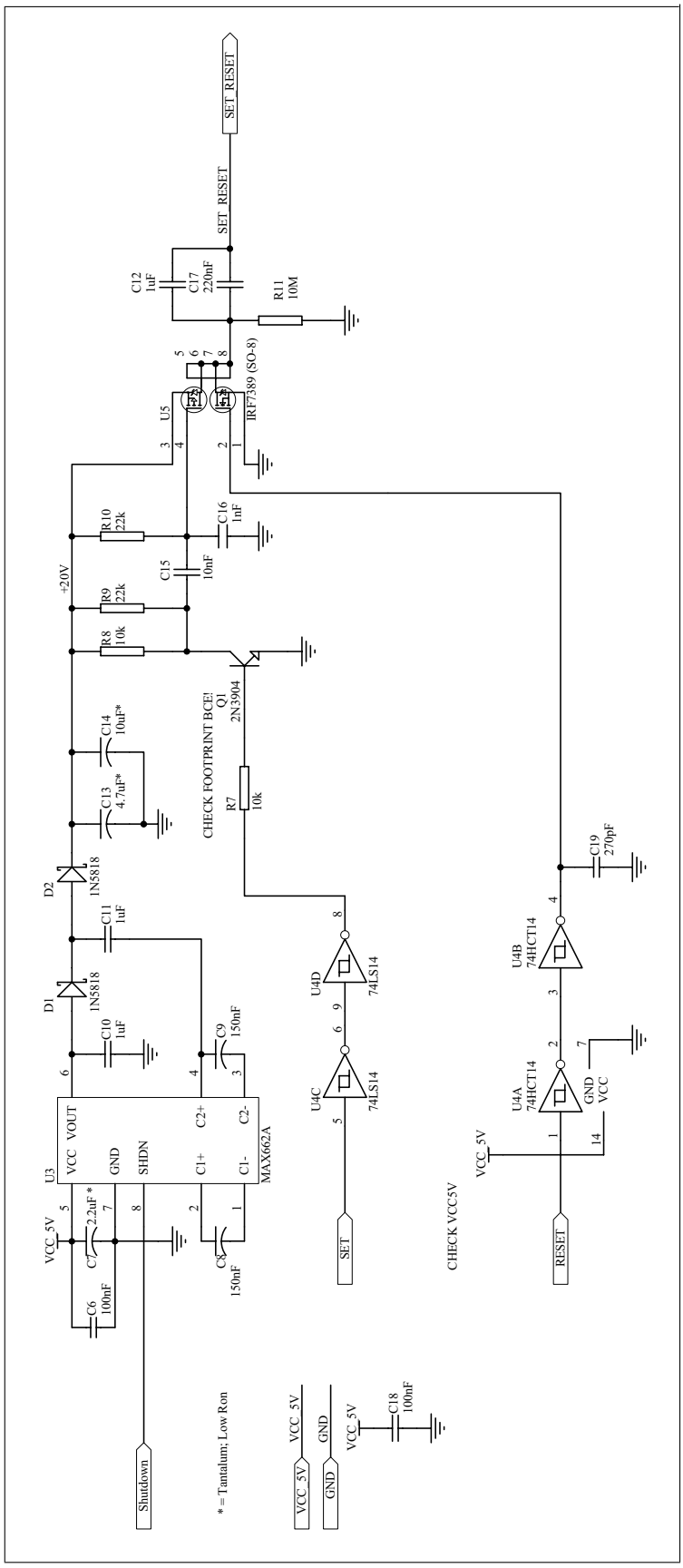

Figure D.5: *Designed Set/Reset pulse circuit for HMC2003 sensor*

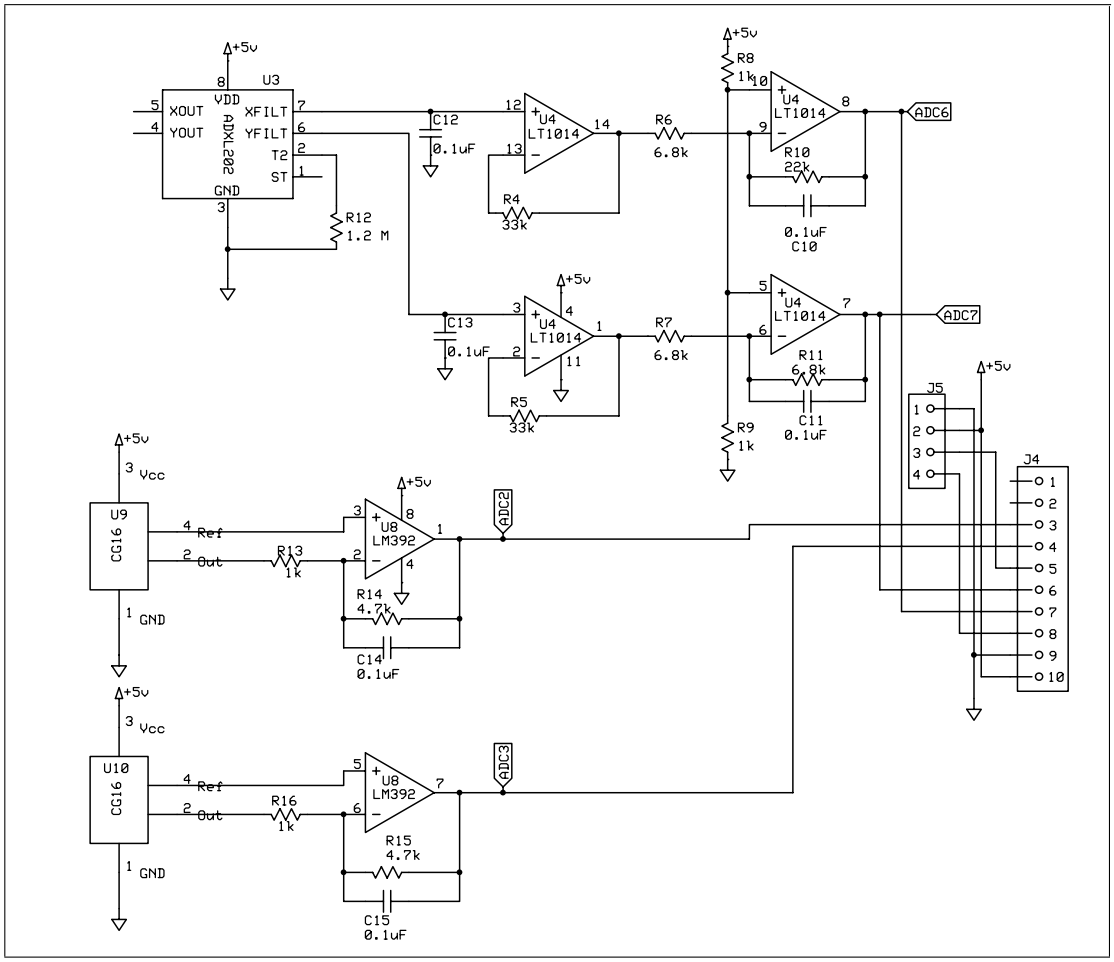

Figure D.6: *Rotomotion IMU XY-axis board schematic (original)*

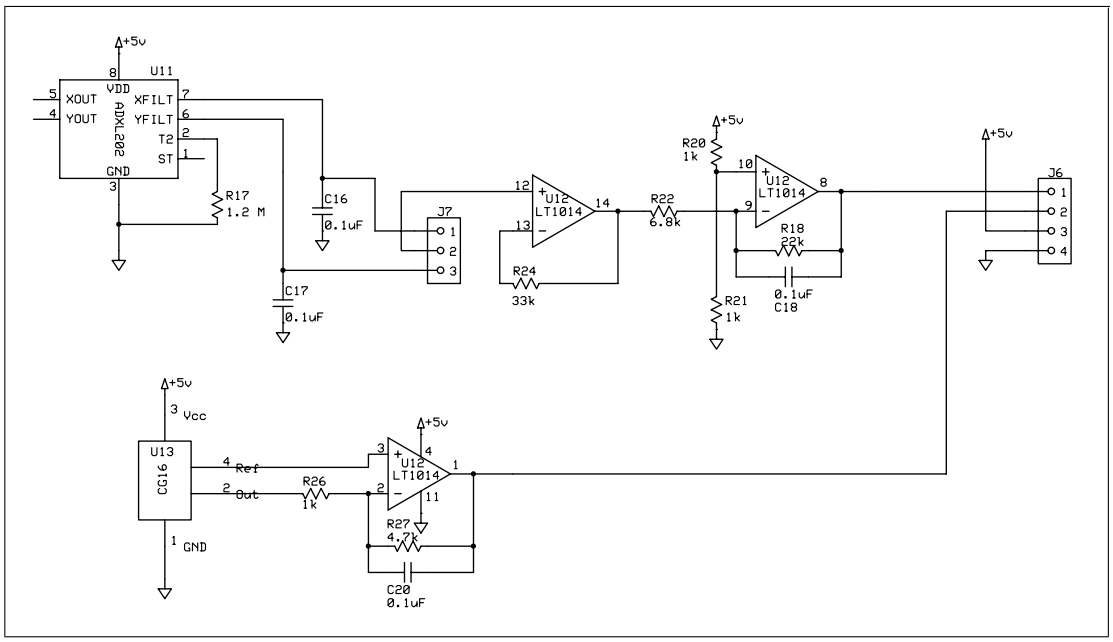

Figure D.7: *Rotomotion IMU Z-axis board schematic (original)*

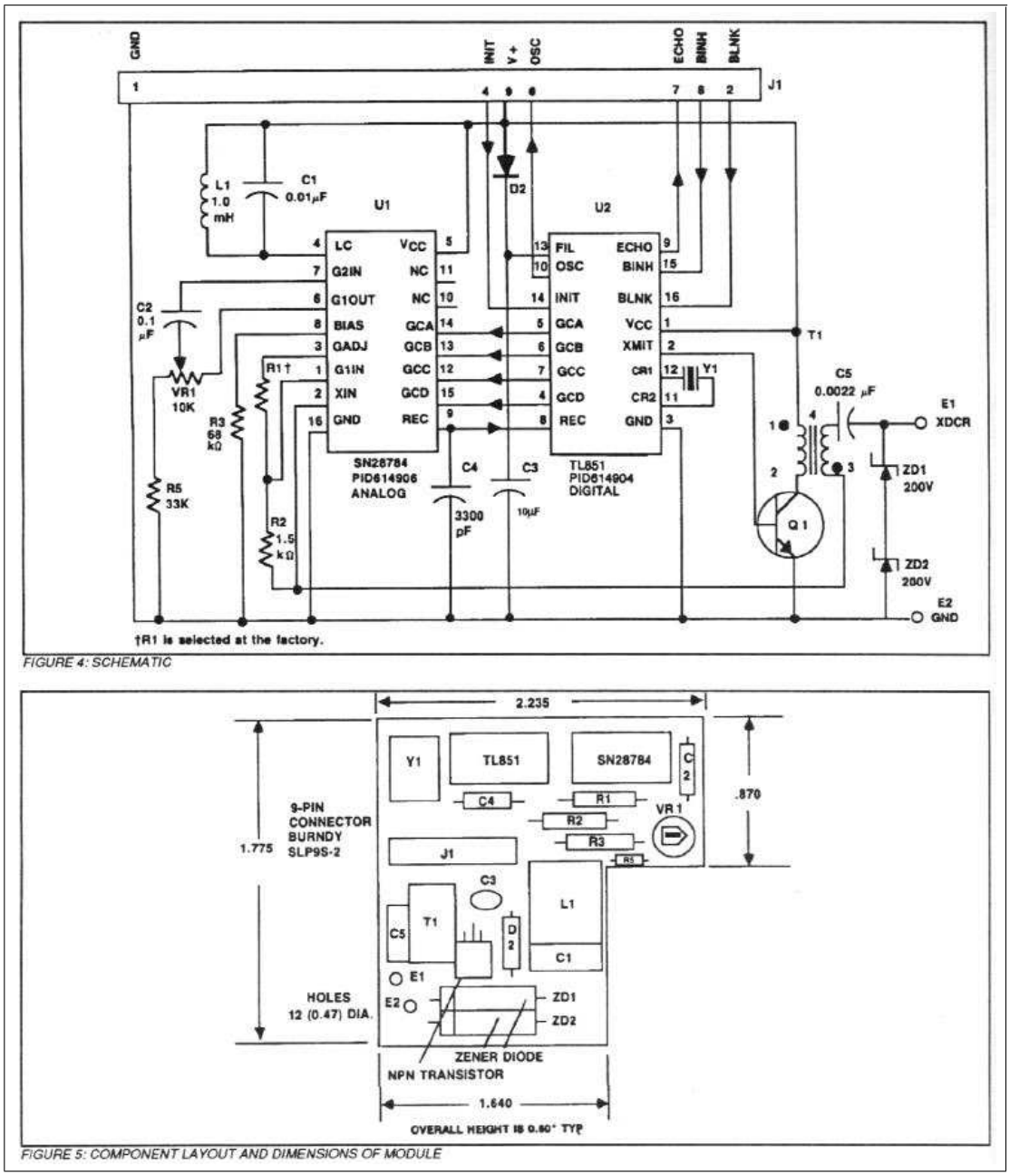

Figure D.8: *Schematic and Component Layout of Polaroid 6500 ultrasonic range sensor used*